Development and Characterization of Ethanol-Compatibilized PPO-based EPMM Membranes

by:

Qiang Wang

A thesis submitted to the Faculty of Graduate and Postdoctoral Studies in Partial fulfillment of the requirements for the degree of

Master of Applied Science

in the

Department of Chemical and Biological Engineering

University of Ottawa

May 2011

ABSTRACT

Emulsion polymerized mixed matrix (EPMM) membranes is a new category of membranes, which incorporate silica-based inorganic nanoparticles dispersed in continuous phase of an organic polymer. The uniqueness of the EPMM membranes comes from the fact that they may combine otherwise incompatible inorganic and organic phases. This is achieved by the synthesis of the inorganic nanoparticles from a silica precursor in a stable emulsion, in which an aqueous phase is dispersed in a continuous phase of the polymer solution. More specifically, the silica precursor soluble in the polymer solution polymerizes in contact with the aqueous phase, and consequently the latter acts as finely dispersed micro reactors.

The objective of this work was to optimize the previously developed protocol for the synthesis of poly (2,6-dimethyl-1,4pheneylene oxide) (PPO) based EPMM membranes, and to characterize their physical and gas transport properties. In particular, the effects of inorganic loading and the membrane post-treatment protocol on the permeability and selectivity of the membranes were of interest. However, the results showed that the obtained permeation and separation were virtually not affected by the theoretical Si loading and the post-treatment protocol. Moreover, in comparison to the base PPO membranes, the observed O_2 permeability and the O_2/N_2 permselectivity have generally decreased. The differential scanning calorimetry (DSC) analysis of the synthesized membranes showed an important scatter of the glass transition temperatures (T_g) of the EPMM membranes with the values generally lower than the T_g of the base PPO. Moreover, the inductively coupled plasma mass spectrometry (ICP-MS) showed the silica content in selected EPMM membranes to be far below the expected theoretical level. This, in

combination with the ^{29}Si nuclear magnetic resonance (^{29}Si NMR) results, showed that most of the already low silica content comes from the unreacted silica source (tetraethylorthosilicate) and have led to the second phase of the project in which a modified synthesis protocol has been developed.

The major differences of the modified protocol compared to the original one include the replacement of a surfactant, 1-octanol, by ethanol and using greater concentrations of the reactants. To study the effect of different parameters involved in the synthesis protocol, a Gravimetric Powder experiment, in which the inorganic polymerization is carried out in an emulsion with a pure solvent rather than a polymer solution, has been designed. The Gravimetric Powder experiments have confirmed polymerization of tetraethylorthosilicate (TEOS) in the emulsion system. Using the conditions, which resulted in the maximum production of the polymerized TEOS in the Gravimetric Powder experiments, one set of new EPMM membranes has been synthesized and characterized.

The new EPMM membranes have the T_g of 228.2^{o}C, which is distinctly greater compared to the base PPO, and contain one order of magnitude more of silica compared to the old EPMM membranes. More importantly, the ^{29}Si NMR analysis has proven that the silica content in the new EPMM membranes originates from the reacted rather than unreacted TEOS. Interestingly, the observed conversion of TEOS in the new EPMM membranes, exceeding 20%, is greater than the largest conversion in the Gravimetric Powder experiments. The oxygen permeability in the new EPMM membrane of 33.8 Barrer is more than twice that of the base PPO membrane. Moreover, this increase in O_2 permeability is associated with a modest increase in the O_2/N_2 permselectivity (4.75 versus 4.67).

RÉSUMÉ

Les membranes mixtes préparées par un procédé de polymérisation en émulsion (EPMM) forment une nouvelle catégorie de membranes. Cette méthode permet l'incorporation de nanoparticules inorganiques à base de silice dans la matrice continue d'un polymère organique. La caractéristique unique des membranes d'EPMM vient du fait qu'elles peuvent combiner des phases inorganiques et organiques autrement incompatibles. Ceci est réalisé par la synthèse des nanoparticules inorganiques à base de silice à l'intérieur d'une émulsion stable formée par une phase aqueuse dispersée dans une phase continue de la solution de polymère. Plus spécifiquement, le précurseur de silice, soluble dans la solution de polymère, polymérise en contact avec la phase aqueuse, et par conséquent les composantes de l'émulsion agissent en tant que micro-réacteurs finement dispersés.

L'objectif de ce travail était d'optimiser un protocole précédemment développé pour la synthèse de membranes à base d'oxyde de 2,6 dimethyl-1,4 pheneylene (PPO) et d'EPMM, et de caractériser leurs propriétés physiques et de transport de gaz. Les effets du chargement inorganique et du protocole après traitement des membranes sur la perméabilité et la sélectivité des membranes étaient d'intérêt. Cependant, la perméation et les résultats obtenus de séparation n'ont montré pratiquement aucun effet du chargement théorique de Si et du protocole après traitement sur la perméabilité O_2 et la permselectivitée O_2/N_2. D'ailleurs, par rapport aux membranes de base en PPO, la perméabilité O_2 observée et le permselectivité O_2/N_2 ont généralement diminué. L'analyse par calorimétrie différentielle (DSC) des membranes synthétisées a montré une grande variation des températures de transition (T_g) des membranes

d'EPMM avec des valeurs généralement inférieures au T_g du PPO. D'ailleurs, la méthode de spectroscopie de masse / plasma couplé par induction (ICP-MS) a montré que le contenu de silice dans des membranes choisies d'EPMM était considérablement au-dessous du niveau théorique prévu. Ceci, en combinaison avec les résultats de résonance magnétique nucléaires ^{29}Si (^{29}Si RMN), ont prouvé que la majeure partie du contenu déjà bas de silice vient de la source non réactive de silice (tetraethylorthosilicate). Ces résultats ont mené à la deuxième phase du projet dans laquelle un protocole modifié de synthèse a été développé.

Les différences principales du protocole modifié sont le remplacement d'un agent tensio-actif, 1-octanol, par l'éthanol et l'utilisation de plus grandes concentrations de réactifs. Pour étudier l'effet de différents paramètres impliqués dans le protocole de synthèse, une Méthode Gravimétrique fut développée, dans laquelle la polymérisation inorganique est effectuée dans une émulsion avec du solvant pur plutôt qu'une solution de polymère. Les expériences avec cette nouvelle méthode ont confirmé la polymérisation du tetraethylorthosilicate (TEOS) dans l'émulsion. Utilisant les conditions qui ont mené à la production maximale de TEOS polymérisé dans la méthode de poudre sèche, un ensemble de nouvelles membranes d'EPMM ont été synthétisées et caractérisées.

Les nouvelles membranes d'EPMM ont un T_g de 228.2 ^{o}C, qui est plus élevé que celui du PPO de base, et contiennent un ordre de grandeur supérieur de silice comparé aux membranes originales d'EPMM. L'analyse ^{29}Si RMN a montré que le contenu de silice dans les nouvelles membranes d'EPMM provient du TEOS qui a réagi plutôt que du TEOS qui n'a pas réagi. La conversion observée du TEOS dans les nouvelles membranes d'EPMM est de 20% supérieure à la plus grande conversion dans les expériences utilisant la méthode gravimétrique. La

perméabilité à l'oxygène de 33.8 Barrer dans la nouvelle membrane d'EPMM est plus de deux fois celle de la membrane contenant seulement du PPO. D'ailleurs, cette augmentation de la perméabilité d'O_2 est associée à une augmentation modeste de la permselectivité O_2/N_2 (4.75 contre 4.67).

Acknowledgements

I would like to express my gratitude to my supervisor, Dr. Boguslaw Kruczek for his guidance, advices, supervision and support of this project. Especially I wish to thank Dr Kruczek for his patience and help in improving the language of this thesis. This thesis would not have been done without his fruitful instruction and comments throughout the work.

The financial support from National Science and Engineering Research Council of Canada is appreciated.

I would like to thank my wife and my parents for their moral support and encouragement.

I would like to thank to Louis Tremblay, Gérard Nina and Franco Ziroldo for their technical assistance during this work.

I would like to thank to Dr. Andre Y. Tremblay, Dr. Marc Dubé and their teams for the support on the ultrasound dismembrator.

Finally, I would like to thank to Siamak Lashkari, Forouzan Sadeghi, Muhammad Tawalbeh and all my friends in Chemical and Biological department at University of Ottawa.

Table of Content

List of Tables

List of Figures

NOMENCLATURE

ABBREVATION

CVS	Constant Volume System
CPS	Constant Pressure System
DSC	Differential Scanning Calorimetry
EPMM	Emulsion Polymerized Mixed Matrix
EtOH	Ethanol
GC	Gas Chromatography
ICP-MS	Inductively coupled plasma mass spectrometry
NMR	Nuclear Megnetic Rosennance
PPO	Poly (2,6-dimethyl-1,4-phenolyne oxide)
STP	Standard Temperature and Pressure conditions
TCE	Trichloroethylene
TEOS	Tetraethylorthosilicate
TMOS	Tetramethylorthosilicate
W/O	Water in Oil

SYMBOLS

c, C	concentration	[mole/L]
D	diffusion coefficient, or diffusivity	$[cm^2s^{-1}]$
H	hydrolysis degree	
J	permeation flux	$[cm^3(STP)cm^{-2}s^{-1}]$
k	kinetics coefficient	
l, L	thickness of membrane	[cm]
p	pressure	[cmHg]
P	permeability coefficient	[Barrer]
S	solution coefficient or solubility	$[cmHg^{-1}]$

T	temperature	[K]
T_g	glass transition temperature	[˚C]
Tm	melting temperature	[˚C]
x	mole fraction in feed side	
y	mole fraction in permeate side	
z	distance from membrane feed side surface	[cm]

GREEK SYMBOLS

α	actual separation factor or actual selectivity
α*	permselectivity or ideal selectivity
γ	activity coefficient

SUBSCRIPTS

0	at initial state
A, B	components in the binary gas mixture
f	membrane feed side
i	component i
M	inside the membrane
p	membrane permeate side

Chapter 1. Introduction

1.1. Motivation and Objectives

Membrane gas separation has become the topic of intensive research in the last three decades mostly because of many advantages: energy efficient, compact, easily adaptable with other units, and simple in operation alternative to other gas separation methods. The intensive research in this field has lead to a fast growing market in several applications including the production of high purity nitrogen from air, the separation of natural gas, the recovery of hydrogen from gas mixtures, and separation of vapour from other gases. From the year 2000 to year 2020, it is expected that the gas separation membrane market will increase from 150 million dollars per year to 760 million dollars per year (Baker, 2002).

Despite of the fast growing market opportunities, the number of commercial membrane gas separation applications remains relatively low in comparison to the membrane competitors, and high manufacturing cost is the major limiting factor to a wider usage of membranes in the gas separation field. Development of new membrane materials with improved permeability and selectivity as well as good mechanical properties and thermal stability has become a focus to overcome this obstacle. Nanocomposite materials, which incorporate well-dispersed zeolite and molecular sieve particles in a continuous

phase of organic polymers, are considered as a possible solution.

The major challenge in developing nanocomposite membranes is the incorporation of the inorganic phase into the polymer phase, which often leads to the formation of non-selective voids or defects. The improper dispersing of inorganic particles into the polymer membranes can lower the selectivity of the gas separation membranes significantly (Mahajan and Koros, 2000).

There are three major routes by which nanocomposite membranes are synthesized, which include solution blending, in situ polymerization, and the sol-gel method. Recently, an alternative method to the three listed above, referred to as an Emulsion Polymerized Mixed Matrix (EPMM) method, has been used in the system with poly (2,6–dimethyl-1,4-phenyl oxide) as the organic polymer in our laboratory (Sadeghi, 2007; Sadeghi et al., 2007). The uniqueness of the EPMM membranes comes from the fact that they may combine otherwise incompatible inorganic and organic phases. This is achieved by the synthesis of the inorganic nanoparticles from a silica precursor in a stable emulsion, in which an aqueous phase is dispersed in a continuous phase of the polymer solution. More specifically, the silica precursor soluble in the polymer solution polymerizes in contact with the aqueous phase, and consequently the latter acts as finely dispersed micro reactors.

The original objective of this work was optimize the previously developed protocol for the synthesis of 2,6-dimethyl-1,4pheneylene oxide (PPO) – based EPMM membranes,

and to characterize their physical and gas transport properties. Considering the exploratory nature of the previous work by Sadeghi (2007), the major objective of this project was to systematically study the effect of inorganic loading on the properties of EPMM membranes. One of the specific objectives of this work was to implement a comprehensive membrane testing protocol to include steady state and transient experiments with single gases and gas mixtures. Another specific objective of this work was to determine the actual inorganic content in the final EPMM membranes and its chemical nature by implementation of inductively coupled plasma mass spectrometry (ICP-MS) and ^{29}Si nuclear magnetic resonance (^{29}Si NMR) techniques in membrane characterizations. In addition, since the previously synthesized membranes had a lower glass transition temperature (T_g) than the host PPO, which was attributed to the presence of a residual surfactant, 1-octanol, and/or residual unreacted tetraethylorthosilicate (TEOS) in the final membranes, a special focus was given to the investigation of the effect of different post-treatment protocols on the properties of the EPMM membranes, in particular their T_g.

While working towards the original objectives of this project, it became apparent that the emulsion polymerization of TEOS under the settings inherited from the previous work is difficult to control and leads to erratic results. This has led to the second phase of the project, in which the major objective became to ensure the emulsion polymerization of TEOS. This required designing an intermediate experimental protocol, referred to as a

Gravimetric Powder method, which allowed readjustment of the originally used settings for the synthesis of EPMM membranes. One set of new EPMM membranes were synthesized and characterized, and their properties are discussed in this thesis.

1.2. Organization of this thesis

This thesis is divided into six Chapters. In addition to the current Chapter, which provides an overview of this project, there are 5 more Chapters. Chapter 2 provides information on: i) classification of different membrane materials, ii) hybrid membranes including synthesis of nanocomposite membranes and properties of the polymer used in this project, iii) the mechanism and kinetics of polymerization of TEOS in different environments, including in the environment of the aluminum hydroxonitrate aqueous solution, and iv) solution diffusion model and basic terms used for characterization of gas separation membranes. Chapter 3 presents a detailed description of the experimental procedures, including the preparation of casting emulsions, membrane synthesis and membrane characterization.

Chapter 4 presents the results and discussion pertaining to the original objectives of this project. Chapter 5 presents the critical analysis of the original synthesis protocol of EPMM membranes, followed by the concept of a Gravimetric Powder method, which has led to the improved synthesis protocol of EPMM membranes, along with the results of

characterization of new EPMM membranes. Chapter 6 provides the concluding remarks and the recommendations for the future work.

Details on sample calculations, raw and calculated data are presented in the Appendices.

Chapter 2. Literature Review

This project aimed at the development and characterization of a novel method of dispersing inorganic materials into glassy polymer matrices, i.e., at the formation of hybrid membranes. Before discussing the literature pertaining to the development of hybrid membrane materials, a general classification of membrane materials is presented. This is followed by the classification of hybrid materials, with special attention given to the emulsion polymerized mixed matrix (EPMM) membranes. The chemistry of inorganic polymerization, with a special focus on the polymerization of tetraethylorthosilicate (TEOS) in the presence of the aluminum complex, Al_{13}^{7+}, which is the key aspect of this project, is then discussed. Finally, the concepts related to the characterization of gas transport properties of membranes, including the basic membrane terminology is presented.

2.1. Classification of membrane materials

A membrane can be defined as a selective barrier between two phases that restricts the transport of various chemical species (Porter, 1990). The feed to the membrane is separated into two streams: the retentate and the permeate. Either the retentate or permeate could be the product stream. In principle, all materials that form sufficiently thin and

stable films can be used as membranes. This includes metals, glasses, ceramics and polymers as well as liquids. As a result, a membrane can be homogenous or heterogeneous, symmetric or asymmetric, charged or uncharged, dense or porous, and solid or liquid. Membranes are normally classified according to their pore size, the material they are made of, and their morphology.

Membranes can be classified according to their pore size. Membranes with pore sizes larger than 10 μm are considered as filters. Microfiltration membranes have pore sizes in the range of 0.1 – 10 μm and are capable of removing suspended and colloidal particles like blood cell, bacteria, and latex emulsions. Ultrafiltration membranes have pore size in the range of 2 – 100 nm and can remove dissolved molecules such as proteins like albumin or pepsin. Reverse osmosis membranes have pore size less than 10 Å and are capable of separating of very small species, as small as monovalent ions, such as Na^+ and Cl^- from solutions. The membranes capable of separation of divalent salts, sugar and dissociated acids are often referred to as "loose reverse osmosis" or nanofiltration membranes. Separation of gases requires membranes with pore size less than 5 Å. On the other hand, gases are primarily separated using so-called nonporous membranes (Shekhawat et al., 2003).

Membranes can be also classified according to the materials they are made of as natural or synthetic. Synthetic membranes can be further subdivided into organic, inorganic, hybrid and liquid membranes. Organic membranes include polymers, whereas

examples of inorganic membranes are ceramic, carbon and metal membranes. Hybrid membranes on the other hand, are a combination of organic and inorganic materials, while the liquid membranes can be either organic or inorganic. Liquids with an appropriate carrier are used for facilitated transport and they are held within the pores of organic or inorganic membranes (Mulder, 1996).

Polymeric membranes are categorized into two distinct groups: glassy membranes and rubbery membranes. The glass transition temperature is lower than the ambient temperature for the rubbery membranes and higher than the ambient temperature for the glassy membranes. When it comes to the permeation and separation of gases, the two categories behave differently. Glassy membranes are selective to smaller molecular size gas molecules whereas rubbery membranes are often selective for the more condensable gases of larger molecular size. Polymeric membranes could be either symmetric, where the properties of the membrane do not change throughout the cross section of the membrane or asymmetric, where the membrane is composed of a thin selective layer on the top of a non-selective porous support layer, which provides the mechanical strength for the membrane (Kesting, 1985). The asymmetric membranes in which the selective and porous layers are from the same polymer are referred to as integrally-skinned while those in which the selective layer is made from a different material than the porous sub layer are referred to as composite membranes.

Polymeric membranes are in general preferred under mild temperatures (20-100^{o}C). They are favoured in large scale operations. Organic polymers can form both porous and nonporous membranes. The former ones contain fixed pores the dimensions of which determine the selectivity of the membrane, and they are typically used for liquid separations. The nonporous membranes on the other hand are used in gas separation and pervaporation (Koros and Pinnau, 1993). The permeability and the selectivity of these membranes are determined by the intrinsic properties of the material.

Inorganic membranes include ceramic, carbon and metal membranes. Ceramic membranes are characterized by being more fragile and more expensive compared to polymer membranes. However, these materials are also characterized by their ability to withstand harsher chemical environments and higher temperatures and can be cleaned on site. Inorganic membranes include also carbon membranes, which are intermediate between polymeric membrane and ceramics membrane. Carbon membranes originate from thermosetting organic polymers that undergo the process of carbonization, which leads to the structure and properties similar to those of ceramic membranes. Inorganic membranes are normally considered as porous membranes, with the exception of metal membranes. The best example of the metal membranes is the palladium membrane, which is used for separation of hydrogen from gas mixtures (Smith and Collins, 1992; Hamilton, 1995).

Hybrid membranes on the other hand, are synthesized from organic and inorganic materials. Principally, there are two ways to synthesis the hybrid membranes, either by

dispersing inorganic nano-particles in a continuous polymer phase (solution blending), or by in situ polymerization within the pores of a porous inorganic structure (Julbe, 2007). The rationale behind hybrid membranes is to overcome the disadvantages of organic and inorganic membranes while synergistically combining the selectivity of inorganic materials and processability of organic polymers. Hybrid membranes have attracted a lot of research interests in the last decade, in particular in the area of membrane gas separation.

2.2. Hybrid Membranes

The term hybrid material is defined as "a material that includes two moieties blended on the molecular scale" (Kickelbick, 2007). One of the two compounds is usually an organic material and the other one an inorganic material. In addition, there must be certain interactions between the molecules of the two compounds. When the structural unit of one of the components is in size range of 1-100 nm, the material may also be referred to as a nanocomposite material.

The term “hybrid materials” is often interchangeably used with the term mixed matrix materials. On the other hand, the latter is more specifically used when zeolite or molecular sieve materials are dispersed in a polymer matrix. The effect of loading of the dispersed phase on the properties of the mixed matrix material is presented in Fig. 2.1. When loading of inorganic phase, for example a zeolite, is low (Fig. 2.1a), the zeolite acts as filler

forming small islands in the continuous polymer phase, and the amorphous portion of the polymer material increases. The diffusivity of gas molecules in such a hybrid material will increase according to the Maxwell-Wagner-Sillar model (Bouma et al., 1997).

With an increase of the zeolite loading, the zeolite islands may connect to each other forming continuous channels. The loading at which this occurs is referred as percolation threshold. If the effective pore size of these continuous channels is relatively large, the gas permeability of the resulting material may increase significantly. At this point the permeability may be entirely controlled by the inorganic phase of the hybrid material. The overall permeability of the mixed-matrix material with continuous channels formed by the connected inorganic particles follows the Maxwell's equation (Baker, 2004).

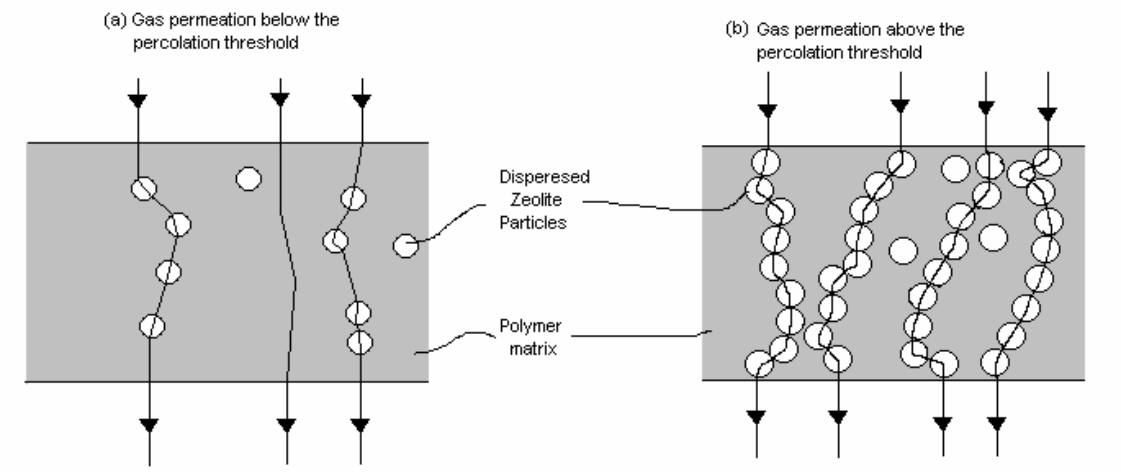

Figure 2.1 Gas permeation through mixed matrix membranes with a) low, and b) higher loading of zeolite dispersed

2.2.1. Synthesis of hybrid materials

There are several methods to disperse inorganic components into the continuous polymer phase. These include: the solution blending method, the in Situ polymerization method and the sol-gel method (Kickelbick, 2007).

In the solution blending method the inorganic nanoparticles are mixed with the organic phases at the level of polymer solution. The actual mixed matrix membrane is then made by evaporation of solvent. Due to its simplicity with no chemical reaction involved in the process, the solution blending method can be used for almost all kinds of inorganic nanoparticles. Moreover, this method allows for an easy control of the concentrations of the polymer and inorganic components in the final material. On the other hand, while the inorganic phase does not need to be soluble in the polymer solution, it should have sufficiently strong interactions with the solvent dissolving the polymer. A lack of such strong interactions makes difficult to achieve good physical dispersion of the inorganic particles at the first stage, i.e., at the level of the polymer solution. Even, when inorganic particles are well dispersed in the polymer solution, upon evaporation of the solvent, they may aggregate, in case of which the final membranes lacks the physical strength and is often defective, which renders it not suitable for any separations (Sharp, 1998).

In case of the in Situ method, nanoparticles containing functional groups such as hydroxyl and carboxyl groups are dispersed in a solution containing organic monomers and the resulting dispersion is coated on a support. The polymerization of the organic monomer

is initiated by high energy radiation, plasma or other means which allow generation of radicals or ions from the function groups of nanoparticles (Laine, 2005). The in Situ method leads to hybrid materials in which polymeric chains are strongly connected to inorganic phase. This allows preventing gaps, which act as defects at the interphase between the organic and inorganic phases. On the other hand, since the dispersion is coated on the support and the reaction is initiated by a high energy source, the thickness of the final membrane is hard to control. Moreover, apart from polymerization of the organic monomer on the surface of functionalized nanoparticles, the nanoparticles may also form aggregates held together by the covalent bonds. Aggregation of nanoparticles, regardless of the synthesis method used has always adverse effects on the properties of the final membrane.

The sol-gel method is the most widely used method to form hybrid membranes. The sol-gel method requires a solvent that can dissolve both the organic polymer and the reaction medium. The polymer is first added into the solvent to form a solution. Then the sol-gel reaction medium, usually an inorganic alkoxide along with an acid or base acting as a catalyst, is added to the polymer solution. The gelation reaction occurs at the functional or chemically modified polymer chain ends, (Brinker & Scherer, 1990). By the sol-gel method, the concentrations of the organic and inorganic components are easy to control and these components are bonded together at a molecular or even at a nanometer level in the membranes. However, finding a solvent that can meet the miscibility requirement of the

sol-gel medium and the organic polymer is not easy. Moreover, the size of the synthesized inorganic particles is not easy to control.

The application of the sol-gel method is not limited to the synthesis of hybrid membranes. The sol-gel method also plays an important role in synthesis supported of dense ceramic layers, surface modification of ceramic membranes and the synthesis of zeolite materials.

2.2.2. Emulsion polymerized mixed matrix membranes

All three methods of synthesis of hybrid membranes discussed above require a solvent, which is compatible with both the organic phase or its precursor and the inorganic phase or its precursor. In case of the in Situ and the sol-gel methods, the respective chemical reactions occur in single phase solutions. However, most organic polymers and their precursors are not miscible in water while most of the inorganic precursors are not soluble in liquids that are suitable as organic polymer solvents. As a result, it is necessary to use a homogenizer that is miscible with the organic solvent, which at the same time can dissolve the inorganic precursor. Finding such a homogenizer is the largest obstacle preventing the in Situ method and sol-gel methods to be applicable for the synthesis of hybrid materials from a large number of combinations of organic polymers and inorganic initiators.

To overcome this obstacle, Sadeghi et al. (2007) has developed a new method, referred to as the Emulsion Polymerized Mixed Matrix (EPMM) method. This method, discussed

next, represents an extension of the in Situ and sol-gel methods.

An emulsion is a heterogeneous system consisting of at least one immiscible liquid dispersed in another in form of droplets (Becher, 1965). In the EPMM method, instead of using a solvent that dissolves both the organic and inorganic reactants, the reaction takes place in an emulsion consisting of two phases. Using a source of energy, such as microwave, plasma, laser, ultra-sound or stirring, one phase, normally the aqueous phase containing the inorganic precursor, is broken into small droplets. Each droplet then acts as a micro reactor and the reaction occurs at the interphase. Despite a generally much smaller reaction rate constant for the reactions in an emulsion compared to a solution reaction, decreasing the size of the dispersed phase and thus increasing its surface area is thought to result is a sufficient conversion of an inorganic precursor into the inorganic nanoparticles (Sadeghi, 2007).

The EPMM method therefore, avoids the strict requirement of finding the general solvent and thus can be applied to more combinations of organic / inorganic systems. The biggest obstacle of the EPMM method is the aggregation of aqueous phase droplets, which can significantly slow down the reaction by reducing the total surface area. On the other hand, sonication and alcoholic solvents can enhance the stability of the emulsion while at the same time promoting the hydrolysis of alkoxides (Vollet et al., 1996).

2.2.3. Organic / inorganic system

As already stated, the EPMM method allows synthesis of hybrid materials from a much wider pool of combinations of organic polymer / inorganic precursor systems. The system of poly (2,6-dimethyl-1,4-phenylene oxide) (PPO) and tetraethylorthosilicate (TEOS) is an example of a combination, for which the sol-gel method is not applicable. This is because PPO is a hydrophobic polymer and solvents that can dissolve it, are not miscible with water, which on the other hand is required for the hydrolysis of TEOS. The following, provides a brief description of the properties of PPO and TEOS.

Poly (2,6-dimethyl-1,4-phenylene oxide)

Poly(2,6-dimethyl-1,4-phenylene oxide), which is the best known representative of the family of polyphenyelene oxides, shows one of the highest permeability to gases among glassy polymers, which is attributed to absence of polar groups in the polymer backbone. The chemical structure of the repeatable unit of PPO is shown in Fig. 2.2. It has a linear structure. The presence of the 2,6-disubstituted phenyl group and two methyl groups in its backbone makes any rotation of the polymer chains around their axes difficult, which leads to a high glass transition temperature (T_g) of PPO. The presence of ether linkage in PPO backbone ensures its chemical and thermal stability and its good mechanical properties.

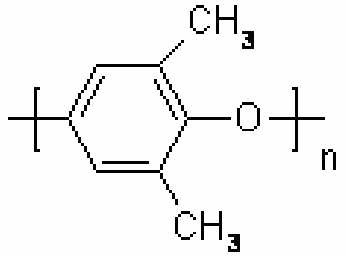

Figure 2.2 Repeatable unit of poly (2,6-dimethyl-1,4-phenylene ether)

PPO is synthesized by oxidation of 2,6-dimethylphenol catalyzed by a copper salt (Hay et al., 1959). The resulting polymer is soluble in toluene, benzene and halogenated hydrocarbons; it also shows a partial solubility in aliphatic hydrocarbons, acetone, alcohols, and tetrahydrofuran (Krause et al., 1978). Solubility of PPO in these solvents and viscosity of the resulting solutions strongly depend on the molecular weight of the polymer. The T_g of PPO also depends on its molecular weight, with values ranging from 206°C (Wrasidlo, 1972) to 225°C (Karasz et al., 1965) when the molecular weight increases from 26 000 to 400 000. As a thermoset, PPO does not melt; it decomposes between 456°C (Karasz & Reilly, 1965) and 464°C (Tran, 2004).

PPO can be easily modified by various electrophilic substitutions including bromination, carboxylation and methyl esterified carboxylation, sulfonylation and acylation, sulfonation and by introduction of trialkyl-silyl, hydroxyethylene and ethyleneoxytrialkyl-silyl groups in the polymer backbone (Kruczek & Matsuura, 1998). A series of novel PPO-based materials have been developed in recent years. The C_{60} modified PPO membrane shows an enhanced permeability for O_2 and CO_2 when C_{60} is

bonded to PPO (Kruse et al., 2007). PPO is also compatible with carbon nanotubes (Liu et al., 2008).

Tetraethylorthosilicate

Alkoxide precursors in form of $M(OR)_n$ including silicone alkoxides, $Si(OR)_4$, and metal alkoxides such as $Zr(OR)_4$, $Al(OR)_3$, $Ti(OR)_4$, and $Sn(OR)_4$, where -OR is the alkoxide group, are commonly used as the starting materials of the inorganic network in the sol-gel process (Bradly et al., 1978). The existence of the M-OR structure enables these compounds to undergo hydrolysis and polycondensation in the presence of water to form the interconnected M-O-M bonds in colloidal particles. These colloidal particles connect to each other to form a gel with a 3-dimentional network (Hench & West, 1990).

Metal alkoxides are very sensitive to moisture that their hydrolysis and polycondensation process are difficult to control. Among metal aloxides, silicon alkoxides have gained the most research interests as inorganic precursors (Xu, 2009). Tetraethylorthosilicate (TEOS) and tetramethylorthosilicate (TMOS) are the most widely used silicon alkoxides precursors for dispersion into organic phase. It is reported by Eliseev et al. (1999) that the presence of the aluminium hydroxonitrate in the aqueous solution enhances the polymerization rate of TEOS and the formation of Al-O-Si bonds. This idea was utilized by Sadeghi (2007) for the formation EPMM membrane based on PPO / TEOS system.

2.3. Chemistry

After a general introduction to the concept of the EPMM method in the preceding sections, the chemistry of the hydrolysis and poly-condensation of TEOS in the presence the aluminium hydroxonitrate is presented next.

2.3.1. Keggin structure

Dissolving aluminium hydroxonitrate in water may lead to different Al-complexes depending on the pH of the aqueous solution. By itself, the aluminum hydroxonitrate is a weak acid and its aqueous solution has a pH of 3.6. When the pH is below 3, the Al^{3+} ion coordinates with 6 water molecules to form: $[Al(OH_2)_6]^{3+}$ (Akitt & Farthing, 1981). As the pH increases beyond 3, $[Al(OH_2)_6]^{3+}$ undergoes the following hydrolysis:

$$[Al(OH_2)_6]^{3+} + hH_2O \rightarrow [Al(OH)_h(OH_2)_{6-h}]^{(3-h)+} + hH_3O^+ \qquad (2.1)$$

where *h* is the molar ratio of the hydrolysis, which is the ratio of the concentration of hydroxyl groups and the concentration of $[Al(OH_2)_6]^{3+}$ groups. Using different base concentrations, different hydrolysis products have been reported with different *h* values (Bottero et al., 1980). For example, at high base concentration, a large poly-nuclear complex is produced: $\{AlO_4[Al(OH)_2(H_2O)]_{12}\}^{7+}$. This Al-complex is said to have a Keggin structure (Furrer et al., 1992), which is presented in Fig. 2.3.

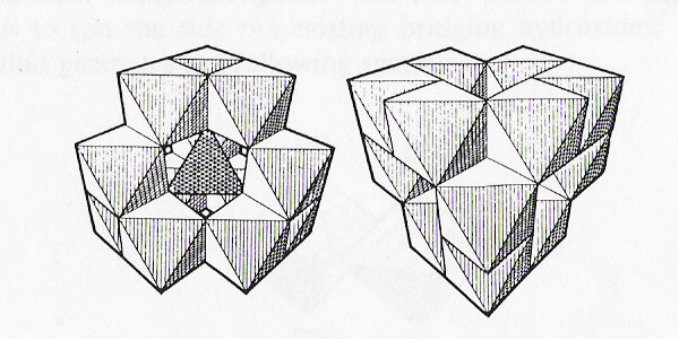

Figure 2.3 Al-complex: $\{AlO_4[Al(OH)_2(H_2O)]_{12}\}^{7+}$ having Keggin structure (Brinker and Scherer, 1990).

As shown in Figure 2.3, a tetrahedral $AlO_{4/4}^{+}$ center is surrounded by 12 $[AlO_{1/4}(OH)_{4/2}(H_2O)]^{0.5+}$ units. Thus, $\{AlO_4[Al(OH)_2(H_2O)]_{12}\}^{7+}$ is a polyprotic acid with 12 identical functional groups and a symmetrical structure. For the sake of brevity the Al-complex in the Keggin structure is abbreviated as Al_{13}^{7+}. According to ^{27}Al NMR, there are two types of Al bonds in Al_{13}^{7+}: Al IV and Al VI. At ambient temperature and the *h* value of 2.5, Al_{13}^{7+} has a half-life of 2 years. The decomposition of Al_{13}^{7+} is accelerated by higher temperatures and higher pH values.

2.3.2. Polymerization of Tetraethylorthosilicate (TEOS) in water

During the hydrolysis of TEOS in water the oxygen atom contained in water molecule attacks the silicon atom and the alkoxide group [-OEt] is replaced by hydroxyl group, as shown by the following reaction

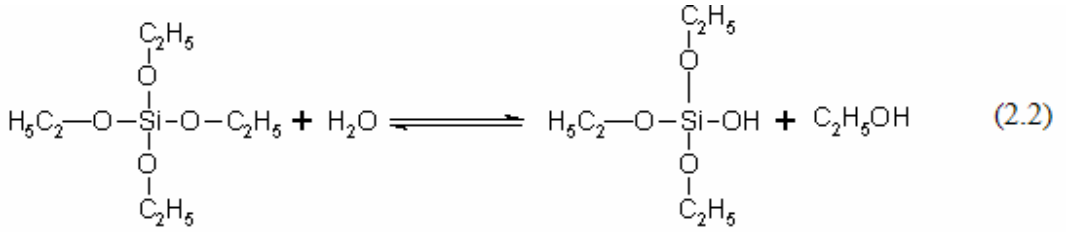

(2.2)

Since TEOS contains more than one [-OEt] group, the TEOS molecules can be hydrolyzed more than once, therefore in general the hydrolysis of TEOS is represented by the scheme (2.3)

$$Si(OEt)_4 + nH_2O \rightarrow Si(OEt)_{4-n}(OH)_n + nEtOH \qquad (2.3)$$

where *n* is the number equal to or less than 4.

The completely or partly hydrolyzed TEOS may then undergo a polycondensation reaction, leading to water molecule as a by-product (water condensation) or ethanol molecule as a by-product (ethanol condensation). Both the water and ethanol condensation reactions lead to siloxane bonds (Si-O-Si). These two condensation reaction are shown schematically below.

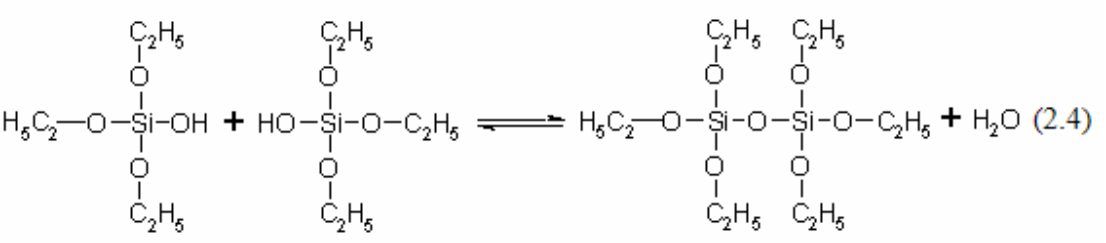

(2.4)

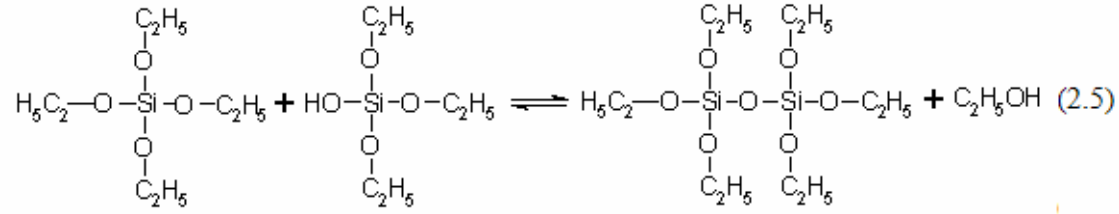

(2.5)

It is important to note that the hydrolysis of TEOS may be accelerated by the addition of homogenizing agents such as alcohols and acetone. On the other hand, adding water and ethanol shifts the equilibrium of the water and alcohol condensation reactions to the left. Therefore, these additives have a dual, opposite effect on the polymerization of TEOS in water. In addition, the product of the poly-condensation of TEOS may still contain [-OEt] groups, which means that it can be further hydrolyzed and poly-condensed with other molecules containing [Si-OH] groups to form a more complex 3-D networks (Brinker & Scherer, 1990).

Under most conditions, the hydrolysis reaction is considered to be the rate controlling step in the whole process. The reaction rate of hydrolysis can be enhanced by employing acid or base catalysts. The reaction rate is also influenced by the concentration and the strength of the catalyst.

2.3.3. Acid-catalyzed polymerization of TEOS

Under acidic conditions, the [-OEt] groups of TEOS might be protonated. The silicon atom, which is electrophilic, is then attacked by the water molecules. The bond between the positively charged [-OEt] group and silicon is then broken and [-OEt] group is reduced and converted to the ethanol molecule, which is a by-product of the acid catalyzed hydrolysis of TEOS. The acid-catalyzed hydrolysis of TEOS is shown in the

reaction scheme (2.6):

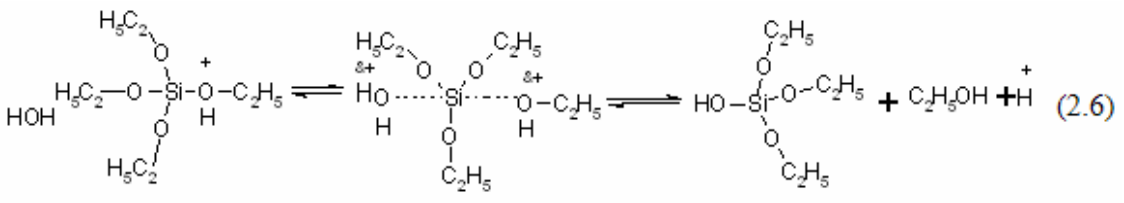

(2.6)

The acid-catalyzed condensation occurs between the protonated silanol atom and the hydrolysis product. The positively charged silanol is more susceptible to nucleophilic attack. Although the poly-condensation step is accelerated by the acidic catalyst, when the water/TEOS ratio is smaller than 4, the hydrolysis process is still the rate controlling step in the polymerization process (Hui et al., 1989). The details of the acid-catalyzed condensation of TEOS is presented in the reaction scheme (2.7):

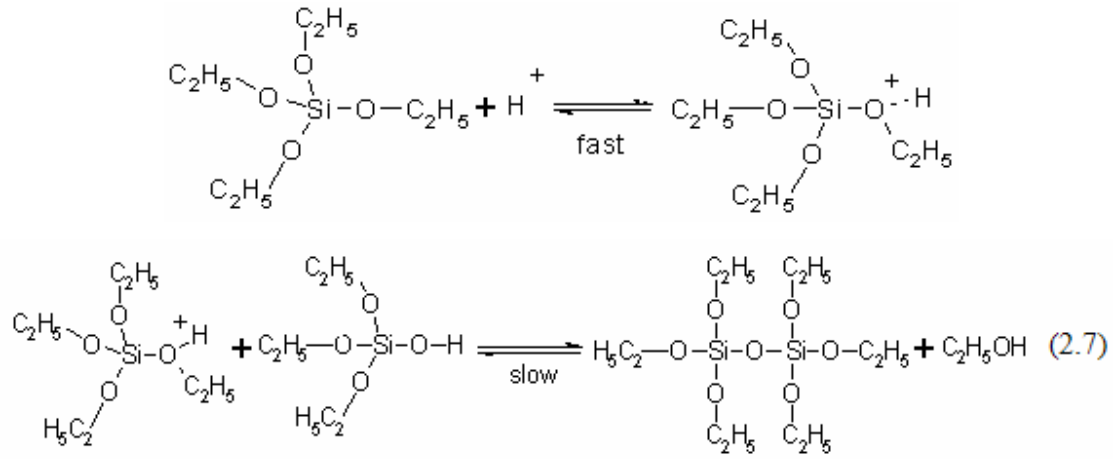

(2.7)

2.3.4. Base-catalyzed polymerization of TEOS

Under basic conditions, water molecules dissociate to produce nucleophilic hydroxyl

ions and these hydroxyl ions attack silicon atom in TEOS. The base-catalyzed hydrolysis of TEOS is shown in by the reaction scheme (2.8):

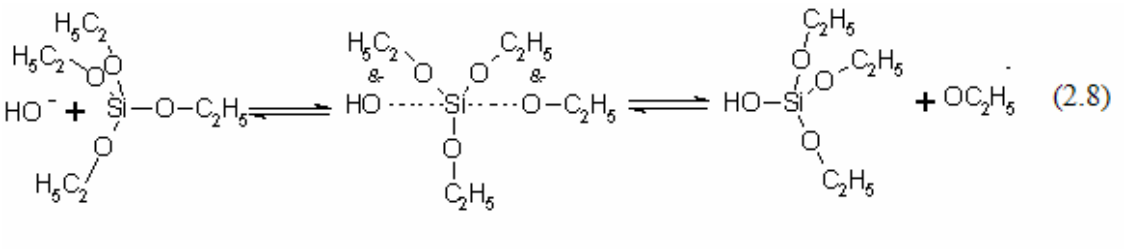

(2.8)

The hydroxyl ions also attack the product of the hydrolysis process and deprotonate the silanol group. This reaction is very fast. The neutral silicon atoms are then attacked by the deprotonated silanol groups which results in the formation of the Si-O-Si bonds. The latter reaction is slow. The two reactions are shown in the reactions schemes (2.9) and (2.10):

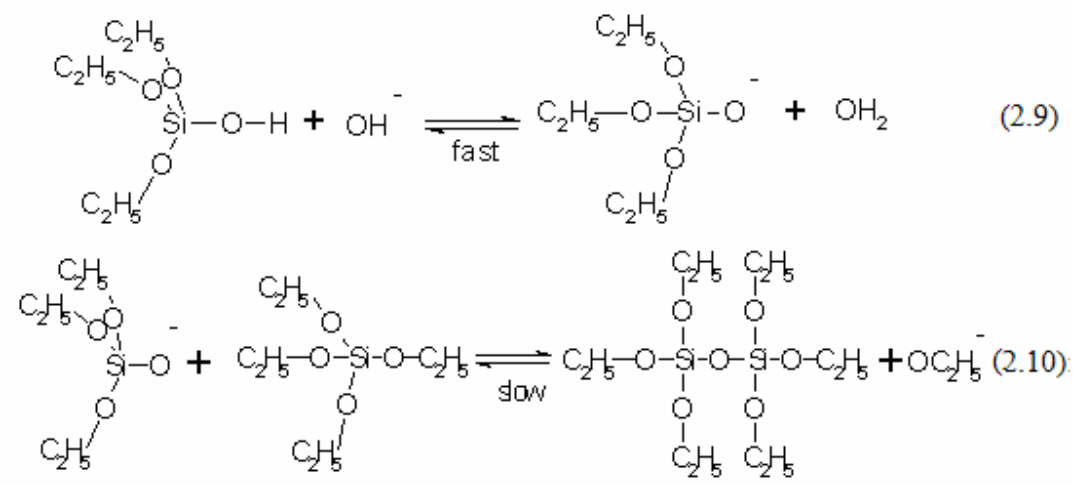

(2.9)

(2.10)

In base-catalyzed polymerization of TEOS, the hydrolysis step is still the rate controlling step.

2.3.5. Co-polymerization of aluminium hydroxonitrate and TEOS

The polymerization of TEOS in the presence of aluminium hydroxonitrate aqueous solution was investigated by Eliseev et al. (1999). When the aluminium hydroxonitrate dissolves in water it forms a Keggin structure, shown in Fig. 2.3. The [OH] groups contained in the Keggin structure have a lower partial charge than the free water molecules. As a result, under the acidic conditions, these aluminum coordinated [OH] groups are more likely to attack TEOS molecules than the free water molecules (Eliseev et al., 1999). The overall reaction between the aluminum hydroxonitrate forming the Keggin structure and TEOS is shown by following the reaction scheme:

$$Si(OEt)_4 + \left[Al(OH)_x(H_2O)_y\right]^{m+} \rightarrow EtO-\left[Si(OEt)_2\right]-O-\left[Al(OH)_{x-1}(H_2O)_y\right]^{m+} + EtOH \quad (2.11)$$

It is reported that for a high degree of hydrolysis of aluminum hydroxonitrate (h > 1.9), the hydrolysis of TEOS occurs rapidly and the resulting gel is not transparent. When the degree of hydrolysis of aluminium hydroxonitrate is less than 1.9, the hydrolysis of TEOS takes a much longer time, and the resulting gels are pellucid. Therefore, the reaction between aluminum hydroxonitrate and TEOS is accelerated by the presence of high degree of hydrolysis of aluminum hydroxonitrate, which in turn depends on the actual pH of the solution. The ^{27}Al NMR of gels obtained at different pH values of the aqueous solutions confirms that the presence of the aluminum in the Keggin structure complex accelerates the polymerization of TEOS.

2.3.6. Kinetics of TEOS polymerization

From the above discussion on the mechanism of polymerization of TEOS in different environments, one can conclude that regardless of the environment and the actual mechanism the rate controlling step is the hydrolysis of TEOS. In this section, the actual rate equations for the polymerization of TEOS in different environments are presented.

Kinetics of acid-catalyzed TEOS polymerization

The kinetics of the acid-catalyzed polymerization of TEOS was studied by Sanchez et al., (1992). Since the hydrolysis is the rate control step, by assuming an irreversible polycondensation reaction, the consumption rate of TEOS was found to have a first-order dependence on the concentration of TEOS, water, and H^+ anion, which is mathematically expressed by the following equation:

$$-\frac{d[TEOS]}{dt} = k[TEOS][H^+][H_2O] \qquad (2.12)$$

Since in the polymerization process water is in large excess and the concentration of water can be considered as constant, Eq. (2.12) simplifies to:

$$-\frac{d[TEOS]}{dt} = k[TEOS][H^+] \qquad (2.13)$$

where *k* is the rate constant, which dependents on the reaction temperature and the concentration of a homogenizer agent (alcohol). Therefore, on the one hand, alcohol can improve the reaction by decreasing the activation energy, but on the other hand, large amounts of alcohol in the system will decrease the concentration of TEOS leading to a

negative effect on the reaction rate (Brinker and Scherer, 1990).

Kinetics of base catalyzed TEOS polymerization

Similarly to the acid-catalyzed polymerization of TEOS, since in the base-catalyzed polymerization, the rate controlling step is the hydrolysis of TEOS, the reaction rate of TEOS was found to have a first-order dependence on the concentration of TEOS, water, and OH^- ion. When the water/TEOS ratio is greater than 4, the kinetics expression very similar to the one for the acidic-catalyzed reaction can be obtained (Chang & Fogler, 1996):

$$-\frac{d[TEOS]}{dt} = k[TEOS][OH^-] \qquad (2.14)$$

where *k* is the rate constant, which dependents on the reaction temperature and the strength of the base catalyst. When ammonia is employed as the catalyst and for low water/TEOS ratios, counting in the ionization reaction of ammonia with water, the concentration of water cannot be ignored, and the expression becomes (Harris et al., 1990):

$$-\frac{d[TEOS]}{dt} = k[TEOS][NH_3]^{0.5}[H_2O]^{1.5} \qquad (2.15)$$

Kinetics of TEOS polymerization in presence of aluminium hydroxonitrate

Eliseev et al. (1999), who studied the kinetics of polymerization of TEOS in the presence of aluminum hydroxonitrate, reported that this reaction is of the first order with

respect to the concentration of the aluminum complex. At the same time, since aqueous solution of the aluminum hydroxonitrate has a pH of 3.6 and thus may be considered as a weak acid, the acid-catalyzed hydrolysis of TEOS should also be considered at the same time. Moreover, considering that the concentration of water is much greater than that of the aluminum complex in the aqueous solution, although the concentration of the protons in the solution is low, the acid catalyzed hydrolysis may be competitive to the co-polymerization of the hydrolyzed TEOS and aluminum complex.

In the preceding discussion on the kinetics of the polymerization of TEOS, it was assumed that the reaction occur in a single phase. In case of the synthesis of EPMM membranes, thy hydrolysis and polycondensation of TEOS occurs in an emulsion at the interphase of the dispersed aqueous phase. As a result, the rate constant is expected to be significantly lower than that corresponding to the reaction in the single phase. On the other hand, the energy input into the system, by for example, ultrasonication of the emulsion may significantly increase the rate constant. This is because ultrasonication of the emulsion maximizes the surface area of the interphase, and at the same time, a part of the ultrasonication energy is converted into a thermal energy, which increases the temperature of the emulsion thereby increasing the rate constant of the polymerization reaction. It is also reported that the addition of ethanol to the emulsion can shorten the start-up time of the hydrolysis, but at the same time decreases the reaction rate because of the dilution of TEOS with ethanol (Vollet et al., 1996).

2.4. Solution-diffusion model

The solution-diffusion model is a phenomenological model describing the transport of fluids, including gases, in nonporous membranes. In this model, the transport of a given penetrant occurs in three sequential steps. In the first step, the penetrant is adsorbed on the membrane surface at the high chemical potential side of the membrane, which is followed by its diffusion across the membrane, and desorption at the low chemical potential side of the membrane. It is normally assumed that the adsorption and desorption steps occur instantaneously and the transport process is governed by the diffusion of the penetrant across the membrane. In is important to emphasize that the solution-diffusion is not concerned with the actual mechanism of the diffusion of the penetrant inside the membrane. As are result, it can also be used for the characterization of the transport of fluids in porous membranes. The only requirement is that thermodynamically the penetrant in the fluid phase is different than the penetrant in the membranes phase, and there is an equilibrium correlation, for example Henry's law, relating the penetrant in these two different phases.

The gas transport across the membrane in the solution-diffusion model is characterized by the permeability coefficient (P). In practice, the permeability coefficient is evaluated from the steady state gas permeation rate (Q) through a homogeneous membrane of known thickness (l) and permeation area (A) at the conditions of known partial pressure gradient ($p_f - p_p$) across the membrane:

$$P = \frac{Ql}{A\left(p_f - p_p\right)} \tag{2.16}$$

where p is the partial pressure of the permeating gas, and subscripts f and p refer to the feed (high pressure) side and the permeate (low pressure) side of the membrane, respectively. The permeability coefficient is a product of two other fundamental transport parameters, the solubility coefficient (S) and the diffusivity coefficient (D):

$$P = SD \tag{2.17}$$

The common unit of the permeability coefficient is Barrer:

$$1\,\text{Barrer} = 10^{-10}\,\text{cm}^3\,(\text{STP}) \cdot \text{cm}/\left(\text{s} \cdot \text{cm}^2 \cdot \text{cmHg}\right) \tag{2.18}$$

The permeability, diffusivity and solubility coefficients in the solution diffusion model are considered to be the properties of the membrane material.

In the solution-diffusion model, the selective potential of the membrane material for a given pair of gases A and B is assessed on the basis of their permeability ratio ($\alpha^*_{A/B}$):

$$\alpha^*_{A/B} = P_A / P_B \tag{2.19}$$

The permeability ratio determined from the respective single gas permeation tests is often referred to as ideal selectivity. In contrast, the permeability ratio determined from a mixed gas permeation test is referred to as permselectivity. If S and D are independent of the gas concentration in membrane, the ideal selectivity and permselectivity should be the same (Zolandz and Fleming, 1992). On the other hand, in case of glassy polymers such as PPO, the transport rate of a penetrant is depressed by the presence of an additional penetrant. This flux depression, which lowers permselectivity compared to the ideal selectivity, is due

to the competitive sorption of penetrants in Langmuir sorption sites, which exist in glassy polymers (Sanders and Koros, 1986).

Since the permeability coefficient is the product of *S* and *D*, the permeability ratio can be seen as a product of the solubility selectivity (α_S) and diffusivity selectivity (α_D):

$$\alpha^*_{A/B} = \alpha_S \times \alpha_D = \frac{S_A}{S_B} \times \frac{D_A}{D_B} \tag{2.20}$$

Carrying out a membrane gas separation test involving a gas mixture of *A* and *B* allows the determination of the membrane separation factor, $\alpha_{A/B}$, which is determined based on the composition of feed and permeate:

$$\alpha_{A/B} = \frac{y_A / x_A}{y_B / x_B} \tag{2.21}$$

where *x*, *y* represent the mole fractions in feed and permeate, respectively. It is important to emphasize that Eq.(2.21) is applicable for the tests performed as zero stage cut, that is when the permeate flow rate is negligible compared to the feed flow rate, which is typically the case when testing new materials in the form of small area membranes.

The permselectivity is related to the separation factor through the following equation (Zolandz and Fleming, 1992):

$$\alpha^*_{A/B} = \alpha_{A/B}\left(\frac{x_A(\alpha_{A/B}-1)+1-r}{x_A(\alpha_{A/B}-1)+1-r\alpha_{A/B}}\right) \tag{2.22}$$

where *r* is the ratio of the permeate pressure to the feed pressure. It is evident from Eq.(2.22) that as *r* approaches to zero, the separation factor approaches to the permselectivity. For *r*

to approach to zero, it is necessary to hold a very high feed pressure and/or a permeate pressure approaching zero. The latter is more realistic in practice, by maintaining the permeate side of the membrane under vacuum. For $r > 0$, the permselectivity is greater than the separation factor as seen in Eq.(2.22).

Chapter 3.
Methodology and Experimental Design

In this Chapter, the experimental methods, instruments, and the materials used in this work for synthesizing the EPMM membranes and characterization of their gas transport and other physical properties are presented.

3.1. Membrane synthesis

This section describes the synthesis process of the EPMM membranes, which includes three major steps: preparation casting emulsion, membrane casting using a spin coating machine, and the post-treatment process of the membrane films.

3.1.1. Preparation of casting emulsion

The preparation of casting emulsion involves two major steps, which are shown schematically in Fig. 3.1. In the first step, an aqueous solution containing the aluminum complex is dispersed in a polymer solution containing a surfactant and the resulting emulsion is referred to as a primary emulsion. In the second step, the inorganic precursor

(tetraethylorthosilicate – TEOS), which is soluble in the organic phase (trichloroethylene – TCE) of the primary emulsion, is added under vigorous stirring provided by an ultrasonic dismembrator (Fisher Scientific Model 550 ultrasonic dismembrator). The inorganic precursor upon contacting with the inorganic phase is believed to polymerize, and this creates a concentration gradient of TEOS within a continuous organic phases. As the polymerization of the inorganic precursor continues, the primary emulsion is converted into a secondary emulsion containing well-dispersed inorganic nanoparticles.

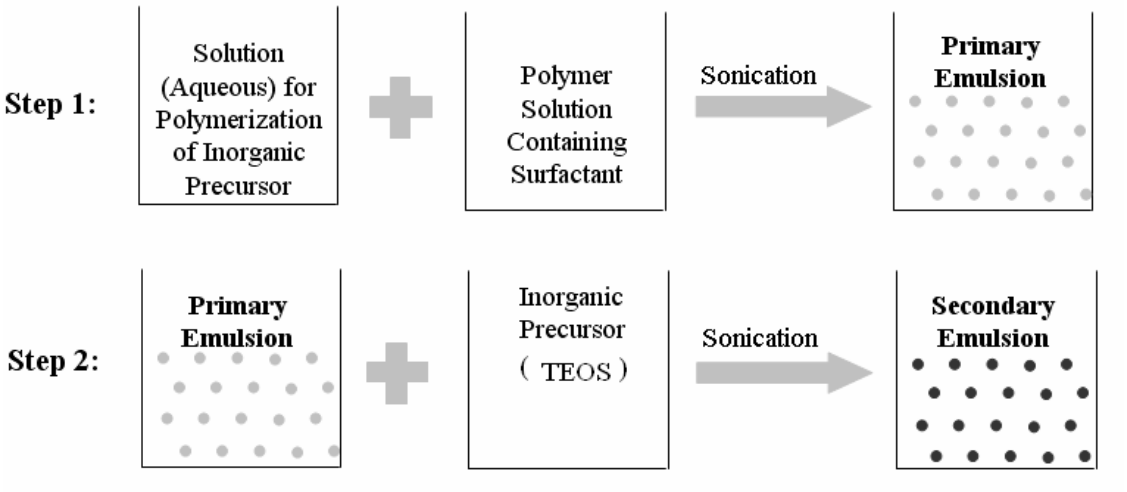

Figure 3.1 The schematic diagram of the steps in preparation of casting emulsion.

3.1.1.1. Preparation of the aqueous solution

The aqueous solution was prepared by dissolving 10.50 g of aluminium hydroxonitrate powder into 15.0 mL of the distilled deionized water. Then 3.00 g of sodium carbonate powder was dissolved in 13.0 mL of the distilled-deionized water to

form the sodium carbonate solution. The sodium carbonate solution was added into the aluminium hydroxonitrate solution while stirring the content using a magnetic stirring bar. Right after the addition of the carbonate solution a precipitate was formed, which however was quickly re-dissolved. The resulting aqueous solution was stirred continuously for 48 hours at room temperature in order to achieve a hydrolytic equilibrium (Swaddle et al., 1994). The concentration of aluminium in the aqueous solution was 1 mole/L. The successfully prepared aqueous solution had no color, and its pH value ranged from 3.6 to 3.8.

To ensure a sufficient degree of hydrolysis of the aluminium hydroxonitrate in the aqueous solution and the desired tetrahedral form of the aluminium complex, a gelation test using the aqueous solution was performed. In the gelation test the aqueous solution was mixed with the solution of TEOS in ethanol and the polymerization of TEOS proceeded in a single aqueous phase. The volumetric proportions of TEOS, ethanol and the aqueous solution were, 1:3:1. Typically, 2 mL of TEOS, 6 mL of 95% ethanol, and 2 mL of aqueous solution were mixed in a 20 mL vial. The ethanol served as a common solvent of the aqueous solution and the TEOS. According to Eliseev et al. (1999), the polymerization of TEOS will proceed only in presence of an aluminum complex in the Keggin structure, and will result in a white gel appearing after in 6 to 8 minutes. Consequently, a successful gelation test serves as an indication of the required Al complex in the Kegging structure, which is the necessary condition for the

polymerization reaction to occur in the actual W/O emulsion.

3.1.1.2. Preparation of the primary emulsion

Polymer solution was prepared by dissolving a high molecular weight polyphenylene oxide (PPO) in TCE to form a 10 w/v% polymer solution. Dissolution of PPO in TCE was facilitated by using a magnetic stirrer. Once a clear polymer solution was formed, a small amount of surfactant, n-octanol, was added to the polymer solution. The volume of the added surfactant depended on the desired inorganic loading in the final membrane.

The primary emulsion was formed adding the appropriate volume of the aqueous solution into 10 mL of the polymer solution containing the surfactant. Formation of the primary emulsion was facilitated by using the ultrasonic dismembrator at the power of 5 for 1 minute. It is important to emphasize that the primary emulsion was attempted to form only with the aqueous solution that had passed the gelation test.

The maximum power of the ultrasonic dismembrator employed in this work was 600W. The power level reading on the ultrasonic dismembrator can be converted to output energy power by the following equation:

$$\text{Output Energy (W)} = \left(\frac{\text{Power level}}{10} \right) \times 600 \qquad 3.1$$

3.1.1.3. Preparation of the secondary emulsion

In the second step, a specific amount of TEOS, which depended on the desired inorganic loading in the final membrane, was added into the primary emulsion and the entire content was mixed for a specific period of time (7 min or 30 min) using the ultrasonic dismembrator at the power level of 3. Each pulse of the ultra-sonication lasted 30 s and between the two pulses, there was a 30 second rest time to avoid overheating of the emulsion. Following the ultrasoniocation period, the emulsions were continuously mixed using a magnetic stirrer until they were taken for membrane casting. The total time between adding TEOS into the primary emulsion and casting of the secondary emulsion is considered as a reaction time, and the purpose of magnetic stirring of the secondary emulsion prior to membrane casting was to prevent aggregation of inorganic particles formed during polymerization of TEOS.

Table 3.1 summarizes inorganic loadings (wt%) of solutions with respect to the mass of dry PPO in the polymer solution, along with the corresponding volumes of the aqueous solution, n-octanol, and TEOS added to the 10% solution of PPO in TCE.

The purpose of using 5% and 10% loadings was to reproduce the data reported earlier by Sadeghi (2007). Since according to this reference, the best performance was achieved by the EPMM membrane having a 5% loading while an increase from 5% to 10% loadings resulted in a decrease in the membrane selectivity, the major focus in this study was given to loadings less than 5%. In addition, to confirm a deterioration of

membrane properties at relatively high loadings, a 15% loading was also used in this study.

Table 3.1. The recipes for the different Si loadings in the final membrane solutions.

Si Loading Wt%	Aqueous solution mL	n-octanol mL	TEOS mL
1	0.0035	0.0021	0.0100
2	0.0069	0.0042	0.0200
3	0.0102	0.0063	0.0300
4	0.0138	0.0083	0.0400
5	0.0172	0.0104	0.0500
10	0.0344	0.0209	0.1000
15	0.0517	0.0312	0.1500

3.1.2. Membrane casting

The actual EPMM membranes were made by spin-coating of the secondary emulsion onto a silicon wafer. Unlike a traditional dip coating technique, spin coating leads to membranes having a very uniform thickness, which is very important when characterizing the gas transport properties of new membrane materials. Since single layer EPMM membranes were too thin to be handled, the actual membrane consisted of at least two layers.

The actual spin-coating process involved depositing a fixed volume of the secondary emulsion (or polymer solution for the purpose of having reference PPO membranes) on a silicon wafer, after which the wafer was accelerated to a high spin speed in a very short

time. The spin speed was kept for a certain period of time following by a rapid deceleration of the wafer to rest.

Before the actual spin-coating process a “dry” spinning at the speed of 3000 rpm for 10 seconds was performed to ensure the proper levelling and positioning of the wafer in the spin-coating machine. Once this was verified, the entire volume of the secondary emulsion, i.e. c.a. 10 mL, was poured onto 10 cm (4 inch) silicon wafers. After depositing of the emulsion, the wafer was accelerated to a speed of 600 rpm and maintained at this speed for 200 s following a rapid deceleration to the rest of the wafer. In the spin coating process, film thinning, which determines the final thickness of the spin-coated film, depends on evaporation of the solvent and convection of the solution (emulsion), and the two are difficult to separate (Yonkoski and Soane, 1992). In our case, in spite of high volatility of TCE, film thinning was mainly due to convection, because most of the emulsion deposited on the wafer was lost during its spinning.

It is important to emphasize the spinning parameters used in this work were not optimized; they were used based on the results from earlier work performed on this particular spin coating machine (Lashkari, 2008; Sadeghi, 2007).

After formation of the first layer, the wafer and its film were allowed to dry in ambient air for at least two hours before adding another layer on top of the first one.

3.1.3. Post treatment of the membrane

There are two major steps included in the post-treatment of the membrane: boiling the free standing films in deionized water and heat-treatment in a vacuum oven.

Before any of these steps, the membrane films were peeled off from the respective silicon wafers by immersing the wafers in the deionized distilled water. The purpose of the treatment of membranes in boiling water was to remove any water soluble residuals; for example, not reacted sodium carbonate and the aluminium hydroxonitrate. The boiling step was carried out for 4 hours, and the time frame for boiling was established previously (Sadeghi, 2007).

Since TCE, n-octanol, and TEOS have limited solubility in water, it was expected that the boiling step removed residuals of these components from the membrane. In turn, the presence of these residuals could plasticize the membrane, thus deteriorating its separation properties. The removal of these components was attempted by extended drying in a high vacuum oven at ambient (25^{o}C) and high temperature (225^{o}C). Ideally, it would be desired removing the residual TCE, n-octanol, and un-reacted TEOS at low temperature (25^{o}C). However, Hatchinson (1995) claimed that in case of glassy polymers, the residual solvents and non-solvents can only be removed by heat treating the polymer above its glass transition temperature (T_g). Since 225^{o}C is just appreciably greater than the T_g of PPO, this temperature was selected in this study.

In addition to facilitation of the residual solvent and non-solvent removal, the high

temperature thermal treatment might also help formation of zeolite structures from the polymerized TEOS, well distributed within a continuous phase of PPO.

In addition to 25°C and 225°C, the thermal post treatment of the synthesized membranes was also carried out at 120°C. The later temperature was used in previous studies involving the formation of PPO-based EPMM membranes (Sadeghi, 2007). Consequently, the thermal post-treatment at 120°C served to synthesize reference membranes, as well to investigate the actual effect of the temperature during the thermal-post treatment on the properties of the membrane.

3.2. Determination of gas transport properties

In this project the permeability of oxygen and nitrogen, as well as the ideal selectivity and permselectivity for the O_2/N_2 system were determined in an automated constant pressure (CP) system with sweep gas, connected to a gas chromatograph (GC), operated at steady state. In addition, dynamic tests were performed in the same system with single O_2 and N_2 gases to determine the respective diffusivities in the synthesized membranes. Knowing the permeability and diffusivity, the solubility of O_2 and N_2 were also evaluated.

In this section, the CP system, as well as its steady state and transient operations is described. In addition, the specific methods for the determination of the above-mentioned gas transport parameters are also discussed.

3.2.1. Constant pressure system

Figure 3.2 presents an overall layout of an automated CP system with sweep gas used in this work. A unique feature of this system, which was designed and built by Lashkari and Kruczek (2008), is its capability of conducting dynamic gas permeation tests, which allow the determination of gas diffusivity in the tested membranes. The heart of the system is a gas permeation cell. The actual system consists of four permeation cells arranged in parallel, so that four membranes can be tested simultaneously. However, for the clarity purposes, Fig. 3.2 shows only one cell.

The permeation cell houses a circular membrane of the diameter of 4.1 cm. The cell is made of a 316 stainless steel, and consists of two detachable parts. The lower part is a high-pressure chamber equipped with the inlet and outlet tubes for the flow of the feed and the retentate streams, respectively. The upper part (a low-pressure side) is also equipped with the inlet and outlet tubes for the flow of the sweep and sweep + permeate streams, respectively. It is important to emphasize that the use of the sweep stream is optional. The membrane is mounted on the stainless steel porous plate having the porosity of 100 μm, which is embedded in the upper part of the cell. The membrane is separated from the porous plate by a filter paper of similar porosity, which prevents damaging of the membrane by the porous plate when the membrane is under the pressure. Under the operating conditions, the porous plate and the filter paper should have no resistance to the gas flow.

The pressure of the feed stream, which should be similar as the pressure of the retentate stream is controlled by a two-stage pressure regulator and monitored by an pressure transducer (PT1) from MKS Instruments, having the reading range of 0.1 to 3.5 MPa (0 - 500 psig). The flow rate of the retentate stream is controlled by a needle valve (NV) and monitored by an MKS mass flow meter (MFM1) having the reading range of 0-10 $\pm$ 0.1 cm^3/min. The flow rate of the sweep stream is controlled by an MKS mass flow controller (MFC) having the control range of 0-10 cm^3/min. The line carrying the sweep + permeate stream is open to atmosphere so that the gas in this stream is at atmospheric pressure. The exact pressure at the permeate side is provided by an absolute pressure transducer (PT2) from MKS Instruments, having the reading range of 0 to 420 kPa (0-50 psia). The flow rate of the sweep + permeate stream is monitored by an MKS mass flow meter (MFM2) identical to MFM1.

In addition to automatic measurements of the flow rates of the sweep + permeate, and the retentate streams by the respective mass flow meters, these flow rates can also be measured manually by a bubble flow meter installed at the outlet from a multi-position valve (not shown in Fig. 3.2) to which the lines carrying these streams are connected. This allows to verify the calibration and if necessary to calibrate the mass flow meters. As already stated, the use of the sweep stream is optional; sweep gas is used only in dynamic experiments. The membrane cell can also be by-passed by the sweep gas stream. This allows the verification of the calibration of the mass flow controller.

The sweep + permeate and retentate lines are connected via the automated multi-position valve (not shown in Fig. 3.2) to a gas chromatograph (GOW-MAC 580 gas chromatograph) equipped with a molecular sieve 5A column for the determination of the composition of the respective streams in gas separation tests. Although not shown in Fig. 3.2, the feed stream could also be connected directly to the GC.

All the transducers, mass flow meters, mass flow controllers, and the GC are connected to a computer and the data is collected by the LabView software.

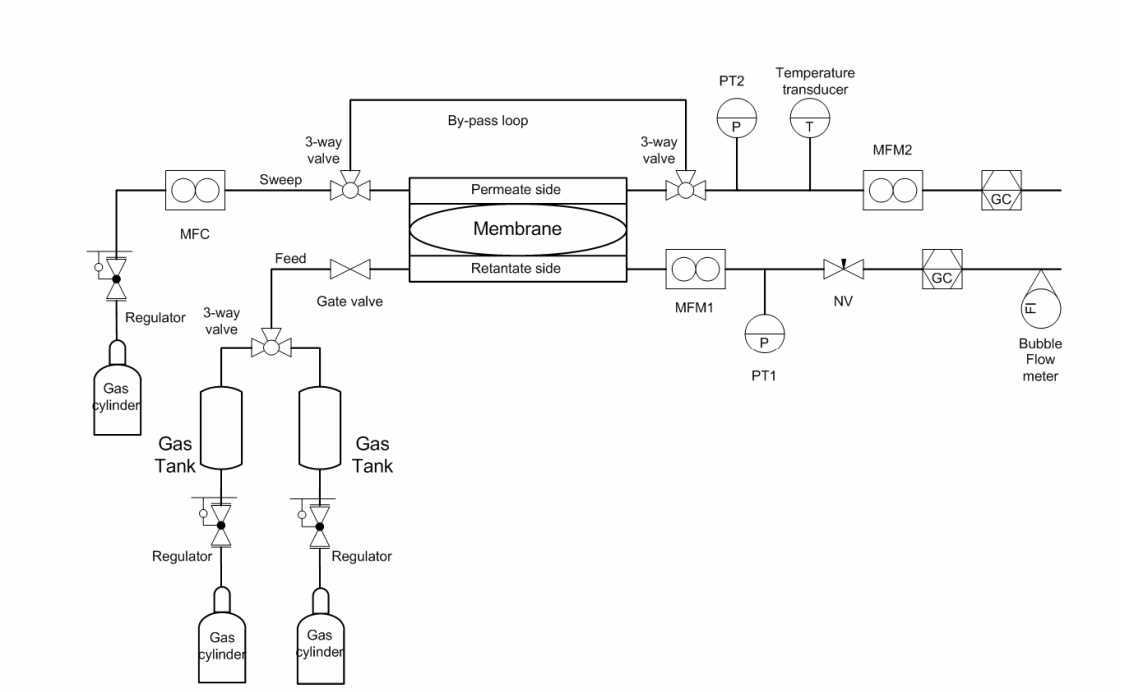

Figure 3.2 The schematic diagram of the automated CP system with sweep gas showing one of four membrane permeation cells.

3.2.2. Analysis of composition using GC

Gas chromatography (GC) is commonly used for the determination of gas composition. In this work we were interested in the analysis of the composition of O_2/N_2 mixtures; consequently, helium was used a carrier gas.

A typical GC results are presented in Fig. 3.3. A series of the voltage signals are plotted as a function of the time starting at the sample injection. It can be observed that at the beginning of the analysis, the voltage of the signals was kept almost constant at the value of 0. At the time point of 90.1 s, the voltage went up sharply and reached the first peak value of 3.68 mV in 6 seconds and then dropped down fast. At the time point of 116.6 s, the signal voltage returned to the level of 0 and was kept at this level for around 15 s. At 129.8 s, the voltage increased again and second peak was found at the time of 137.0 s. The voltage fell back to 0 at 166.3 s and remained at 0 for the rest of the analysis.

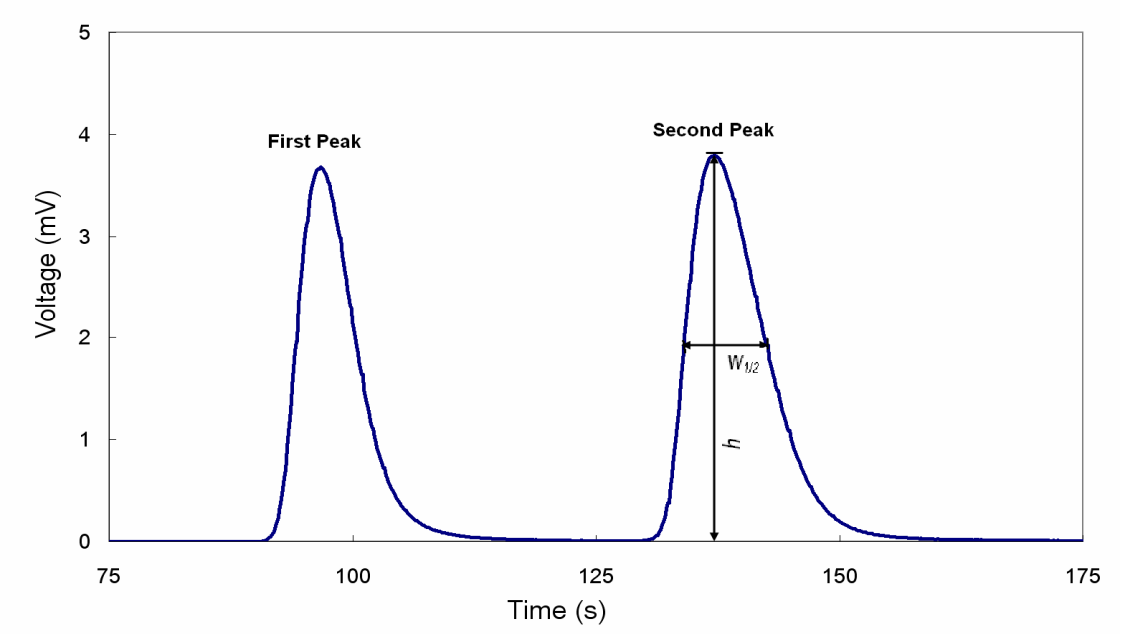

Figure 3.3 A typical GC results of the analysis of permeate composition in air separation test.

The two peaks in Figure 3.3 correspond to the two components in the sample, O_2 – the first peak, and N_2 – the second peak. The area of the peaks can be calculated as,

$$\text{Area}_i = f_i \cdot h_i \cdot w_{i,1/2} \qquad 3.2$$

where h is height of the peak, $w_{1/2}$ is width of the peak at its 1/2 height and f is a correction factor which depends on the temperature of the detector and the category of the gas. In this work, f_{O2} is 1.029 and f_{N2} is 0.988 at detector temperature of 39 °C (Gow-Mac Instruments, 1994). The composition of the sample is directly proportional to the areas of the peaks and the concentration of component i is,

$$c_i = \frac{\text{Area}_i}{\sum \text{Area}_i} \qquad 3.3$$

3.2.3. Steady-state and transient gas permeation tests

The dynamic tests were performed by applying a step change in feed pressure and following the changes in the flow rate of sweep + permeate stream. The step change in the feed pressure was enabled by having the feed line connected to two gas cylinders via a 3-way valve and two respective buffer tanks. Both cylinders contained the same gas but are operated at different pressure. Initially, the feed line is connected to the cylinder operated at low pressure. After a sufficiently long time, the steady state permeation rate across the membrane is established, and the feed line is quickly switched from the low pressure cylinder to the high pressure one. The resulting transient permeation data allows

determination of the gas diffusivity in the tested membrane using a half-time method, which will be described in the subsequent section.

Reaching steady-state condition in a given dynamic test was validated by a constant flow rate of permeate + sweep stream, as determined by the MFM2. It is important to emphasize that to ensure the readings from the MFC2 were within its sensitivity range, dynamic tests were performed using the sweep gas set at sufficiently high, constant flow rate, and the sweep gas and feed gas were always the same. The latter ensured that gas permeation was occurring in only one direction, i.e., from the feed side to the permeate side of the membrane. If the sweep gas were different than the feed gas, apart from the forward permeation of the feed gas, back permeation of sweep gas from the permeate side to the feed side could occur.

In case of gas permeation/separation tests aiming on determination of the permeability and permselectivity of gases in a given membrane, the sweep gas was not used and the steady state permeation rate was determined based on the flow reading determined manually using a bubble flow meter. The bubble flow meter used in this work was the smallest commercially available on the market, and allowed for the measurements of the permeation rates as small as 0.01 mL/min. In addition, in case of gas separation tests, apart from reaching a constant permeation rate, the permeate stream had to reach a composition, which did not change with time, as determined based on the results from the gas chromatograph.

The permeability of O_2 and N_2 in tested membranes was evaluated from Eq.(2.5) based on the steady state permeation rates of the respective gases. The thickness of the membrane was measured using a micrometer (Mitutoyo). The thickness measurements were performed after completion of all the required gas permeation/separation tests. The thickness used in Eq. (2.5) represents an average from at least 10 different points within the permeation area of the membrane. It is important to emphasize that in case of single gas permeation experiments, Δp_i in Eq. (2.5) corresponds to the total pressure gradient across the membrane. In case of mixed gas permeation tests, Δp_i, requires the compositions of the retentate and permeate streams. Since all gas separation experiments were carried out at a stage cut approaching zero (i.e., the flow rate of the retentate was much larger than the flow rate of permeate) the composition of the retentate was similar to the composition of the feed, which was verified experimentally using the GC. Knowing the permeability of individual gases from the feed mixture, the O_2/N_2 permselectivity was evaluated directly using Eq. (2.19). Alternatively, the O_2/N_2 permselectivity could also be evaluated from Eq. (2.20) based on the experimentally measured separation factor defined by Eq. (2.19).

3.2.4. Half-time method

The diffusivity of gases in membranes is typically determined using a time lag method, which normally requires a constant volume (CV) testing system (Ziegel, 1969). In the time lag method, both sides of the membrane are initially at high vacuum, and then

one side of the membrane is pressurized while the rate of pressure increase on the other side of the membrane is recorded, from which the diffusivity is evaluated.

In a CP system, such as the one used in this study, the diffusivity is determined using a half time method (Ziegel, 1969). Similarly to the time lag method, the half time method requires a step change in feed pressure; however, response signal is the permeation rate through the membrane rather than the pressure at the permeate side of membrane. The half time, $t_{1/2}$, is the time measured from the step change in feed pressure until the moment when 50% of the change in the permeation rate had occurred. Consequently, the half time method requires accurate values of the initial steady-state permeation rate before the step change, and the final steady-state permeation rate after the step change in feed pressure. The diffusivity is related to the half time through the following equation (Ziegel, 1969):

$$D = \frac{l^2}{7.025 t_{1/2}} \qquad 3.4$$

where l is the thickness of the membrane.

3.3. Membrane properties characterization

To ensure the polymerization of TEOS taking place and the aluminium well connected to the silica network, the elemental analysis by inductively coupled plasma mass spectrometry (ICP-MS) and nuclear magnetic resonance (NMR) for Si and Al were

conducted. In addition, differential scanning calorimetry analysis of the membrane films was carried out to estimate the glassy transition temperature. Since all these analyses required destruction of the membrane films, only a part of the membrane samples were analyzed with these techniques.

3.3.1. Differential scanning calorimetry (DSC) analysis

Differential scanning calorimetry (DSC) is a technique used to measure the glassy transition state temperature (T_g). A polymer sample around 2.0 mg to 4.0 mg was put into a small aluminium cell. By applying a heat flow to the sample cell and an empty reference cell in an isolated calorimetry, the difference of the heat flow needed can be obtained as the heat needed for the polymer sample. Using this heat rate and other properties of the sample, the heat capacity of the membrane sample was obtained.

The programmed ramping procedure for the DSC analysis of the EPMM membrane samples includes:

1. Equilibrium at 40˚C
2. Heat-up to 250˚C at a rate of 10˚C / min
3. Equilibrium at 250˚C
4. Cool down to 40˚C at a rate of 10˚C / min
5. Repeat step 2 to step 4 for 3 times

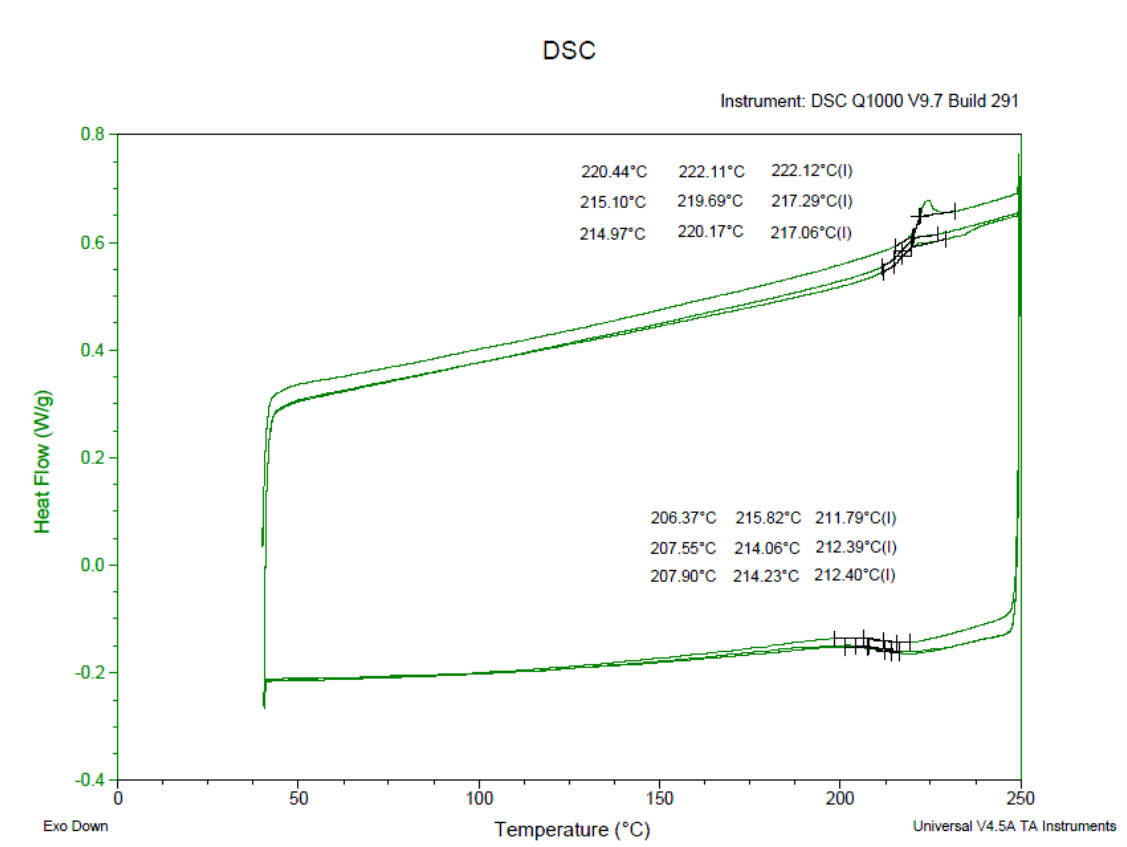

Figure 3.4 A conventional DSC result for a pure PPO membrane.

A typical conventional DSC result of a PPO membrane is plotted in Figure 3.4. In the first heating ramp, it can be observed that the heat flow increased linearly with temperature at low temperature. When the temperature was closed to 220˚C, there is a change in the slope of the heat flow. This high heat flow lasted till the temperature reached 222˚C and another step change appeared. Generally speaking, these would be considered as a phase change or a state change in the middle of the heat flow change where a jump in the heat flow rate took place. In this experiment, the glassy membrane changed its state to the glassy transition state at that temperature range. In the cooling

ramp, the first change occurred at approximately 216˚C and the next change occurred at approximately 206˚C. The T_g of this PPO membrane estimated based on the first heating ramp was 222.11˚C and the T_g got from the first cooling ramp is 211.8˚C. The T_g estimated from the second heating and third heating ramps were 217.3˚C and 217.1˚C, respectively. The T_g obtained from the first heating ramp is slightly higher than the one from the second and third heating ramps since in the first ramp, the membrane sample and the pan might contain some residual solvents, such as water, n-octanol and some other impurities which might decompose in the first heating ramp. The T_g obtained from the second and third cooling ramps were 212.4˚C and 212.4˚C, respectively. These values are very close to the T_g from the first cooling ramp, equal to 211.8˚C. The average value of T_g from the second and third heating ramps, 217.2 ˚C, would be considered the as T_g got from the heating ramps and the average value of T_g got from all three cooling ramps, 212.2 ˚C would be considered the as T_g got from the cooling ramps. The glassy transition temperature of the membrane obtained from the heating ramps was a little higher than that obtained from the cooling ramps and the average value of T_g obtained from the second and third heating ramp would be considered as T_g of this membrane sample.

3.3.2. Inductively coupled plasma mass spectrometry (ICP-MS)

Inductively coupled plasma mass spectrometry (ICP-MS) is a type of high sensitive

mass spectrometry which can determine the composition of the metals inside a given sample and detect metals at the concentration level of part per billion (ppb).

The membrane samples were first burned in a furnace. Then the ash was weighed and dissolved into 10 ml of strong acid, typically the nitrate acid. By detecting the atomic emission of the different elements, the mass concentration of the atoms contained in the samples can be determined.

3.3.3. ^{29}Si NMR and ^{27}Al NMR

When the stable isotopes contain odd numbers of protons or neutrons, they have the instinct magnetic momentum, or a non-zero spin. By applying an electromagnetic pulse in a magnetic field on these isotopes, they can absorb energy from the pulse and radiate energy back at their specific resonance frequencies. By studying the nuclear magnetic resonance (NMR) spectroscopy and comparing the observed frequencies to the known frequencies, the chemical bonds existing in the molecules can be determined.

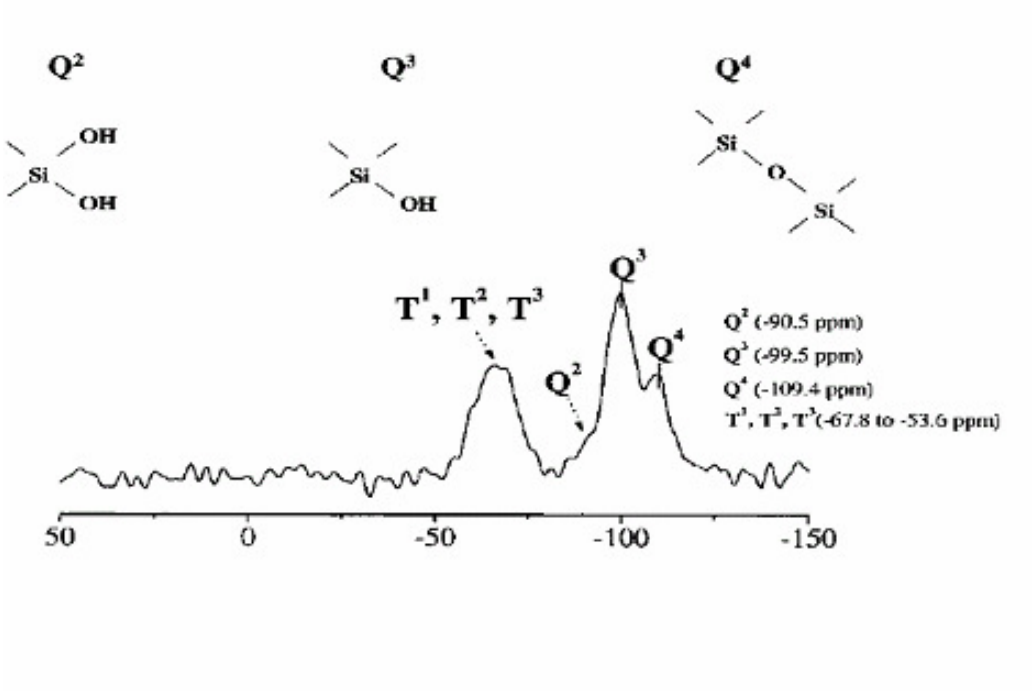

Figure 3.5 The standard ^{29}Si NMR curve for a polymerized TEOS sample (Ruiz-Hitzky et al, 2002).

Fig. 3.5 is a standard curve for the ^{29}Si NMR describing the chemical shifts of the silica in the hydrolyzed TROS and their corresponding chemical bonds. Peak Q_2 is located at -90.5 ppm and it corresponds to the silica nuclei connecting to two OH groups. Q_3 is located at -99.5 ppm and corresponds to the silica connecting to one OH group. Q_4 is located at -109.4 ppm and corresponds to the silica connecting to another silica nucleus via an oxygen nucleus. The co-existence of Q_2, Q_3, and Q_4 means that the TEOS was polymerized and the inorganic network was built. In TEOS polymerization, another peak, Q_0, was able to be found also. Q_0 is located at -82.4 ppm and corresponds to the silica in the unreacted TEOS. The absence of Q_0 means the TEOS was fully reacted. There might be small shifts of the peaks on NMR results while the result would not be affected

significantly.

The area under each peaks also indicated the amount of a particular bound. By integrating the height of the peak, the amount of each type of bounds can be estimated. Combined with the ICP-MS result, the result of NMR analysis can help to understand the structure of the polymer sample.

3.4. Equipment and Materials

Equipment and chemicals employed in this project are tabulated by an alphabet order in Tables 3.2 and 3.3.

3.4.1. Equipment

Table 3.2 Equipment used in this research project.

Equipment	Part No.	Manufacture
Bubble flow meter	0.5 ml	Supelco
DSC	QA-1000	TA Instrument
GC Unit	580 Series	Gow-Mac Instrument
ICP-MS	Agilent HP 4500	Hewlett-Packard
Micrometer	0 - 1”	Mitutoyo
Si and Al NMR	Avance 400 III	Bruker Biospin
Scale	AG204	Mettler Toledo
Stirring Oven	PC-420	Corning
Ultra-sound dismembrator	550	Fisher Scientific
Vacuum Oven	1415M	Sheldon Manufacturing

3.4.2. Chemicals

Table 3.3 Chemicals and gases used in this research project

Chemical	Specification	Source
Aluminium nitrate nonahydrous	ACS reagent	Sigma-Aldrich
Air	Medical grade	Linde Canada
Ethanol	99.50%	Sigma-Aldrich
Nitrogen	Industrial grade	Linde Canada
N-Octanol	99%	Sigma-Aldrich
Oxygen	Industrial grade	Linde Canada
PPO	Powder	GE plastic
Sodium Carbonate anhydrous	ACS reagent	Sigma-Aldrich
Trichloroethylene (TCE)	ACS reagent	Sigma-Aldrich
Tetraethylorthosilicate (TEOS)	ACS reagent	Sigma-Aldrich

Chapter 4. Results and Discussion

The original objective of this work was to implement the major recommendations from the previous work on the development and characterization of PPO-based EPMM membranes (Sadeghi, 2007). These included, post-treatment of the synthesized membranes above the glass transition temperature of the host polymer (PPO), expanding the range of inorganic loading in the synthesized EPMM membranes, and application of additional characterization tools, in particular ICP-MS for the determination of the actual inorganic loading in the synthesized membranes, and ^{29}Si NMR and ^{27}Al NMR for the determination of the actual structure of the inorganic phase dispersed in the membrane.

Since ICP-MS, ^{29}Si NMR and ^{27}Al NMR, as well as DSC, which were used in this study as a characterization tool, are destructive techniques; these analyses were performed only after the complete characterization of the gas transport properties of the membranes. Consequently, in this section the results pertaining to the determination of the permeability, diffusivity and solubility of O_2 and N_2 in the synthesized membranes followed by their O_2/N_2 permselectivity are presented first.

4.1. Gas transport properties of synthesized EPMM membranes

In this section, the results of gas permeation/separation tests are presented and

discussed. The major objective in this section is to identify any correlations between the gas transport properties of the synthesized EPMM membranes and the theoretical Si-loading, and the post-treatment protocol. The latter includes the post-treatment temperature and inclusion or exclusion of a step in which membranes are boiled in deionized water.

Table 4.1 summarizes all new types of EPMM membranes synthesized in this study. In addition, EPMM membranes were also synthesized at the conditions used by Sadeghi (2007), i.e., with the theoretical Si-loadings of 5%, boiled in deionized water and post-treated in a vacuum oven at 120 ˚C for 48 hours.

Table 4.1 Summary of synthesized membranes for properties and performance experiments

Post-Treatment Temperature	25˚C		225˚C	
Si Loading	Boiled	Not Boiled	Boiled	Not Boiled
1	√		√	
2	√		√	
3	√		√	
4	√		√	
5	√	D	√	D
10	√	D	√	D
15	D	D	√	D

An empty cell in Table 4.1 indicates that no membranes at given conditions were synthesized. For all other conditions, at least duplicate membranes were synthesized. The symbol √ indicates that at least one of synthesized membranes was successfully tested in gas permeation/separation experiments. On the other hand, the symbol D indicates that all membranes of the corresponding type were defective. In general the synthesized

membranes did not have any visible defects; therefore, defectiveness of a given membrane was determined by comparable permeabilities of O_2 and N_2, i.e., no or very small ideal selectivity. The tested membranes with the ideal selectivity less than 3.0 were considered as defective and are excluded from further analysis.

It can be noticed that in Table 4.1, all membranes prepared without the boiling step were defective. Boiling EPMM membranes in deionised water; however without any justification, was proposed by Sadeghi (2007). It is hypothesized that this step helps removing all unreacted components of the aqueous phase, which otherwise may lead to development of defects during the final drying step of the membrane. On the other hand, the boiling step should not influence the content (if any) of the unreacted TEOS, because of limited solubility of the latter in water.

4.1.1. Single gas permeation tests

Single gas permeation tests were performed using single oxygen and nitrogen from the respective gas cylinders. They were carried out in both steady-state and transient modes as discussed in Section 3.2. The former allowed evaluation of the permeability of O_2 and N_2, as well as their ratio, i.e., the ideal selectivity of the synthesized EPMM membranes. The latter allowed determination of the diffusivity of O_2 and N_2 in the synthesized membranes. Knowing the permeability and diffusivity, the solubility of the two gases in the synthesized membranes was also evaluated from the ratio of the

permeability and diffusivity.

4.1.1.1. Permeability and ideal selectivity

The O_2 permeability of the EPMM membranes post-treated at 25˚C, 120˚C and 225˚C are plotted in the Figure 4.1 as a function of the theoretical Si-loading in the casting emulsion. In addition, Fig. 4.1 shows the horizontal reference line, corresponding to 19.44 Barrer, which is the average O_2 permeability of five PPO membranes. Similarly to the actual EPMM membranes, the latter were two-layer films prepared using the spin-coating technique. Their post-treatment involved only drying at ambient temperature and pressure for an extended period of time.

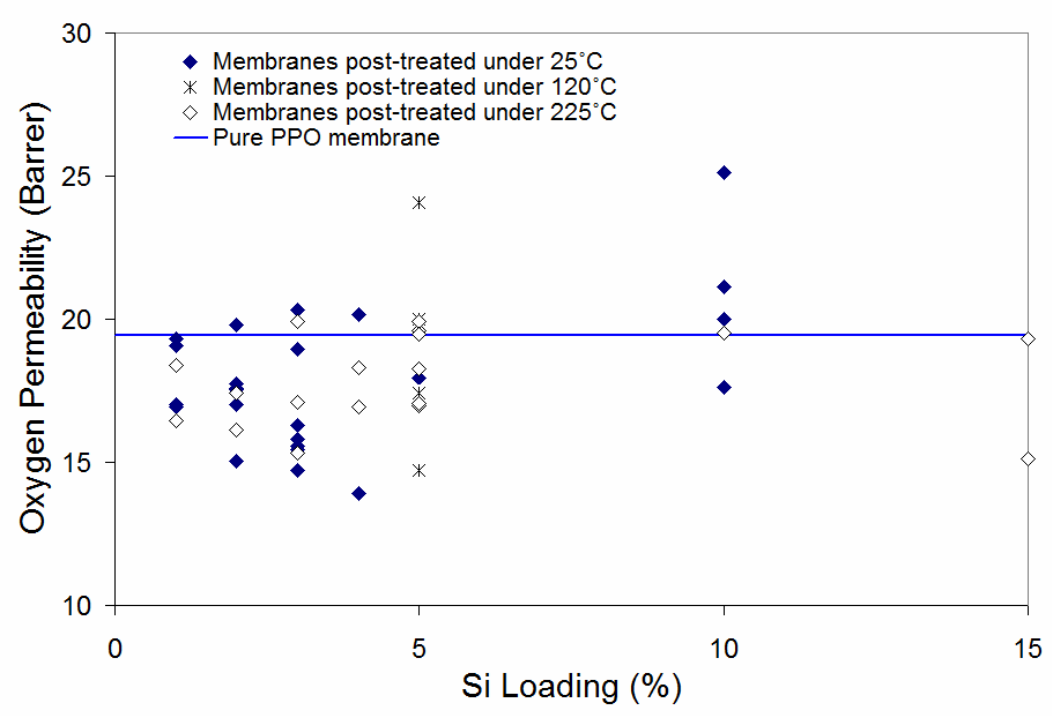

Figure 4.1 Effect of Si loading on permeability of O_2 in EPMM membranes.

The O_2 permeability of EPMM membranes in Figure 4.1 ranges from 14 to 25 Barrer. In comparison to the permeability of the PPO membrane, most of the data points fall below the reference line. At the same time, it is important to emphasize a large variation in the O_2 permeability for a given theoretical Si-loading. For example, in case of the EPMM membranes with 5% theoretical loading, and post-treated at 120^{o}C, the O_2 permeability ranges from 15 Barrer to 24 Barrer. The most important contributor to such a significant variation in the membrane permeability is an uncertainty associated with the measurement of the membrane thickness. The membrane thickness used in the permeability calculations was an average value based on at least 10 micrometer measurements in different points of a given membrane. While the spin coating method improves the reproducibility of the membrane thickness compared to a more traditional method of membrane casting by dip coating (Lashkari, 2008), the resulting uncertainty in the membrane thickness may have prevented observing the effect (if any) of the theoretical Si-loading on the O_2 permeability of EPMM membranes.

To improve the clarity of the figures, from this point on, all the gas performance data, starting from the data shown in Fig. 4.1, will be presented using the average values for given membrane preparation conditions. Fig. 4.2 plots the average permeability for a given theoretical loading and the post-treatment temperature versus the theoretical loading. Looking at the average permeability it is evident that except for the 10% loading, the values in Fig. 4.2 fall below the reference permeability of the PPO membrane.

Interestingly, for both post-treatment temperatures there seems to be a theoretical loading for which the permeability reaches a minimum value. In case of the membranes dried at 25^{o}C, the minimum permeability occurs at the theoretical Si-loading of 2% while in case of those dried at 225^{o}C at the at the theoretical Si-loading of 3%. On the other hand, it is important to note that size of error bars in Fig. 4.2, which represent the standard deviation from all the permeability values for a given theoretical Si-loading and the drying temperature, is comparable to the actual variation of the permeability with the theoretical loading. Therefore, despite the apparent trends between the permeability and the theoretical loading in Fig.4.2, these might not represent the actual trends, and as such the collected data does not allow formulating any definite conclusions about the effect of the theoretical Si-loading on the permeability of the EPMM membranes. On the other hand, assuming that theoretical Si-loading represents the actual Si-loading in the membrane, it can be concluded that dispersing inorganic particles in the continuous phase of the PPO matrix does not improve the membrane permeability. On the contrary, it appears to decrease the O_2 permeability of the EPMM membranes compared to that of the PPO membrane. In other words, the anticipated increase in permeability resulting from dispersing inorganic phase into the polymer network (Kickelbick, 2007), has not been confirmed by the results presented in Figures 4.1 and 4.2.

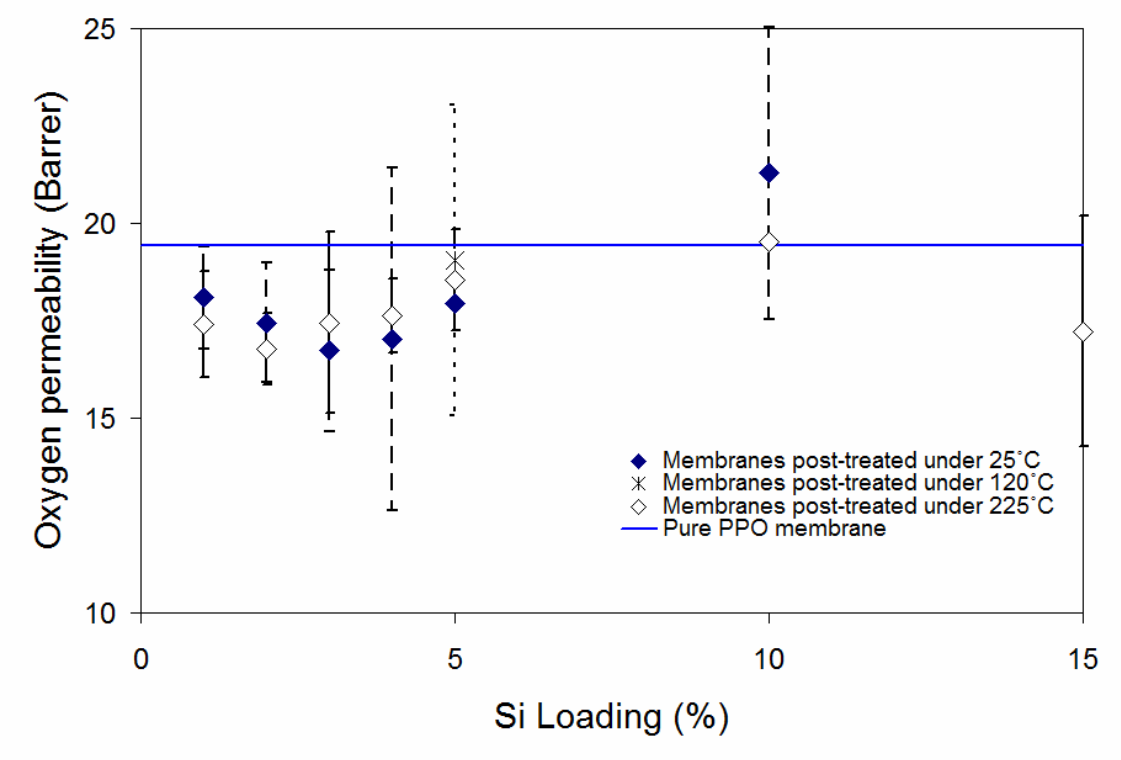

Figure 4.2 Effect of Si loading on oxygen permeability of EPMM membranes.

Figure 4.3 plots the average ideal O_2/N_2 selectivity for a given loading and the post-treatment temperature versus the theoretical Si-loading of the EPMM membranes. The figure also includes a horizontal reference line for the ideal selectivity of 4.96, which corresponds to the ideal selectivity of the PPO membrane. The corresponding standard deviation for each average selectivity is also shown as error bars in this figure.

It can be noticed that, except for the EPMM membrane with the 5% theoretical Si-loading treated at 25^{o}C, the average ideal selectivity for all other loadings fall below the reference ideal selectivity of the pure PPO membrane. In general, it appears that the average ideal selectivity decreases with an increase in the theoretical loading. Assuming

that the theoretical Si-loading corresponds to the actual loading in the EPMM membranes, it can be concluded that dispersing the inorganic phase into a continuous PPO matrix decreases the selective properties of the membrane. This, in combination with the previously discussed effect of the theoretical Si-loading on the O_2 permeability indicates that, contrary to what was expected based on the results of Sadeghi (2007), PPO membranes have superior permeation and selective properties compared to the PPO-based EPMM membranes. It is important to emphasize that Sadeghi (2007) reached her conclusions based on individual membranes, while in this work the properties of all membranes corresponding to a given Si-loading and the post-treatment temperature were averaged. On the other hand, the analysis of the gas transport properties of all EMMP membranes, which is summarized in Appendix A, reveals that there were individual EPMM membranes having superior permeation and selective properties compared to those of the reference PPO membrane. However, these superior properties were not repeatable and consequently are hidden in the average values and the corresponding error bars presented in Figures 4.2 and 4.3.

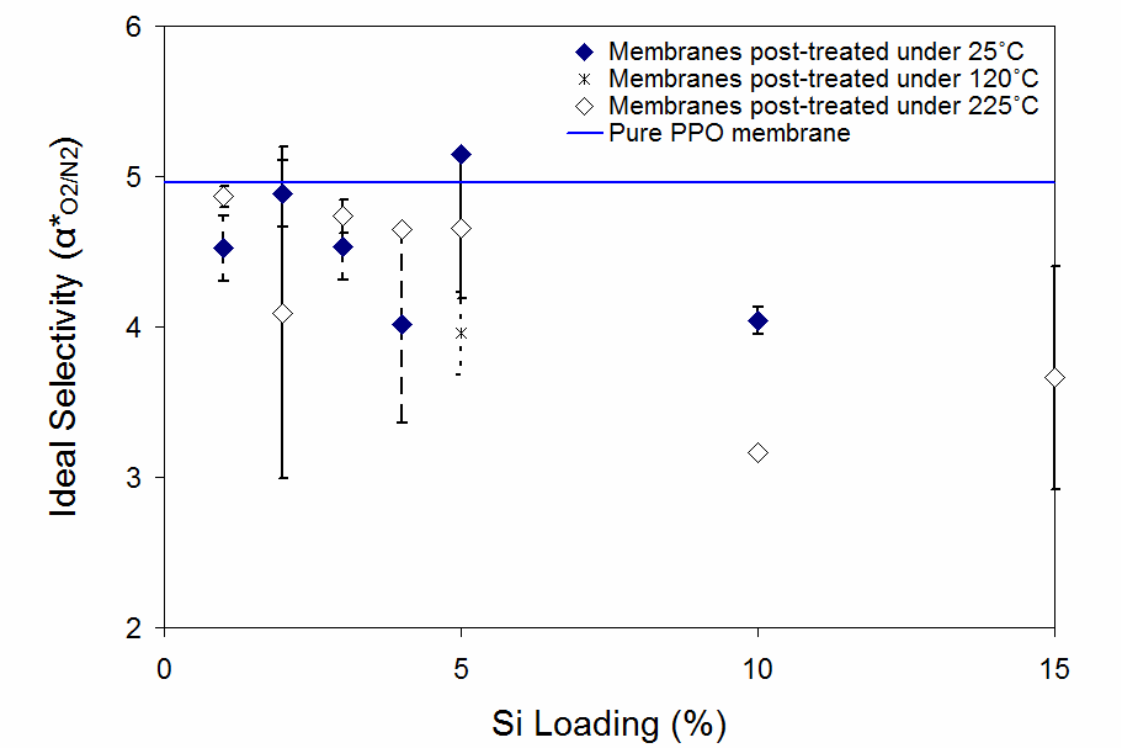

Figure 4.3 Effect of Si loading on the ideal O_2/N_2 selectivity of EPMM membranes.

Focusing on the relative magnitude of the error bars in Fig. 4.3, it is noticed that for some membranes the error bars are large, although they are generally smaller than in Fig. 4.2. It is important to note, that unlike the error bars in Fig. 4.2 those in Fig. 4.3 cannot be attributed to the uncertainty in the membrane thickness measurement. This is because the ideal O_2/N_2 selectivity is the ratio of the respective permeability coefficients, and as a result any error in the thickness measurement cancels out. Consequently, large error bars in case the EPMM membranes with the Si-loadings of 2%, 5% and 15% dried at 225°C as well as that for the Si-loading of 4% dried at 25°C indicate a rather poor reproducibility of the membrane properties even when the same synthesis protocol is followed.

From the discussion so far it becomes evident that the permeability and the ideal selectivity are generally not related with the theoretical Si-loading of the EPMM membranes. Considering this, the EPMM membranes synthesized in this work are compared on the basis of the post-treatment temperature. Figures 4.4 and 4.5 present the effect of the post-treatment temperature on the O_2 permeability and the ideal O_2/N_2 selectivity of the EPMM membranes, respectively. It is important to emphasize that all membranes post-treated at a given temperature were used for the evaluation of the respective average and standard deviation values in Figs. 4.4 and 4.5 regardless of their theoretical Si-loadings.

It can be noticed in Fig. 4.4 that the O_2 permeability increases with the post-treatment temperature. On the other hand, it should be noted that the differences between the average permeability at different temperatures are within the standard deviation for a given post-treatment temperature. One of the reasons to post-treat the EPMM membranes at 225^{o}C, i.e. above the T_g of PPO was to ensure complete removal of residual solvent and/or TEOS from the membrane structure. If these residuals were present in the membrane structure they could act as a plasticizer or antiplasticizer. The exact role of the residuals depends on their concentration. For relatively small concentrations, the residuals act as an antiplasticizer, which occupies a part of free volume otherwise available for the diffusing penetrants through the membrane, thus decreasing the membrane permeability. Consequently, removing of residuals acting as antiplasticizer should increase membrane

permeability, which to some extend is seen in Fig. 4.4.

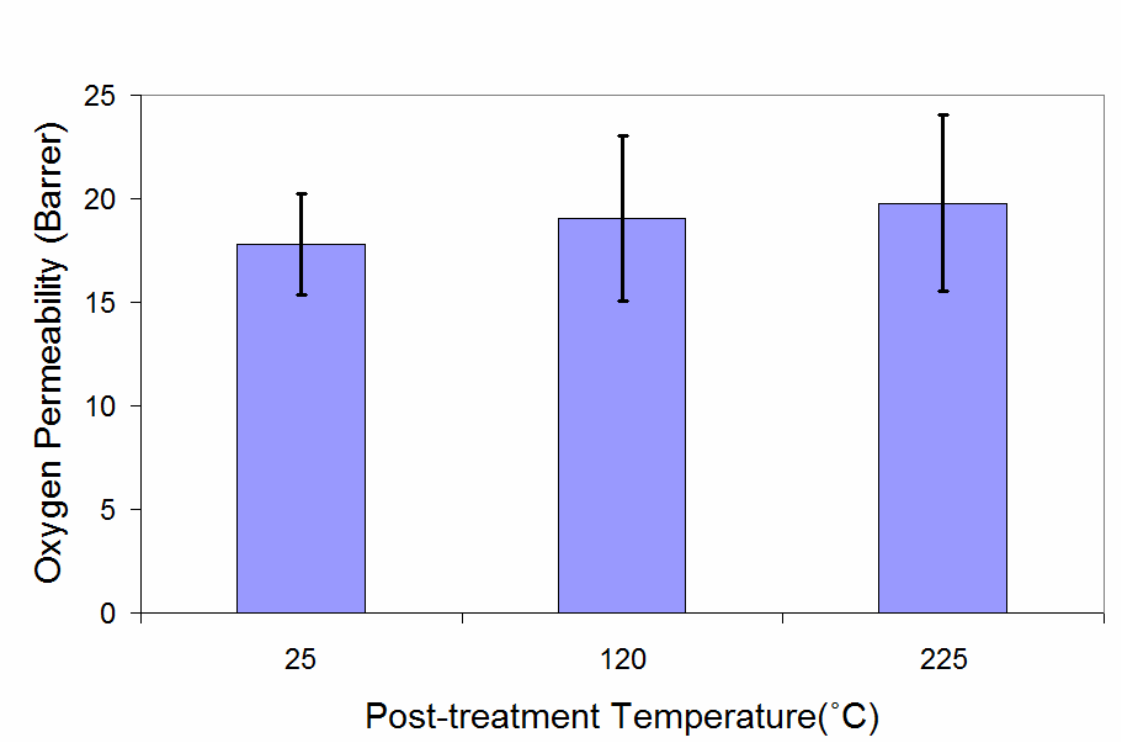

Figure 4.4 Effect of post-treatment temperature on O_2 permeability in EPMM membranes.

On the other hand, considering Fig. 4.5, there is no immediately obvious effect of the post-treatment temperature on the ideal O_2/N_2 selectivity of the EPMM membranes. It can be noticed that the membranes treated at 25°C have slightly greater ideal selectivity than those treated at 225°C. At the same time the ideal selectivity of the membranes treated at 25°C and 225°C is notably greater than those treated at 120°C.

Although similarly to Figs. 4.2 and 4.3 the observation of any effect of the post-treatment temperature on gas transport properties of the EPMM membrane is impaired by relatively large error bars, it appears that the post-treatment temperature is

more important parameter than the theoretical Si-loading. This is completely unexpected result, because while the post-treatment temperature should affect the gas transport properties of the EPMM membranes, these properties should be affected more strongly by the presence of inorganic particles dispersed in the membrane network.

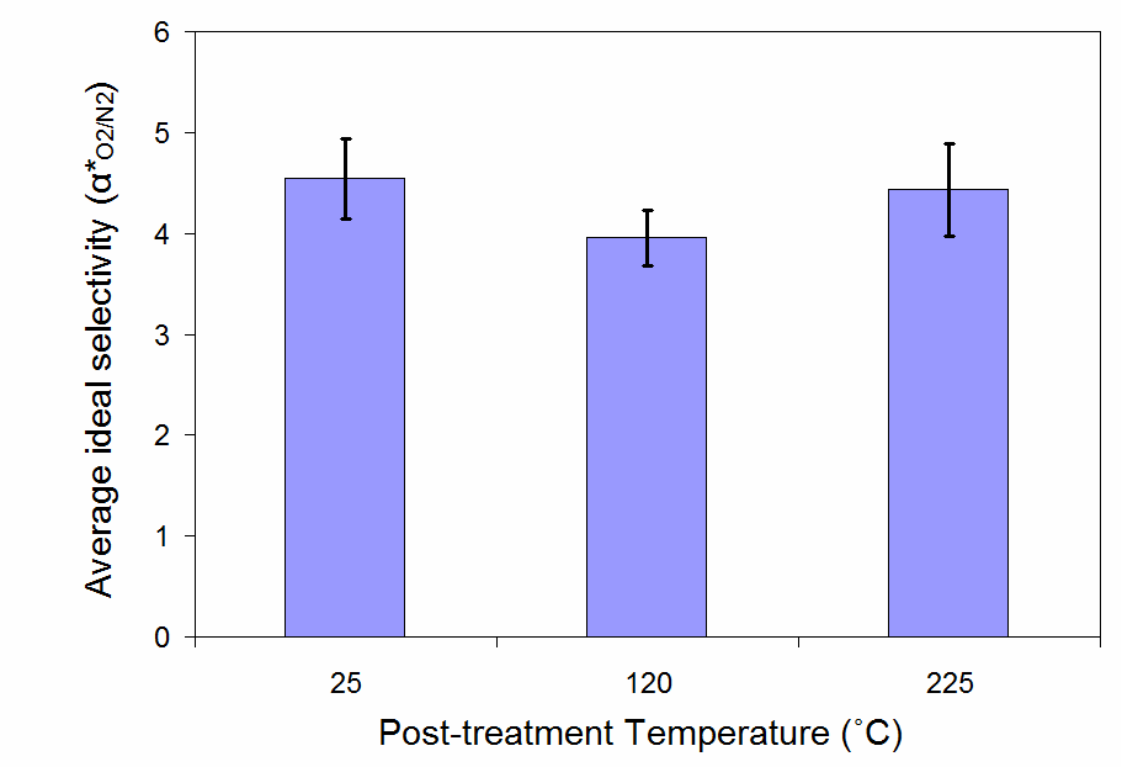

Figure 4.5 Effect of post-treatment temperature on O_2/N_2 ideal selectivity of EPMM membranes.

4.1.1.2. Diffusivity and solubility

A part of the experimental protocol with single O_2 and N_2 gases involved experimental determination of the diffusivity and the diffusivity selectivity and hence the solubility and the solubility selectivity of the synthesized EPMM membranes. It is important to emphasize that a lack of obvious trends between the theoretical Si-loading

and permeability does not preclude the existence of trends between the Si-loading and the diffusivity and/or the solubility of O_2 in the EPMM membrane. However, as shown in Figs. 4.6-4.9, similarly to the permeability and ideal selectivity, the theoretical Si-loading does not affect the diffusivity, diffusivity selectivity, solubility and solubility selectivity of the synthesized EPMM membranes. Since there are no obvious trends the theoretical Si-loading, the error bars are not included in these figures.

Focusing on Fig. 4.6, which plots the average O_2 diffusivity in the EPMM membranes as a function of the theoretical Si-loading, it can be noticed that unlike the average permeability, the average diffusivity of O_2 in the synthesized EPMM membranes is greater than the reference diffusivity of 12.44 x 10^{-12} m^2/s, which corresponds to the diffusivity of O_2 in pure PPO membrane. From a theoretical point of view, the effect of dispersion of an inorganic phase in the membrane depends on the nature of the inorganic phase. If the inorganic phase is impermeable to gases, its dispersion in the membrane may increase the membrane tortuosity leading to a decrease in the membrane diffusivity. At the same time, both permeable and impermeable inorganic particles may increase the free volume of the membrane, which normally leads to an increase in the membrane diffusivity. When the inorganic particles are permeable to gases, which should be the case in this work (the synthesized inorganic phase is expected to be an amorphous silicalate or aluminum silicalate particles), the diffusivity of the PPO-based EPMM membranes was expected to be greater than that of the base PPO membrane, which is actually observed in

Fig. 4.6.

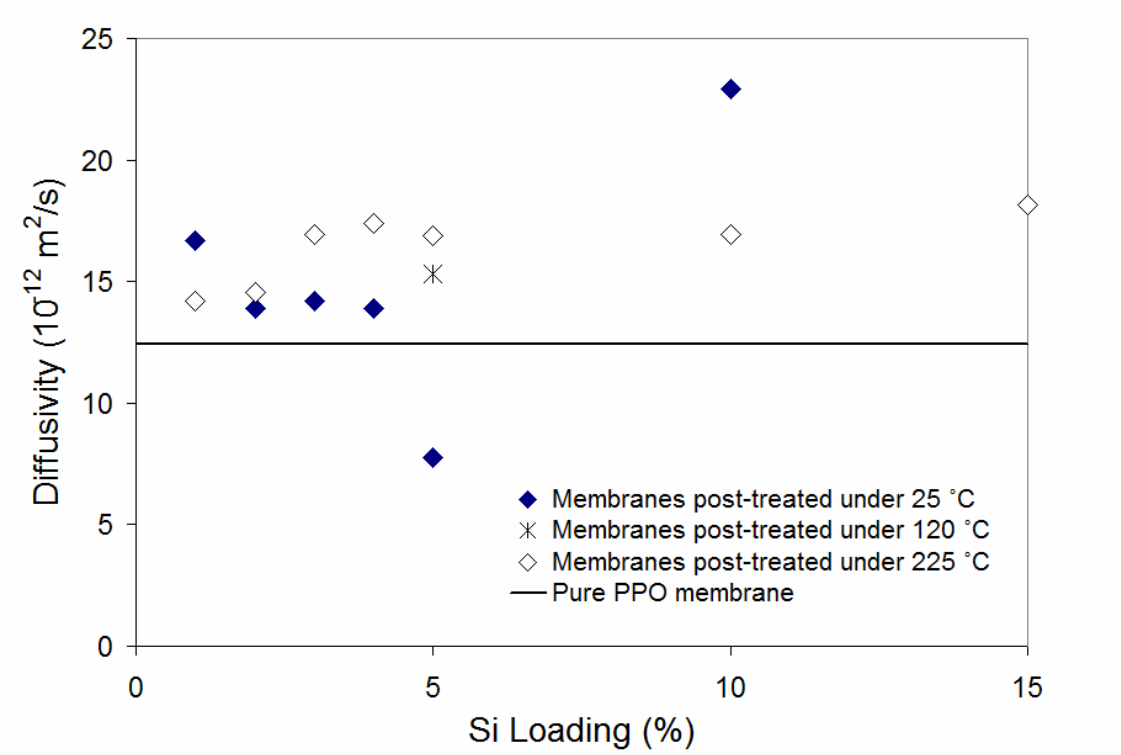

Figure 4.6 Effect of Si loading on diffusivity of O_2 in EPMM membranes.

Out of six different Si loadings for which membranes were post-treated at both 25°C and 225°C, in three cases the diffusivity of the membranes post-treated at 225°C is greater than the diffusivity of the membranes post-treated at 25°C, in two cases the situation is exactly the opposite and in one case the diffusivities of both types of membranes are comparable. As a result, there is also no obvious effect of the post-treatment temperature on the O_2 diffusivity of the synthesized EPMM membranes.

Fig. 4.7 plots the average diffusivity selectivity, i.e., the ratio of the average diffusivity of O_2 to the average diffusivity of N_2, versus the theoretical Si-loading of the

synthesized EPMM membrane along with the reference diffusivity selectivity of the PPO membrane. The diffusivity selectivity can be considered as the ideal diffusivity selectivity and as such is an equivalent to the ideal selectivity. However, unlike the average ideal selectivity, the average diffusivity selectivity of the EPMM membranes is comparable to that of the PPO membrane. Therefore, considering the combination of the O_2 diffusivity and the O_2/N_2 diffusivity selectivity, EPMM membranes appear to have superior properties compared to those the pure PPO membranes.

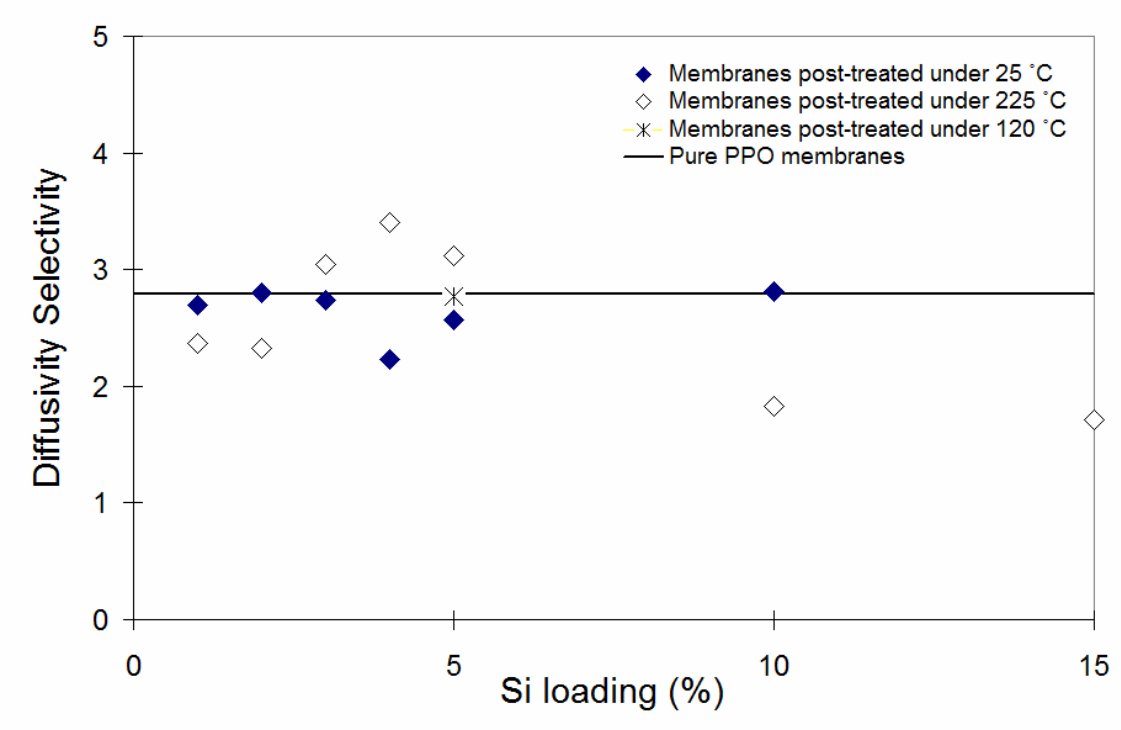

Figure 4.7 Effect of Si loading on the O_2/N_2 diffusivity selectivity of EPMM membranes

Fig. 4.8 plots the average O_2 solubility versus the theoretical Si-loading of the EPMM membranes along with the reference solubility of O_2 in the PPO membrane. It is

important to emphasize that unlike the permeability and the diffusivity, the solubility was not measured experimentally but rather calculated from the ratio of the permeability and diffusivity. Consequently, since the O_2 permeability of the EPPM membranes is generally smaller while the O_2 diffusivity greater, the average O_2 solubility of the EPMM membranes is considerably smaller than that of the pure PPO membrane. The only exception is the EPMM membrane with 5% theoretical Si-loading and post-treated at 25°C, for which the O_2 solubility is significantly greater than that of the PPO membrane. It is important to note however that this abnormally high O_2 solubility is based on the performance of a single membrane of this type since only one membrane of this type was successfully synthesized at these conditions.

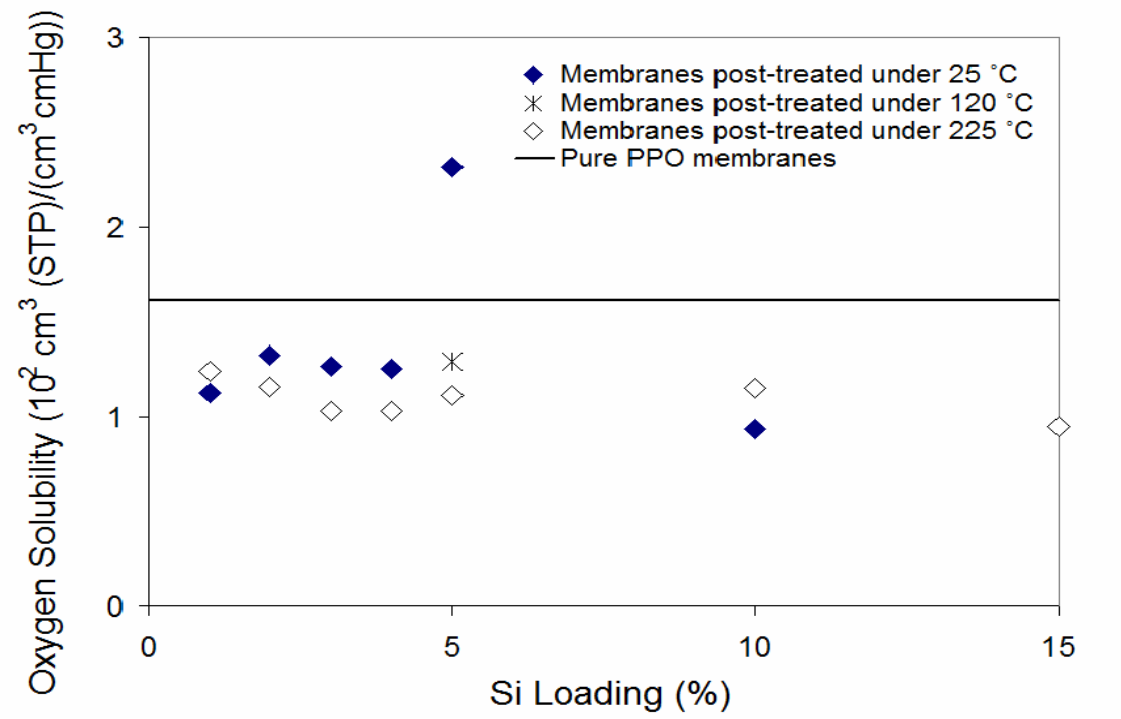

Figure 4.8 Effect of Si loading on solubility of O_2 in EPMM membranes.

The average solubility selectivity of the EPMM membranes post-treated at 25°C, 120°C and 225°C are plotted in Fig. 4.9 versus the theoretical Si-loading. The solubility selectivity of the pure PPO membrane is included in Fig. 4.9 as a reference.

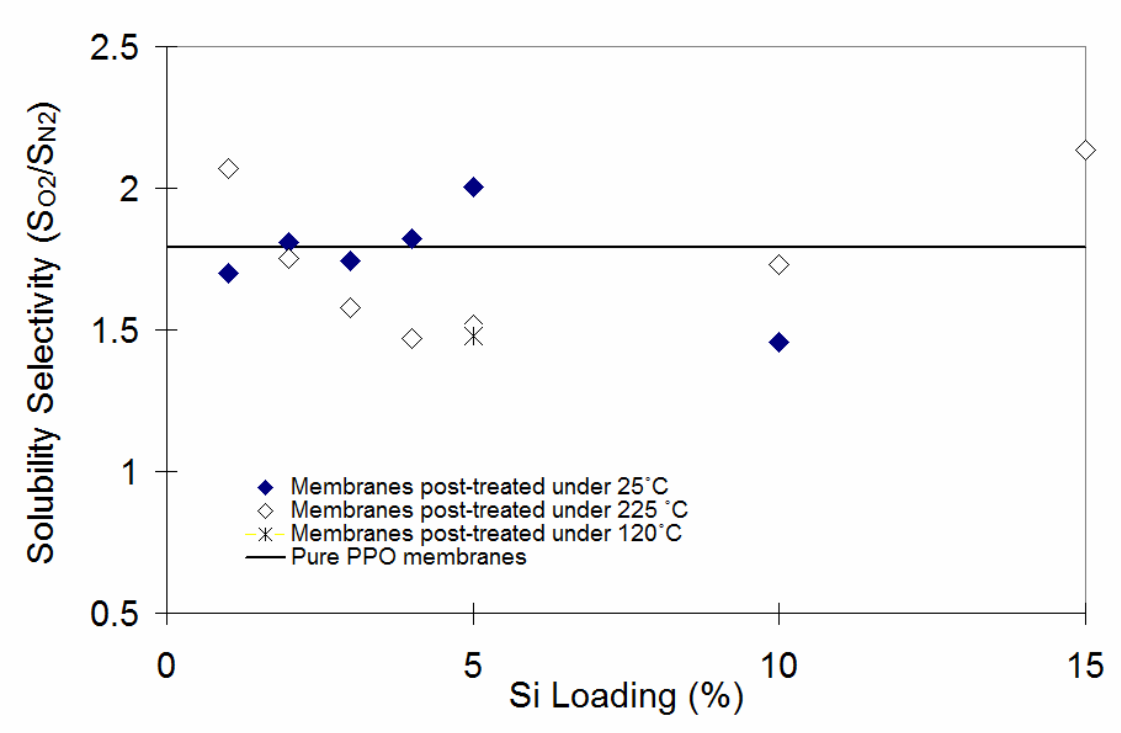

Figure 4.9 Effect of Si loading on the O_2/N_2 solubility selectivity of EPMM membranes.

Similarly to the O_2 solubility, the solubility selectivity is determined from the ratio of the ideal selectivity and the diffusivity selectivity, and as such this is not an independently determined parameter. It can be noticed in Fig. 4.9 that the solubility selectivity of the EPMM membranes is lower than that of the pure PPO membrane. Also, there is no obvious relationship with the theoretical Si-loading, as well while for some Si-loadings the solubility selectivity of the membranes treated at 25°C is greater than that for the

membranes treated at 225^{o}C, there are Si loadings for which the opposite is true.

4.1.2. Gas separation tests

In addition to single gas permeation tests, the results of which were discussed in the preceding sections, the EPMM membranes we also investigated in the air separation tests. Similarly to the single gas permeation tests, the air separation tests allow the determination of the permeability of individual gases present in the gas mixture as well as their ratio. Unlike the ratio of the permeability coefficients determined from the single gas permeation tests, which is referred to as the ideal selectivity, this ratio based on the results from the gas separation tests is referred to as permselectivity. The latter provides a more realistic evaluation of the selective properties of the membrane than the former one. The results obtained from the analysis of the gas separation data are presented next.

Fig. 4.10 plots the average O_2 permeability of the EPMM membranes determined from the air separation tests versus the theoretical Si-loading. For comparison, the O_2 permeability data obtained from the single gas permeation tests, previously presented in Fig. 4.2, is also reproduced in this figure. In addition, the reference O_2 permeability of PPO determined from the mixed and single gas tests are also shown. Similarly to the O_2 permeability from the single gas permeation tests, there is no obvious relation between the O_2 permeability and the theoretical Si-loading. Also, the O_2 permeability of the

EPMM membranes is generally lower than that of the PPO membrane. It can also be noticed that the average O_2 permeability from the air separation tests for any theoretical Si-loading and any post-treatment temperature is consistently less than the corresponding average values determined from the single gas permeation tests.

A decrease in the permeability resulting from the presence of another gas in the feed, in this case a decrease in the O_2 permeability in the presence of N_2 is a well known phenomenon for gas transport in glassy materials. This behavior is a consequence of a dual mode sorption, and more specifically, of a competition for the limited number of adsorption (Langmuir) sites (Sanders & Koros, 1986). In this case, the presence of the other gas decreases the concentration gradient across the membrane so that for the same partial pressure gradient across the membrane the actual driving force for the diffusion is lower in a mixed gas permeation test compared to a single gas permeation test.

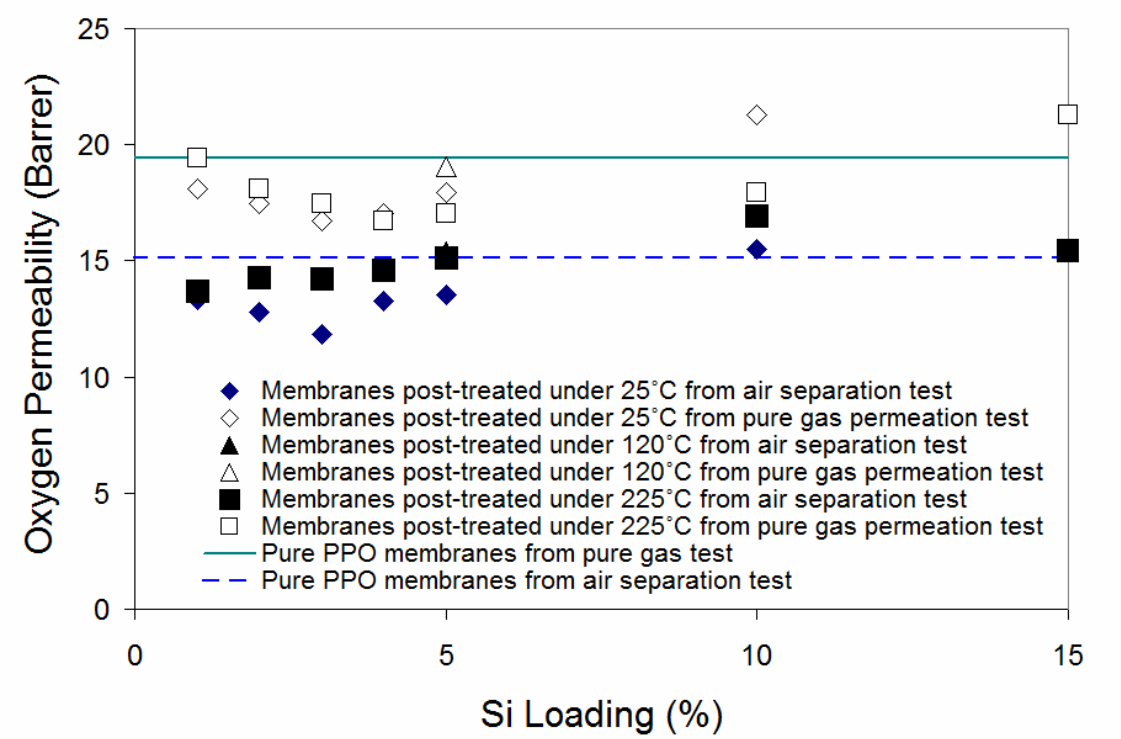

Figure 4.10 Effect of Si loading on the permeability O_2 in EPMM membranes determined from the gas separation experiments. For comparison the data obtained from single gas permeation tests previously presented in Fig. 4.2 is reproduced in this figure.

It can also be noticed in Fig. 4.10 that the effect of the post-treatment temperature is not the same for the average permeability data obtained in single and mixed gas tests. The difference between the average permeability values at a given theoretical Si-loading for the membranes post-treated at 25°C and those post-treated at 225°C changes, and in some cases this difference changes the sign.

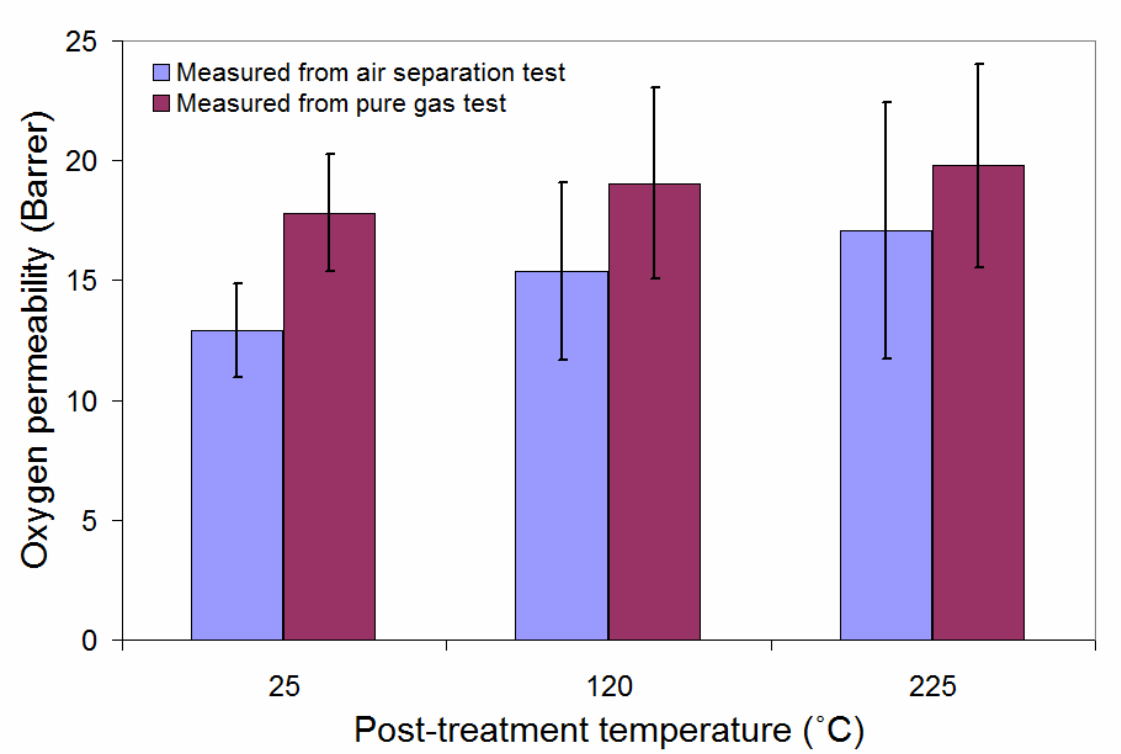

Figure 4.11 Effect of temperature on the O_2 permeability in EPMM membranes determined from the gas separation experiments. For comparison the data obtained from single gas permeation tests previously presented in Fig. 4.4 is reproduced in this figure.

Fig. 4.11 presents the comparison of the effect of the post-treatment temperature on the average O_2 permeability determined from the single and mixed gas experiments. In this figure, all permeability data for a given post-treatment temperature was averaged out regardless of the theoretical Si-loading. The permeability data from single gas permeation tests is reproduced from Fig. 4.4.

Figure 4.12 plots the average O_2/N_2 permselectivity of the EPMM membranes versus the theoretical Si-loading and compares it with the ideal O_2/N_2 selectivity data previously presented in Fig. 4.3. In addition, horizontal lines representing the

permselectivity and the ideal selectivity of the PPO membrane are also included in Fig. 4.12. Similarly to the ideal selectivity data, there is no obvious relation between the O_2/N_2 permselectivity and the theoretical Si-loading. However, unlike the ideal selectivity of the EPMM membranes, which was lower than that of the PPO membrane, the permselectivity of the EPMM membranes is comparable to that of the PPO membrane.

For a given theoretical Si-loading and the post-treatment temperature, the O_2/N_2 permselectivity is lower than the corresponding ideal selectivity. This effect is a consequence of a decrease in the permeability of the more permeable gas, in this case O_2, in the presence of the less permeable gas, in this case N_2, which was already noted in Fig. 4.10. While the permeability of the less permeable gas also decreases in the presence of the more permeable gas, this effect is not that strong, and thus the permselectivity is lower than the corresponding ideal selectivity.

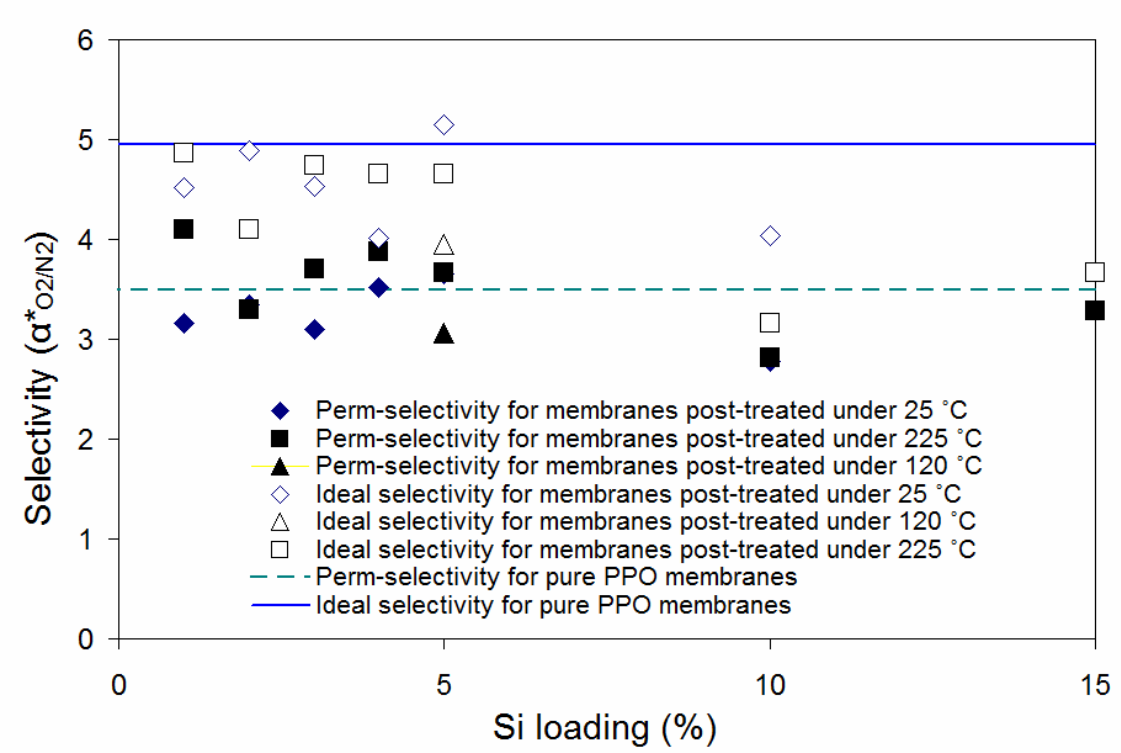

Figure 4.12 Effect of Si loading on the O_2/N_2 perm-selectivity of EPMM membranes. For comparison the ideal selectivity data obtained from single gas permeation tests previously presented in Fig. 4.3 is reproduced in this figure.

The difference between the ideal selectivity and permselectivity is also illustrated in Fig. 4.13, which presents the comparison of the effect of the post-treatment temperature on the average O_2/N_2 permselectivity and ideal selectivity. The latter was reproduced from Fig. 4.5. It is evident that for any post-treatment temperature the ideal selectivity is greater than the permselectivity. Interestingly, the permselectivity of the membranes dried at 225°C is clearly greater than that of the membranes dried at other temperatures. In case of the ideal selectivity, the average ideal selectivity of the membranes dried at 225°C and 25°C were comparable. Similarly to the ideal selectivity,

permselectivity of the membranes post-treated at 120°C is lower than for the membranes post-treated at other temperatures.

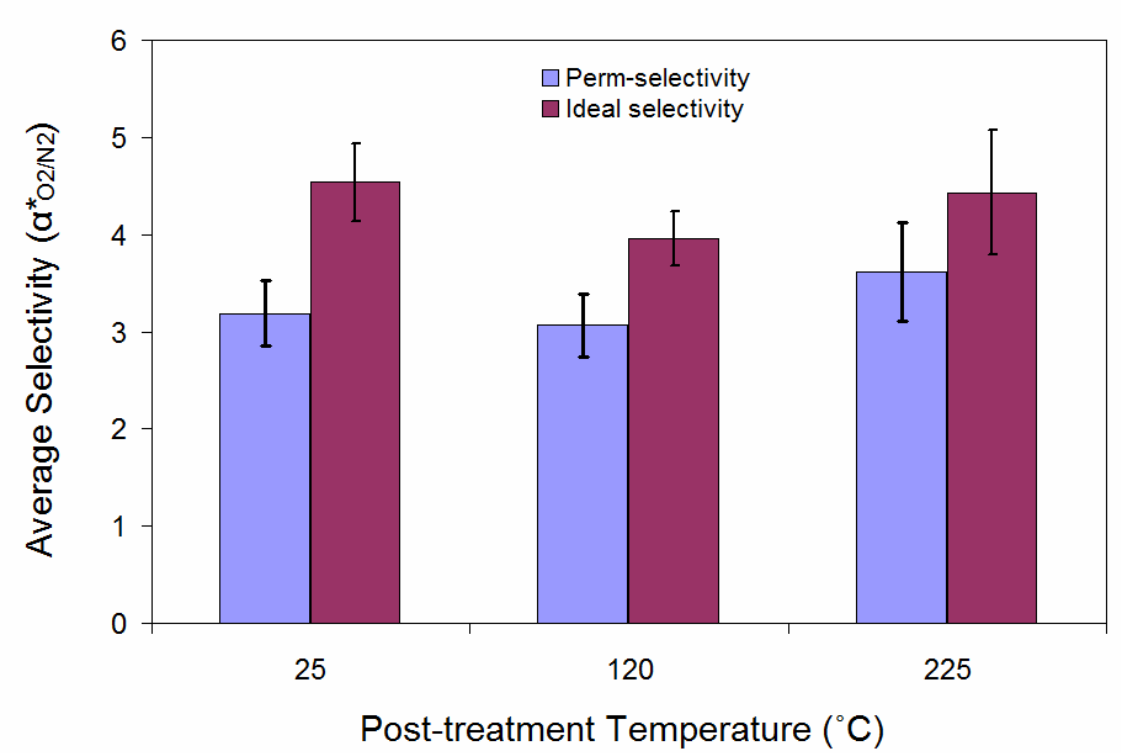

Figure 4.13 Effect of post-treatment temperature on perm-selectivity of EPMM membranes. For comparison the ideal selectivity data previously presented in Fig. 4.5 is also reproduced in this figure.

4.1.3. Summary of gas performance results

From the preceding discussion it is evident that the anticipated effects of the theoretical Si-loading on the permeability of selectivity of the synthesized EPMM membranes are not present. As a matter of fact, it appears that both permeability and selectivity of the EMPP membrane are not related with the theoretical Si-loading, or if they are related to the theoretical Si-loading, these effects are smaller than the variation in

transport properties for a given type of membrane. Moreover, if anything, introduction of the inorganic particles deteriorates the gas transport properties of the EPMM membranes compared to those of the reference PPO membrane. While there were some individual EPPM membranes with the gas transport properties better than those of the reference PPO membranes, these properties could not be reproduced by following the identical synthesis protocol.

A lack of any effect of the theoretical Si-loading on the properties of the EPMM membranes and poor reproducibility of the gas transport properties of the membranes synthesized following identical synthesis protocol, might be an indication of the problem in the synthesis protocols. More specifically, it is possible that the actual Si-loadings of the EPMM membranes might not correspond to the theoretical Si-loadings used as a key parameter in the preceding discussion. More insight to the reasons for the lack of any evident trends between the theoretical Si-loading and the gas transport properties will be available after analysis of the other characterization results, which are presented and discussed in the proceeding sections.

4.2. Analysis of the glass transition temperatures

The DSC analysis can provide an indirect proof of the formation of inorganic particles dispersed in a continuous PPO phase of the EPMM membranes. More specifically, the presence of inorganic phase is expected to decrease the mobility of the polymeric chains

leading to an increase in the glass transition temperature T_g of the EPMM membranes compared to the T_g of the base PPO membranes. It is important to note that in previous research, the opposite was observed, i.e., the T_g of the EPMM membranes was lower compared to the T_g of PPO. Moreover, the difference between the two increased with the Si-loading (Sadeghi, 2007). This unexpected result was attributed to the presence of residual solvent and/or non-reacted TEOS and/or residual n-octanol surfactant, because the EPMM membranes synthesized in previous study were post-treated only at 120°C, i.e., considerably below the T_g of PPO. It is well known that residual quantities of any of these components, which can only be removed completely above the T_g of the base polymer, may plasticize the polymeric chains leading to a decrease in the observed T_g. As a result, some EPMM membranes synthesized in this work were post-treated at 225°C, i.e. above the T_g of PPO.

The T_g of the synthesized EPMM membranes, which had undergone complete gas permeation/separation analysis, were determined by following the procedure discussed in Section 3.3.1. Fig. 4.14 presents the plot of the T_g of EPMM membranes as a function of the theoretical Si-loading for the membranes post-treated at 25° and 225°C. Contrary to what was expected, there is no trend between the T_g and the theoretical Si-loading. On the other hand, at the same Si-loading, T_g may vary from 183°C to 216°C. Considering the post-treatment temperature, it appears that using 225°C as opposed to 25°C does not lead to a greater T_g of the resulting membrane, which undermines the anticipated effect of the

post-treatment temperature, in particular the post-treatment above the T_g of the base polymer.

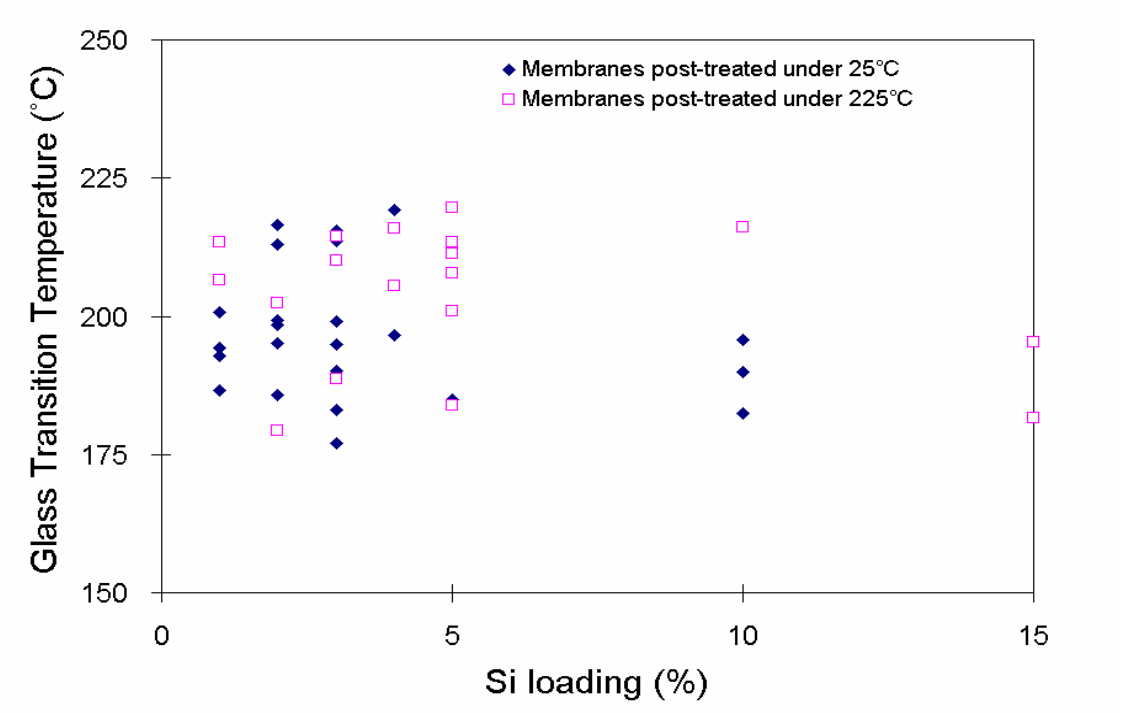

Figure 4.14 The glass transition temperature of the EPMM membranes, post-treated at 25°C and 225°C, as a function of the theoretical Si-loading.

In addition, most T_gs in Fig. 4.14 are less than 217.2°C, which corresponds to the T_g of the PPO membrane. Therefore, assuming that the polymerization of TEOS had occurred; it appears Si loading generally leads to a decrease, rather than an increase, in the glass transition temperature, which is consistent with the results reported by Sadeghi (2007). Interestingly, a few exceptions of the EPMM membranes with the T_g close to or greater than 217.2°C include both the membranes post-treated at 25°C and 225°C.

In conclusion, the results pertaining to the DSC analysis did not yield the expected

results related to the effect of the theoretical Si-loading and the post-treatment temperature on the T_g of the synthesized EPMM membranes. On the other hand, theses results, which show no expected trends, are consistent the results pertaining to gas permeation/separation characterization discussed in Section 4.1.

4.3. The actual inorganic loading and the structure of inorganic phase

The most important variable in this work is the Si-loading in the final EPMM membrane. Up to this point, the Si-loading in the EPMM membranes was represented by the theoretical loading based on the amount of TEOS added to the primary emulsion in the process of the preparation of the casting emulsion. This approximation is valid only when the complete polymerization of TEOS occurs. To determine the actual Si-loading in the synthesized EPMM membranes, after the completion of all gas permeation / separation tests, they were analyzed by inductively coupled plasma mass spectroscopy (ICP-MS). In addition, the actual structure of the inorganic phase in the EPMM membranes was determined by the ^{29}Si NMR and ^{27}Al NMR techniques.

4.3.1. Inductively coupled plasma mass spectrometry (ICP-MS)

The results of the ICP-MS analysis are presented in Fig. 4.15, in which the actual silica content in the EPMM membranes is plotted as a function of the theoretical Si-loading. The results shown in Fig. 4.15 distinguish between the membranes

post-treated at 25°C and 225°C.

If all TEOS in the secondary emulsion had polymerized, the results in Fig. 4.15 should follow a straight line of slope 1. On the other, in case of incomplete polymerization the actual silica content should at least increase with the theoretical Si-loading. However, examination of the data in Fig. 4.15 does not reveal any of the above trends. It appears that the actual silica content is not related to the theoretical Si-loading. Moreover, regardless of the theoretical Si-loading, the actual silica content in the EPMM membranes is very low, with the maximum values reaching 0.9 wt%. In addition, for a given theoretical Si-loading, the actual silica content varies widely from 0.446% to 0.917%.

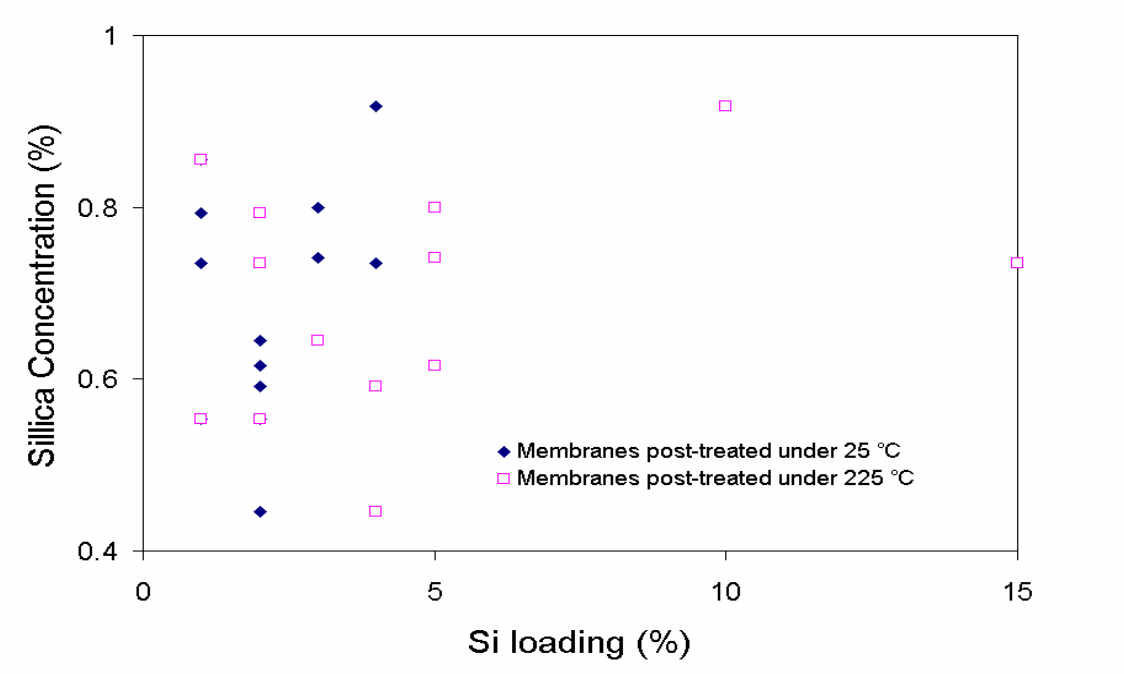

Figure 4.15 The actual silica concentration in the synthesized EPMM membranes, determined by ICP-MS analysis, as a function of the theoretical Si-loading.

For the theoretical loadings for which the analysis was performed with the membranes post-treated at both 25°C and 225°C, the actual silica content does not seem to be affected by the post-treatment temperature. This finding is important, because on the one hand, a lack of any correlation between the actual silica content and the theoretical Si-loading, as well as very low actual silica contents may suggest that polymerization of TEOS had not occurred at all. In this case, the detected silica by the ICP-MS analysis would originate from a non-reacted TEOS remaining in the EPMM membranes as residual. On the other hand, if the entire silica content originates from non-reacted, residual TEOS, the actual silica content in the membranes post-treated at 25°C should be greater than that for membranes post-treated at 225°C. This is the case for the theoretical loadings of 3% and 4% but not for the theoretical loadings of 1% and 2%. Therefore, it appears that some of the silica content detected by the ICP-MS is coming from the polymerized TEOS, in particular in the case of the EPMM membranes post-treated at 225°C.

Another component that was sought in the ICP-MS analysis was aluminum. Aluminum hydroxonitrate was a part of the aqueous solution, which apart from providing the desired pH for the polymerization of TEOS could also participate in the actual polymerization. Fig. 4.16 presents the plot of the actual aluminum concentration in the synthesized EPMM membranes as a function of the theoretical Si-loading. It can be noticed that the detected amounts of Al does not exceed 0.05 wt%, which is more than

one order of magnitude less than the actual silica content. Similarly to Fig. 4.15, the actual Al content in the EPMM membranes cannot be correlated with the theoretical Si-loading.

Due to its solubility of in water, any non-reacted aluminum hydroxonitrate should be readily removed during the boiling of the synthesized membranes in de-ionized water. Therefore, the presence of Al could indicate its incorporation into the silica network resulting from the polymerization of TEOS. On the other hand, the presence of the Al at such a low concentration level is not a convincing proof for the copolymerization of TEOS with the aluminum hydroxonitrate.

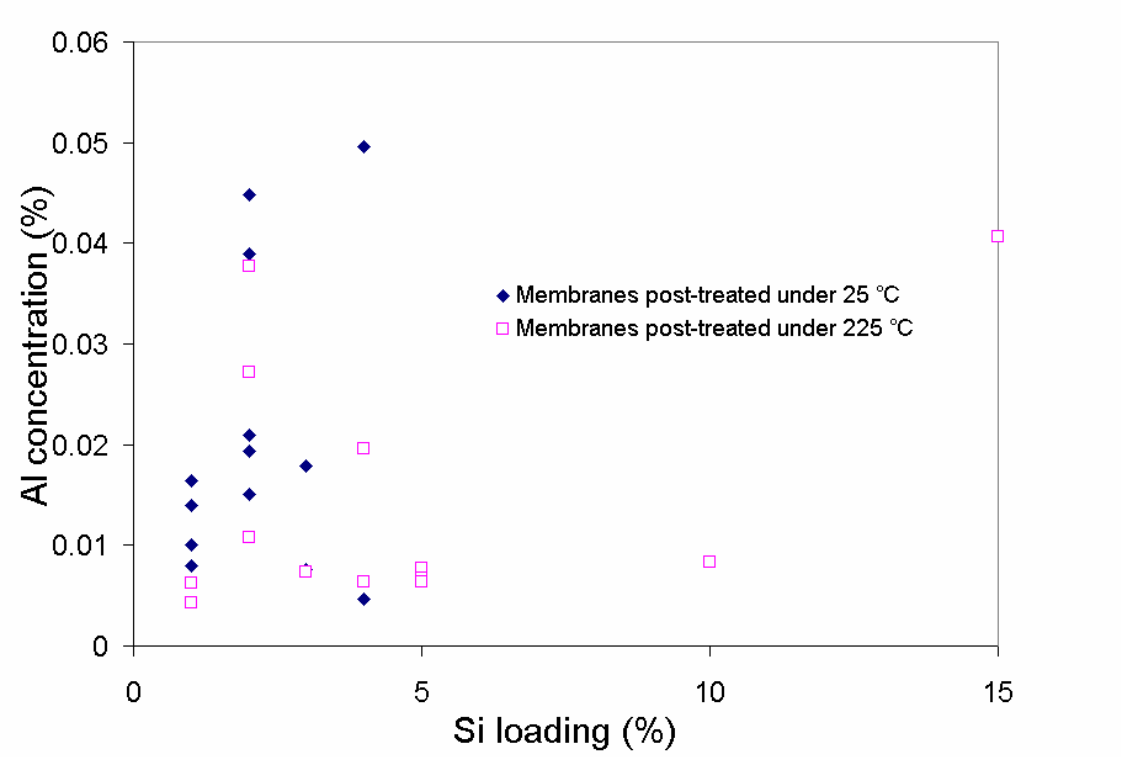

Figure 4.16 The actual alumina concentration in the synthesized EPMM membranes, determined by ICP-MS analysis, as a function of the theoretical Si-loading.

The ICP-MS analysis showing the actual content of silica in the synthesized EPMM, which is much less than the theoretical Si-loading, explains the lack of any relationship between the theoretical Si-loading and the membrane performance. Fig. 4.17 plots the permselectivity and the ideal O_2/N_2 selectivity as a function of the actual silica content. However, similarly to the theoretical Si-loading, there is no correlation between the actual silica concentration and the performance of the membrane.

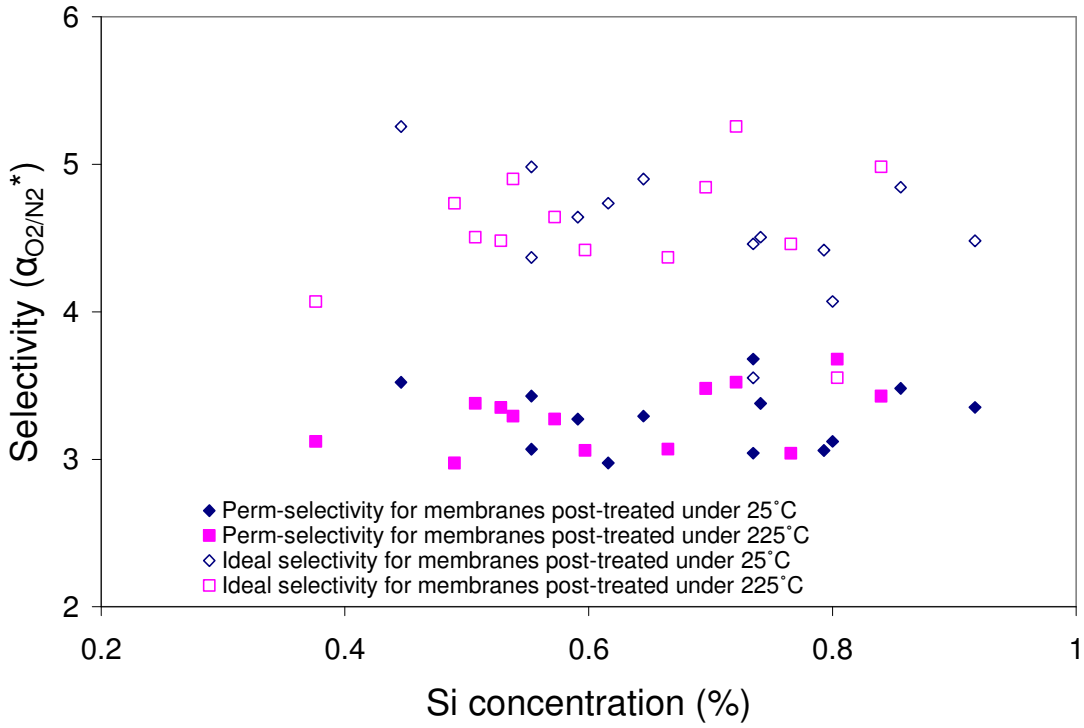

Figure 4.17 Permselectivity and ideal O_2/N_2 selectivity as a function of the actual silica concentration in the EPMM membranes.

4.3.2. ^{29}Si NMR

From the discussion so far, it is evident that the actual silica content in EPMM membranes was far below to what was expected based on the amount of TEOS used for the preparation of the casting emulsion. Moreover, because of a lack of any correlation between the actual silica concentration and membrane performance, it becomes questionable where the detected silica comes from? If all non-reacted TEOS were removed during the post-treatment, the detected silica would be coming from the polymerized TEOS. At the other extreme, the detected silica could be coming entirely from non-reacted TEOS, which was not removed during the post-treatment process. It is also possible from that the detected silica is coming both from the polymerized TEOS and non-reacted, residual TEOS. To answer this question, ^{29}Si NMR of selected EPMM membranes was performed. Since both, ICP-MS and ^{29}Si NMR are destructive techniques, when a membrane was tested by ICP-MS it could not be tested by ^{29}Si NMR and vice versa. Moreover, the latter required a sample in form of a powder, but the EPMM membranes could not be crushed even in liquid nitrogen; therefore, they had to be cut manually into a very small pieces, which was very tedious and time consuming.

In addition to the ^{29}Si NMR analysis of EPMM membranes, this technique was also used to analyze the powder produced during the gelation tests, the results of which are presented in Fig. 4.18. Considering this figure, it is evident that there are three overlapping peaks, which can be resolved to the following positions: -95.58 ppm, -101.93

ppm and -108.86 ppm. These positions correspond exactly to the positions of the Q_2, Q_3 and Q_4 peaks, which represent the silicon atom connected through the oxygen atom to two, three, and four silicon atoms, respectively (Ruiz-Hitzky et al., 2002). Essentially, the presence of these three peaks Q_2, Q_3, and Q_4 directly proves polymerization TEOS in the gelation test.

Figs. 4.19 and 4.20 present the ^{29}Si NMR spectra of two EPMM membranes having the same theoretical Si-loading of 5%, which were post-treated at 25^{o}C (Fig. 4.19) and 225^{o}C (Fig. 4.20). The two spectra are similar to each other showing a single peak at approximately -82.2 ppm, which corresponds to hydrolyzed TEOS (Ruiz-Hitzky et al., 2002). It is clear that there are no Q_2, Q_3 or Q_4 peaks in Figs. 4.19 and 4.20. This indicates that all silica present in these two EPMM membranes, following the post-treatment process and all gas permeation/separation tests, comes from a residual, non-reacted TEOS. It is important to note that the size of the pick relative to the base line in Figs 4.19 and 4.20 is quite different. Assuming that the size of the pick increases with the amount of the component being detected, there is much more residual TEOS in the membrane post treated at 25^{o}C than in the membrane post treated at 225^{o}C.

The ^{29}Si NMR results presented here prove that there was a serious problem with the synthesis protocol of the EPMM membrane. Essentially, the assumed polymerization of TEOS had not occurred, at least not in the two membranes that were randomly picked for the ^{29}Si NMR analysis. At the same time, TEOS did polymerize in all gelation tests. It

is important to emphasize that in the latter case, the aqueous solution containing aluminium in the required Keggin structure was mixed with TEOS in ethanol, and because of the miscibility of ethanol and water the polymerization of TEOS was taking place in a single phase. On the other hand, because of insolubility of PPO in ethanol, in the case of the actual casting emulsion, TEOS was dissolved in TCE, which had already contained PPO and the dispersed aqueous solution with the aluminum in the Keggin structure. For the polymerization to occur, TEOS had to be first hydrolyzed, which, because of insolubility of TEOS in water, could occur only at the boundary between the aqueous and the TCE phases. This could have severely limited the extent of polymerization of TEOS in the casting emulsion.

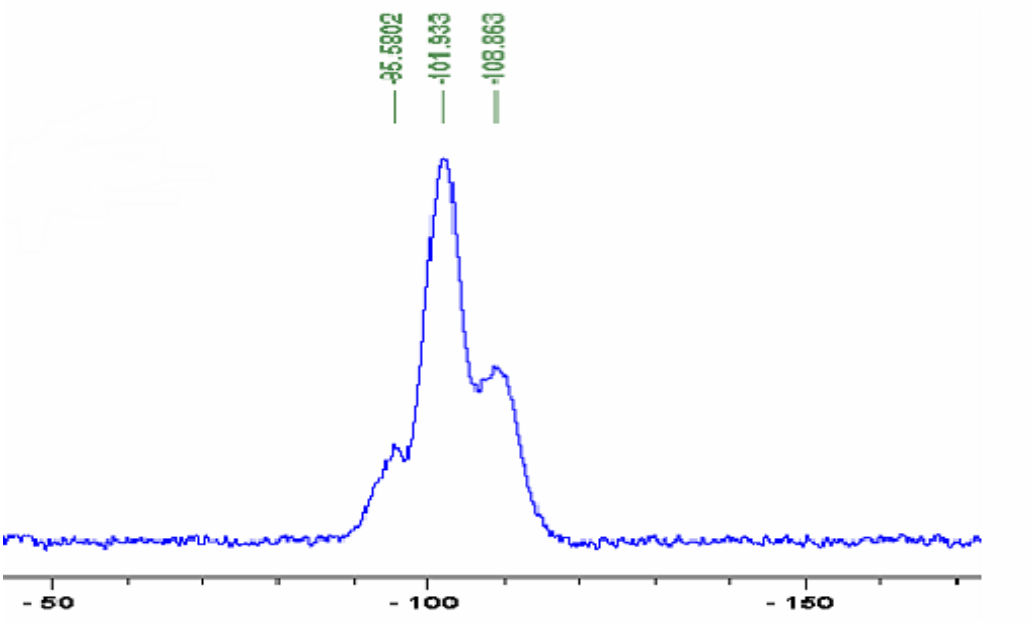

Figure 4.18 The ^{29}Si NMR spectrum of the polymerized TEOS powder synthesized in a gelation tests.

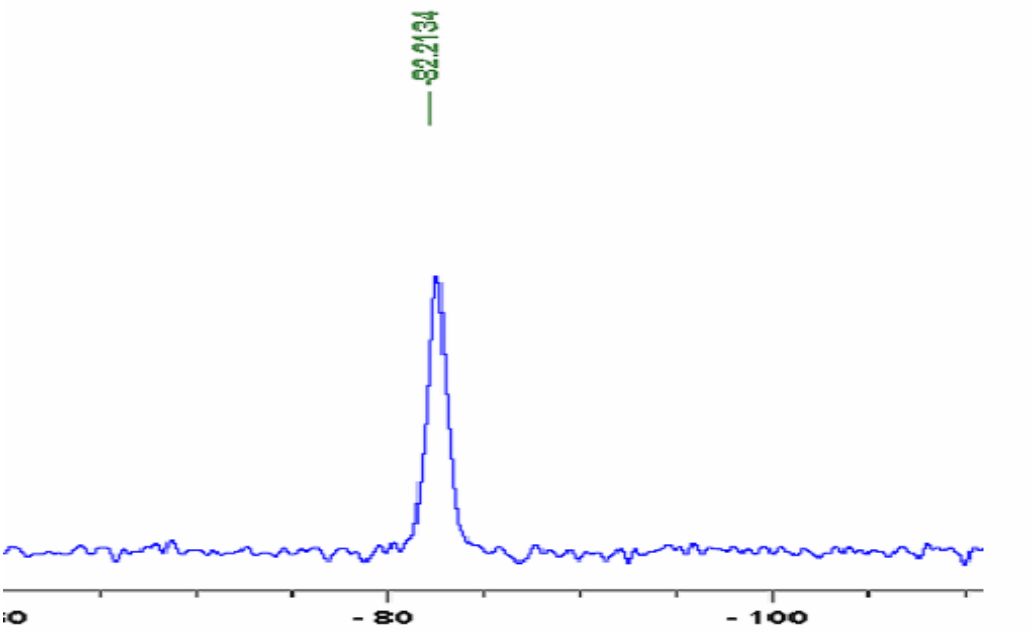

Figure 4.19 The ^{29}Si NMR of the EPMM membrane with the theoretical Si-loading of 5%, which was post-treated at 25^{o}C.

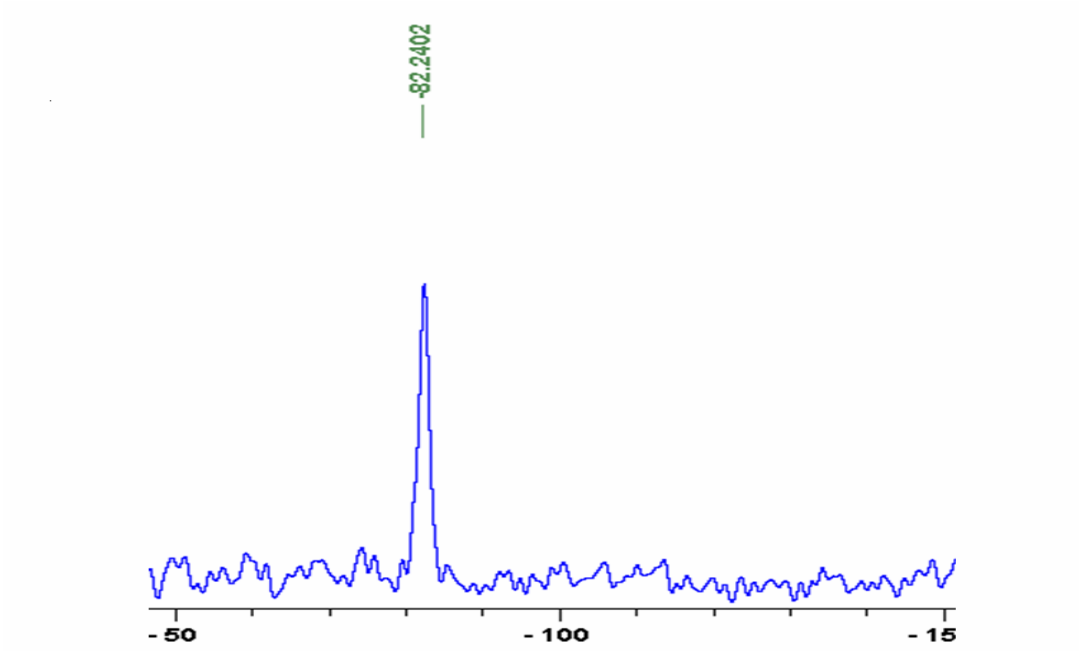

Figure 4.20 The ^{29}Si NMR of the EPMM membrane with the theoretical Si-loading of 5%, which was post-treated at 225^{o}C.

Chapter 5.
Second Phase of the Project

As discussed in the previous Chapter, the membrane synthesis protocol adapted from the previous work by Sadeghi (2007) was not successful. Consequently, the continuation of the project required fundamental changes in the synthesis protocol to ensure the polymerization of TEOS in the casting emulsion. This has led to the second phase of this project. The results of the second phase of the project, which are presented in this chapter, are divided into three parts. First, the reasons that could have prevented the polymerization of TEOS in the old synthesis protocol are presented, and the factors affecting the rate of TEOS polymerization are discussed. The second part presents a new gelation protocol, which allows the investigation of the key parameters of the polymerization reaction in the environment similar to the one in the actual casting emulsion. In the third part, the parameters established in the second part are applied for the synthesis of new EPMM membranes. The properties of the new EPMM membranes are determined and discussed.

5.1. Critical Analysis of the Synthesis Protocol

According to the results discussed previously, the silica in the old EPMM membranes originated from the non-reacted TEOS. The absence of the polymerized TEOS could indicate that either the conditions required for the polymerization to take place were not present in the casting emulsion, or that the reaction rate was insufficient to form an appreciable amount of the polymerized TEOS during the time allowed for the reaction.

As indicated in Chapter 3, before every synthesis, a gelation test was performed, which was essentially a single phase polymerization of TEOS, and the emulsion synthesis were carried only after a successful gelation test. Table 5.1 provides a detailed comparison of the reaction conditions for the gelation tests and the synthesis of the EPMM membranes.

Table 5.1 Comparison of the gelation test solution and the casting emulsion.

Parameter	Gelation Test	Casting Emulsion
Solvent of Phase 1	Ethanol	TCE
Solvent Concentration in Phase 1 (%)	60.0	94.1
Solvent of Phase 2	Water	Water
Number of Phases	1*	2
Surfactant	N/A	1-Octanol
Surfactant concentration (%)	N/A	0.313
TEOS concentration (%)	20.0	1.50
Aluminum hydroxonitrate concentration (%)	20.0	0.517
Max Reaction time (min)	8	60

* One phase in gelation test because of miscibility of Ethanol and Water

The most fundamental difference between the reaction conditions in the two systems is the fact that the gelation tests were carried out in a single phase while the polymerization of TEOS during the membrane synthesis was carried out in a two-phase system. The presence of ethanol in the gelation test enabled TEOS to be miscible with an aqueous phase containing aluminum hydroxonitrate, which leads to the solution polymerization of TEOS. On the other hand, during the synthesis of EPMM membranes, the polymerization could only take place at the surface of the emulsion droplets, which must had led to much lower reaction rates compared to the single phase system. This difference was known ahead of time; however, it was assumed that increasing the interphase area by decreasing the size of the droplets would lead to sufficient reaction rates in the emulsion system.

In addition to the above fundamental difference, the concentration of the reactants in the gelation test and the actual synthesis process were quite different. It can be noticed that the concentration of the reactant, TEOS, in the gelation system was 13.3 times greater than that in the casting emulsion. At the same time, the overall concentration of aluminum hydroxonitrate was 39 times greater in the gelation system compared to the casting emulsion. The difference in the reactants concentrations may have also been responsible for slowing down the rate of the TEOS polymerization in the casting emulsion.

The kinetics of polymerization of TEOS, both in a single phase and in water-in-oil (W/O) emulsion was reported by Sanchez and McCormick (1992). In both cases, the

polymerization kinetics was observed to be strongly dependent on the concentration of TEOS, the concentration of water and the concentration of a catalyst. In case of the polymerization of TEOS in the presence of aluminum hydroxonitrate, since the latter takes part in the reaction and with a large excess of water, the rate of the reaction is expected to be governed by the following equation:

$$-\frac{d[TEOS]}{dt} = k[TEOS]^x \left[Al_{13}^{7+}\right]^y \qquad 5.1$$

where, [TEOS] and $[Al_{13}^{7+}]$ are the concentrations of TEOS and Al_{13}^{7+} functional groups, k is the reaction rate constant, and x and y are the orders of [TEOS] and $[Al_{13}^{7+}]$, respectively. Since TEOS and aluminum hydroxonitrate were added into emulsion with a stoichiometric amount, the above equation simplifies to:

$$-\frac{d[TEOS]}{dt} = k[TEOS]^{x+y} \qquad 5.2$$

According to Eq. (5.2), the reaction rate depends on the $(x+y)^{th}$ order TEOS concentration, where the sum of x and y in single phase reaction system was reported to be equal to unity (Chang and Fogler, 1996). At time t, the amount of the reacted TEOS can be expressed as:

$$[TEOS]_{reacted} = [TEOS]_0 (1 - \exp^{-kt}) \qquad 5.3$$

where $[TEOS]_0$ is the initial concentration of TEOS in the emulsion. According to Eq. (5.3), for the difference in concentrations of TEOS in the gelation system and the casting

emulsion, a much longer reaction time is required for the polymerization reaction to reach a reacted silicon concentration detectable with ^{29}Si NMR. Furthermore, as already stated, in the latter case the reaction can occur only at the boundary of the two phases, which decreases the reaction rate constant significantly. As a result, and for a given reaction time, the amount of the polymerized TEOS would decrease accordingly.

Based on the above consideration, to achieve a higher amount of the polymerized TEOS in the new synthesis protocol it was decided to:

- Use compatibilizer (ethanol) instead of surfactant (1-octanol)
- Increase the reactant concentrations
- Increase the reaction time

5.2. Development of new synthesis protocol

The rationale behind the replacement of 1-octanol by ethanol in the new synthesis protocol was to allow the polymerization of TEOS in a single phase. However, in the system involving PPO as a polymer and TCE as its solvent, it is impossible to obtain a single phase regardless of the amount of ethanol used. While ethanol is miscible with TCE, which is used as a PPO solvent, PPO is not soluble in ethanol. However, the ethanol added to the emulsion, is split between the aqueous phase and the PPO solution phase. Consequently, the aqueous phase may become soluble for TEOS, and as a result,

the polymerization of TEOS could occur in the bulk aqueous phase rather than just at its boundary.

5.2.1. Gravimetric Powder Method

A definite verification of the validity of the new synthesis protocol in the actual casting emulsion would require the ^{29}Si NMR and ICP-MS analyses. However, these analyses, since we did not have direct access to the relevant equipment were subcontracted to an outside lab. It took up to four months to obtain the ^{29}Si NMR and ICP-MS results reported in the previous chapter.

To avoid a long turnover for the ^{29}Si NMR and ICP-MS results, we have developed a method, which is referred to as a Gravimetric Powder Method, for indirect assessment of the polymerization of TEOS in the emulsion system. Compared to the new synthesis protocol for the EPMM membranes, the polymerization of TEOS in the Gravimetric Powder Method is carried out in the emulsion system with only the solvent rather than the polymer solution. The rationale for the Dry Powder Method can be explained by considering the volatility of species involved in the synthesis of EPMM membranes, which are listed in Table 5.2. A species is considered to be volatile when it leaves no residual after a prolonged evaporation. Consequently, the non-reacted TEOS is considered as a volatile species while the polymerized TEOS is a non-volatile species. As a result, the extent of polymerization of TEOS in casting emulsion could be assessed on

the basis of an increase in the mass of non-volatile species in the system.

The problem with this approach in the actual casting emulsion arises from the fact that the polymer constitutes the largest non-volatile mass. Consequently, the detection of an increase in the mass of nonvolatile species due to the polymerization of TEOS in the actual casting emulsion might not be feasible. On the other hand, when the continuous phase is a pure solvent rather than a polymer solution, the mass of the residuals after their extensive evaporation on drying, becomes very sensitive to the progress of the polymerization reaction. This represents the basis for the Gravimetric Powder Method.

Table 5.2 The species in the casting emulsion and their volatility.

Species	Volatile
Water	Yes
Ethanol	Yes
TCE	Yes
TEOS	Yes
Na salt	No
Al-Si complex	No
Al salt	No
PPO	No

The protocol of the Gravimetric Powder Method is presented schematically in Fig. 5.1. In the first step the primarily emulsion was formed by combining 0.1 mL of aluminum hydroxonitrate solution with 0.3 mL of ethanol and 10 mL of TCE, and then ultrasonication of the mixture at a specific power level for one minute. Apart from using pure solvent and ethanol rather than a polymer solution and 1-octanol, respectively, the

volume of the aluminum hydroxonitrate solution was twice that of the largest theoretical inorganic loading of the old synthesis protocol. In the second step, a specific amount of TEOS was added into the primary emulsion and the system was ultrasonicated for a specific period of time at power level of 3 followed by magnetic stirring for a specific period of time. The total time of the ultrasonication and the magnetic stirring is considered to be the reaction time. In the third step, the emulsion was transferred to a Petri dish to evaporate all volatile components and the resulting powder was dried until a constant mass.

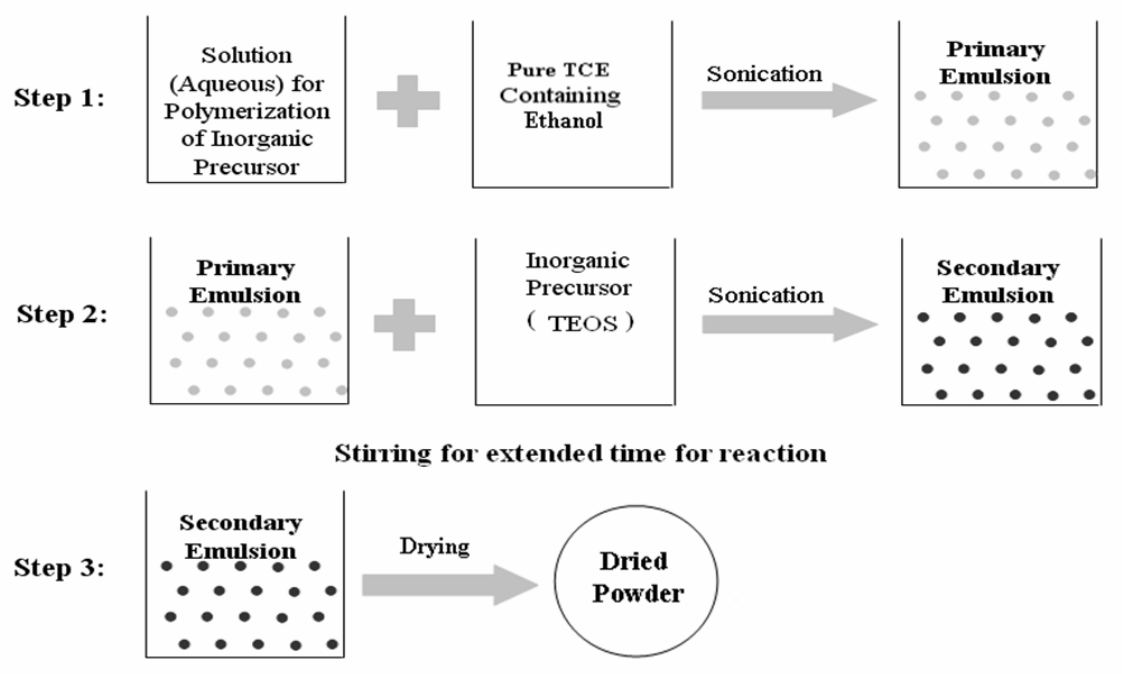

Figure 5.1 The protocol for the Gravimetric Powder experiment.

If there were no chemical reaction, the dried powder would be constituted of the

aluminum hydroxonitrate and sodium carbonate used in the preparation of the aqueous solution. For 0.1 mL of the aqueous solution and the concentrations of the aluminum nitrate and sodium carbonate described in Chapter 3, the calculated mass of the residual was 0.0305 g. The experimental average residual content from 0.1 mL of the aqueous solution was determined to be 0.0308 g, which is in an excellent agreement with the theoretical value. On the other hand, evaporation of 1.0 mL of pure TEOS did not leave any detectable residual. Therefore, the mass of 0.0305 g was considered to be a threshold value in the Gravimetric Powder experiments.

Apart from providing a proof for the emulsion polymerization of TEOS in a system similar to the new EPMM synthesis protocol, the objective of the Gravimetric Powder experiments was to evaluate the effect of some parameters on the extent of the emulsion polymerization of TEOS. In particular, the effects of the ultrasonication power level in the 1st step of the procedure, the ultrasonication time in the 2nd step, the total reaction time and the volume of TEOS used were of interest. Table 5.3 summarizes the parameters of interest along with the levels at which these parameters were investigated.

Table 5.3 Experiment parameter setting for the Gravimetric Powder experiments.

Ultra-sonication power level in Step 1	3	4	5	6	7		
Ultra-sonication time in Step 2 (min)	0	1.5	3	7	15	30	60
Total reaction time (h)	1	2	4	8	16	24	48
Volume of TEOS (mL)	0.2	0.3	0.5	0.75	1.0		

5.2.1.1.Effect of the total reaction time

In the synthesis of the EPMM membranes the total reaction time was defined from the moment a specific volume of TEOS was added to the primary emulsion, until the secondary emulsion was used for casting the membrane. During the reaction time the emulsion was either ultrasonicated or magnetically stirred. For the consistency, the total reaction time in the Gravimetric Powder Method is defined in the same way, except the end of the reaction time is marked by transferring the emulsion to a Petri dish.

Figure 5.2 presents the effect of the total reaction time on the mass of the dried powder. The figure presents two curves, one for the experiments in which the secondary emulsion was ultrasonicated for 7 minutes and the other one for the experiments with 30 min ultrasonication. It should be noted that as indicated in Chapter 3, to avoid overheating of in the ultrasonicated emulsion, the ultrasonication step was performed in a 30 s of / 30 s off mode. Consequently, ultrasonication for 7 minutes indicates the net ultrasonication time, while the total time for the ultrasonication step, which includes the off periods, is twice the provided ultrasonication time. In all experiments shown in Fig. 5.2 the primary emulsion was ultrasonicated at the power level 5 for one minute and the stoichiometric amount TEOS was used.

It can be noticed in Fig. 5.2 that regardless of the ultrasonication time and the total reaction time, the amount of the dried powder is greater than the threshold mass of 0.0308 g with the maximum amount of 0.0678 g. Moreover, it is evident that the mass of

the dried powder increases with the reaction time, in particular in the first 24 hours. On the other hand, the mass of the dried powder for 48 hr is comparable to that for 24 hr of the total reaction time. Fig. 5.2 also shows that for a given total reaction time, the amount of powder formed in the experiments in which the secondary emulsion was ultrasonicated for 30 min is significantly greater than that in the experiments in which the secondary emulsion was ultrasonicated for only 7 min.

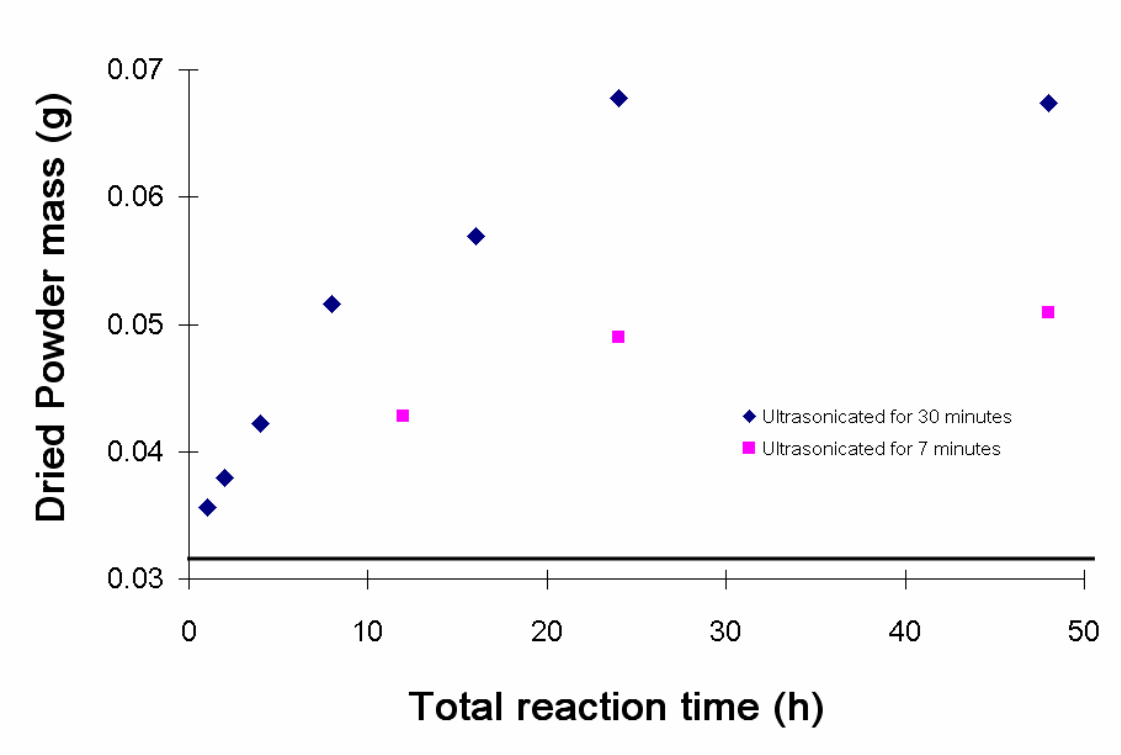

Figure 5.2 Effect of extended reaction time on mass of the dried powder. Primary emulsion ultrasonicated at the power level 5 for 1 min. Polymerization with the stoichiometric amount of TEOS relative to the aluminum hydroxonitrate.

5.2.1.2.Effect of the amount of TEOS

Figure 5.3 presents the effect of amount of TEOS used on the mass of the dried powder. In this series of experiments, the primary emulsion was ultrasonicated at the power level 5 for one minute, followed by the addition of different volumes of TEOS ranging from 0.2 mL to 1 mL, and the ultrasonication of the secondary emulsion for 30 min followed by the magnetic stirring for the total reaction time of 24 h. According to the stoichiometry of the reaction between the aluminum hydroxonitrate and TEOS, using 0.1 mL of the aqueous solution requires 0.29 mL of TEOS. Therefore, the smallest volume of TEOS of 0.2 mL used in this series experiments represents 69% of the required stoichiometric amount of TEOS. In all other experiments the volumes of TEOS used were either stoichiometric or in excess with the latter as large as 245%.

It is evident that increasing the amount of TEOS added to the emulsion increases the mass of the dried powder. Consequently, using the excess of TEOS in the casting emulsion system should increase the actual inorganic loading of the new EPMM membranes. In case of the Gravimetric Powder method there is no limit to the excess of the TEOS used. However, in case of the actual membrane synthesis protocol, a large excess of TEOS could significantly decrease the viscosity of the emulsion, which could lead to the problems in spin coating of the membranes from the emulsion. In addition, because of low volatility of TEOS its complete removal, even at temperatures above the glass transition of the polymer, might be difficult.

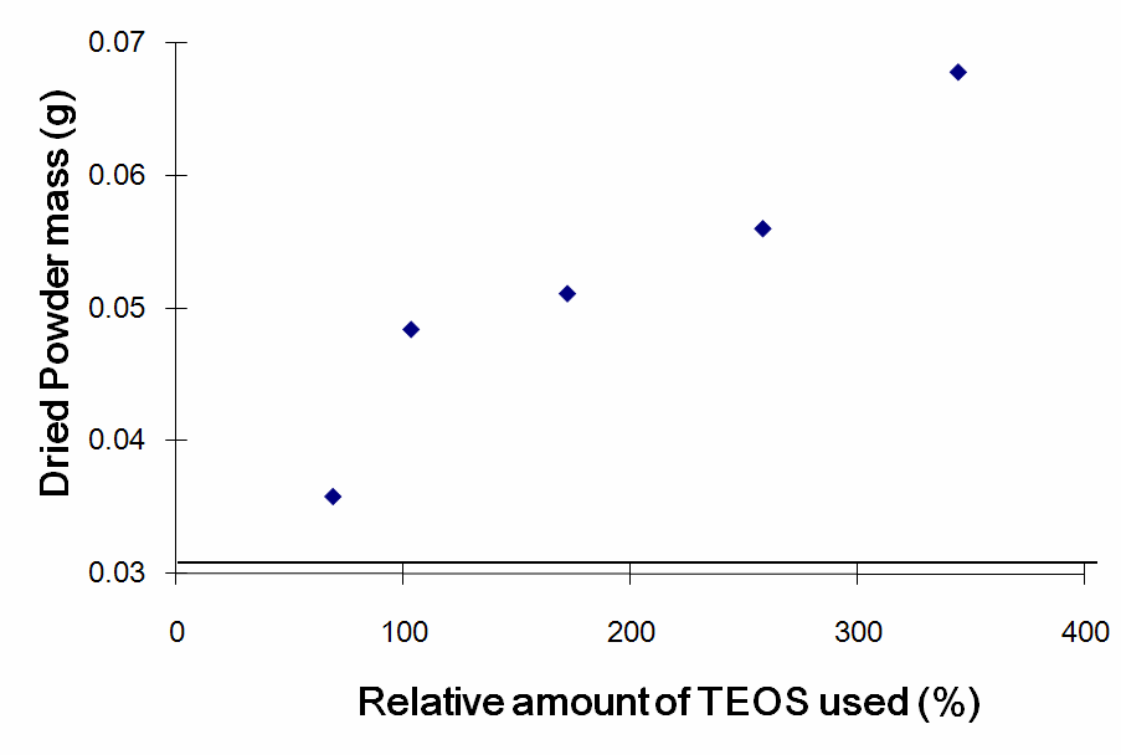

Figure 5.3 Effect of the relative amount of TEOS used on the mass of the dried powder. Primary emulsion ultrasonicated at the power level 5 for 1 min; secondary emulsion ultrasonicated at the power level 3 for 30 min followed by the magnetic stirring for the total reaction time for 24 hr.

5.2.1.3.Effect of ultra-sonication time in of the secondary emulsion

Figure 5.4 presents the effect of the ultrasonication time of the secondary emulsion on the mass of the dried powder. In this series of experiments, the conditions in the primary emulsion (ultrasonication for one minute at the power level 5) and the amount of TEOS added (0.3 mL) were the same. The secondary emulsion was then ultrasonicated at the power level 3 for different times ranging from 3 min to 60 min. Following the

ultrasonication step, the emulsion was further mixed using a magnetic stirrer. The total reaction time, i.e., the time during which the secondary emulsion was mixed by ultrasonication or by magnetic stirring was the same in all experiments and equal to 24 hours.

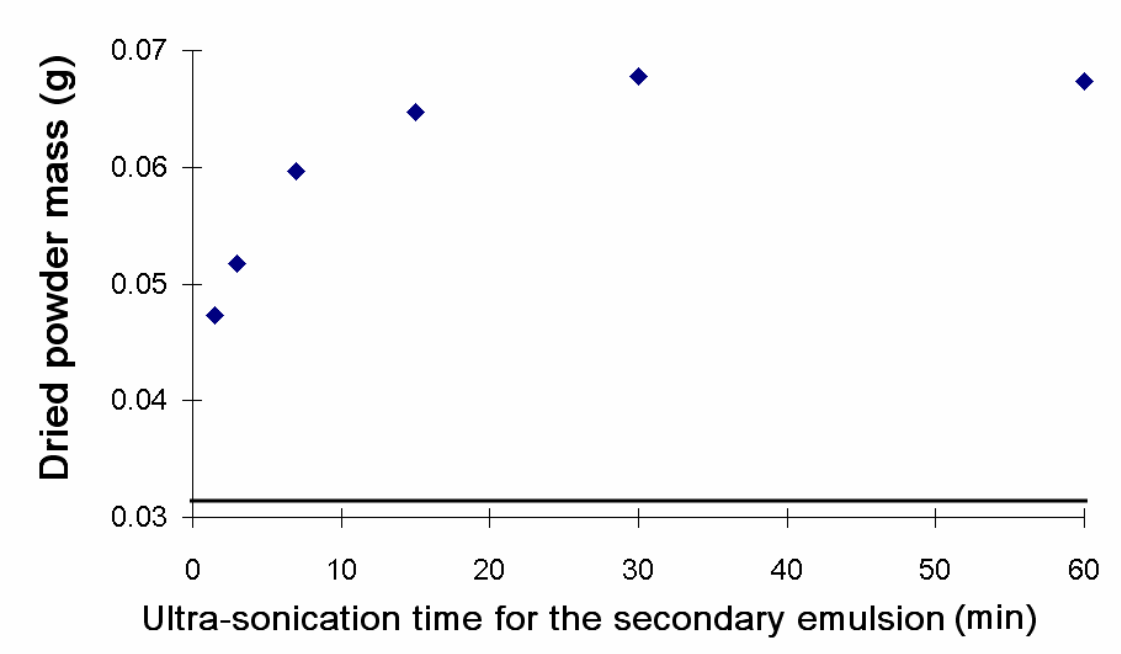

Figure 5.4 Effect of ultra-sonication time of the secondary emulsion the mass of the dried powder. Primary emulsion ultrasonicated at the power level 5 for 1 min; Polymerization with the stoichiometric amount of TEOS for the total reaction time of 24 hr.

It can be noticed in Fig. 5.4 that for short ultrasonication times (< 15 min) the mass of the dried powder is very sensitive to the actual ultrasonication times. Considering that following the ultrasonication the secondary emulsion was continued to be mixed using the magnetic stirring, during which the reaction could also progress, the actual effect of

the ultrasonication time could actually be even stronger than that shown in Fig. 5.4. On the other hand, there is a little difference between the mass of the dried powder for the ultrasonication times of 15, 30 and 60 min. Combining Figs. 5.2 and 5.4 it can be concluded that while ultrasonication is superior to magnetic stirring as a means of promoting the polymerization of TEOS, the former is effective for a relatively short time after the addition of TEOS into the primary emulsion.

5.2.1.4.Effect of ultra-sonication power level in Step 1

The ultrasonication power level in Step 1 plays an important role on the size of the aqueous phase droplets dispersed in the continuous organic phase. The size of the droplets determines the interphase area. In turn, although in the modified synthesis procedure it is expected that TEOS can polymerize not only at the interphase but also inside the droplets, it is expected that increasing the interphase area by decreasing the size of the aqueous droplet should increase the conversion rate of TEOS.

Fig. 5.5 presents the effect of the power level in Step 1 on the size of the aqueous droplets in the primary emulsion. The size of the droplets was determined using a dynamic light scattering (DLS) instrument (Malvern Zetasizer, UK), capable of measuring droplets size in the 0.4 nm - 10 μm range.

As expected the size of the droplet in the primary emulsion decreases with an increase

in the power level. More specifically, in case of the emulsions depicted in Fig, 5.5 the size of the droplets decreases from approximately 1890 nm at the power level of 3, to 1315 nm at the power level of 7. In principle the power level of the ultrasonicator could be increased to the maximum setting of 10; however, at the power level of 8 it was observed that part of the emulsion was lost from the container.

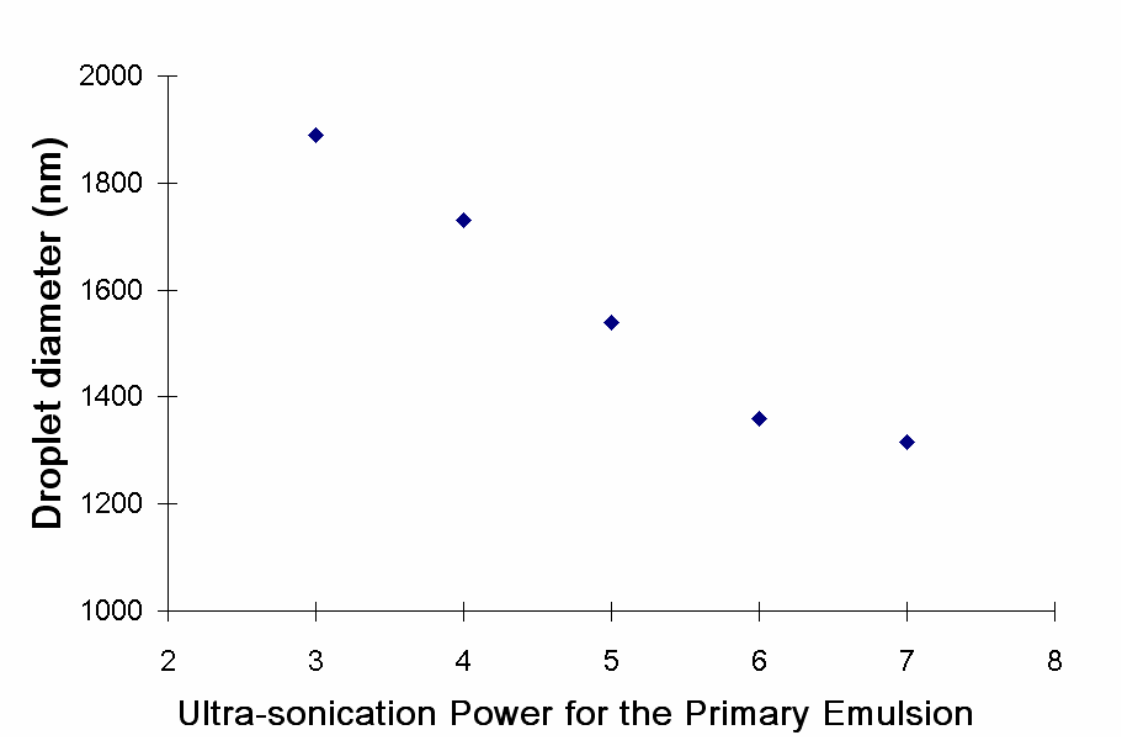

Figure 5.5 Effect of ultra-sonication power on the size of aqueous phase droplets in the primary emulsion. All samples had the same volume and were ultrasonicated for the same time of 1 min.

Fig. 5.6 presents the effect of the effect of the power level in ultrasonication of the primary emulsion on the mass of the dried powder. In this series of experiments, following the ultrasonication of the primary emulsion for 1 min and adding a stoichiometric volume of TEOS, the secondary emulsion was ultrasonicated for 30 min

followed by the magnetic stirring for the total reaction time of 24 h. It is evident from Fig. 5.6 that the ultrasonication power in the primary emulsion strongly affects the mass of the power, which varies from 0.0354 g for the power level of 2 to 0.0764 g for the power level of 7. The dependence of the mass of powder on the power level is particularly strong between the settings 3 and 5.

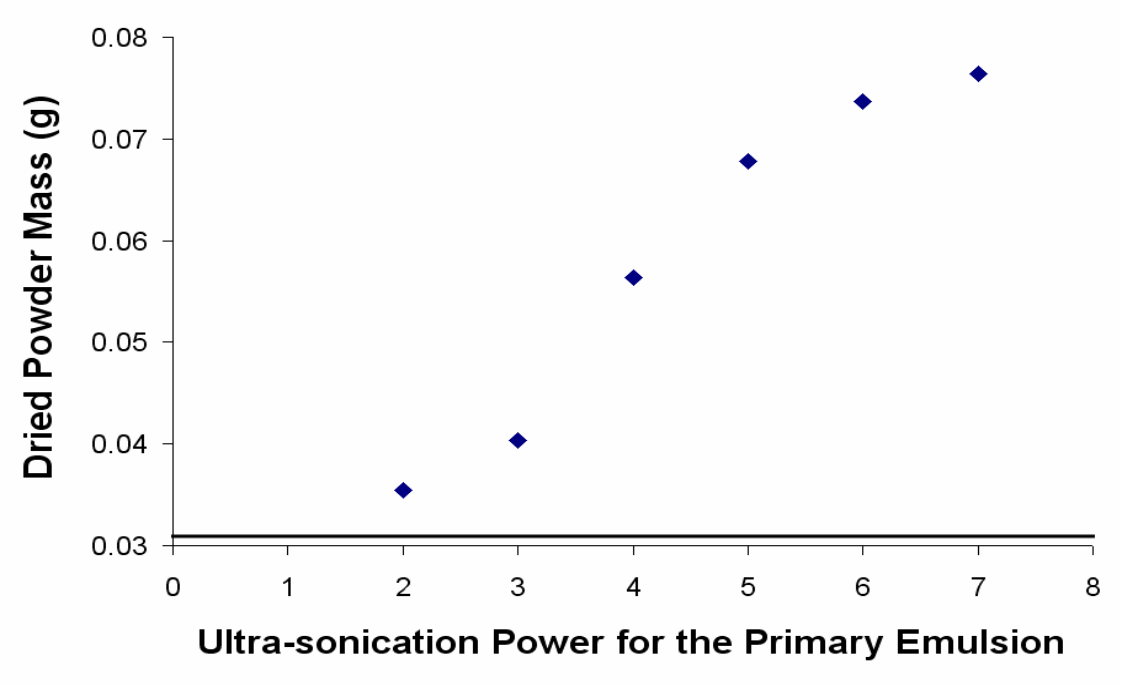

Figure 5.6 Effect of ultra-sonication power in the primary emulsion on the mass of the dried powder. Primary emulsion was ultrasonicated for 1 min followed by polymerization of the stoichiometric amount of TEOS for the total reaction time of 24 hr, of which the reaction emulsion was ultrasonicated for 30 min at the power level of 3.

5.2.2. ^{29}Si NMR result of the dried powder

To validate the Gravimetric Powder experiments and to provide the direct proof of polymerization TEOS in the emulsion system, the dried powder sample was sent to ^{29}Si

NMR analysis. The obtained ^{29}Si NMR results are shown in Fig. 5.7.

There are three overlapping peaks in Fig. 5.7. The major peak near -102 ppm is associated with two smaller peaks at around -96 ppm and -112 ppm. These three peaks correspond to Q_3, Q_2 and Q_4 bounds, respectively. The existence of these three peaks confirms polymerization of TEOS. Moreover, the absence of peaks corresponding to Q_0 and Q_1 bounds indicate complete removal of an unreacted TEOS from the powder that was sent for the analysis.

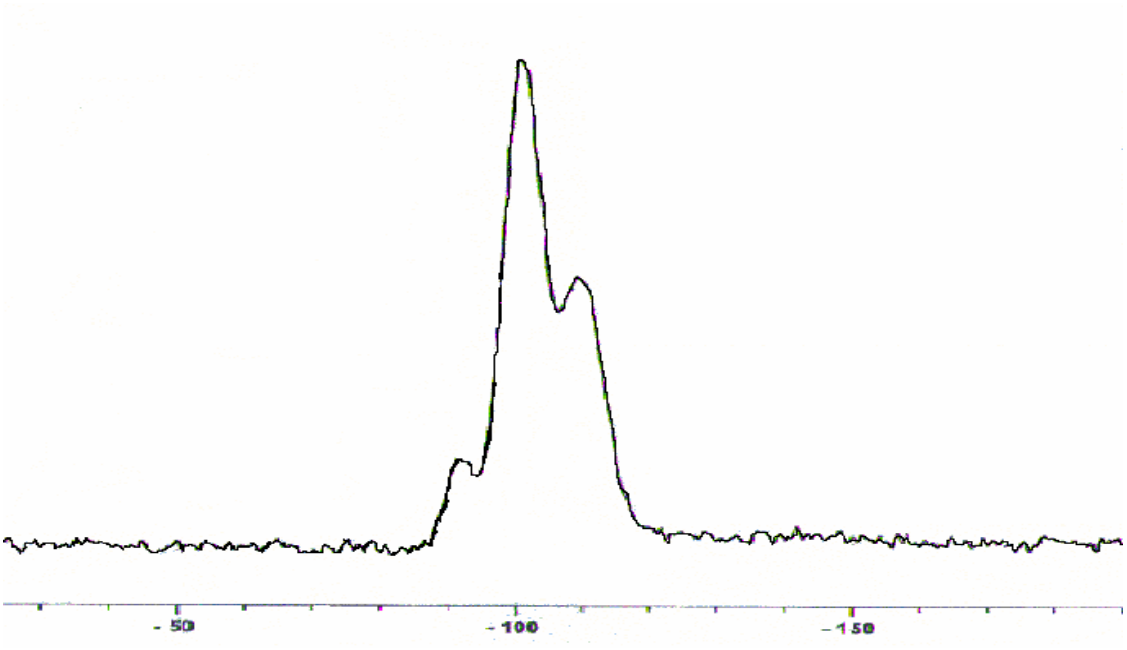

Figure 5.7 ^{29}Si NMR results spectra of the powder synthesized in the Gravimetric Powder Method.

In addition, the fact that there are no peaks other than Q peaks in Fig. 5.7 may indicate that TEOS did not copolymerize with the aluminum hydroxonitrate, as one would expect based on the literature review presented in Chapter 2. In this case, the aqueous solution of aluminum hydroxonitrate with its pH of 3.6 would play only a role a

weak acid catalyst rather than the catalyst and a co-polymerization reactant.

5.2.3. Conversion of TEOS in emulsion polymerization

Combining the results from the Gravimetric Powder Method with ^{29}Si NMR results allows for a rough estimation of the conversion of TEOS in the emulsion polymerization with pure solvent, using the following assumptions:

- Aluminum hydroxonitrate did not copolymerized with TEOS
- Only one kind of Si bond exists in the powder.

The details of the conversion calculations are presented in Appendices A1 and A2. Considering the ^{29}Si NMR spectrum shown in Fig. 5.7, the second assumption is not valid, because there at least three types of bonds present in the analyzed powder corresponding to Q_2, Q_3 and Q_4, respectively. Table 5.4 presents the example of the conversion calculations, subject to the above assumptions, using the results obtained in the experiment in which the primary emulsion was ultrasonicated at the power level of 5 for 1 min, followed by the reaction with 1.0 mL of TEOS for the total reaction time of 24 hours, of which the secondary emulsion was ultrasonicated for 30 min at the power level of 3. In this experiment the total of 0.0677 g of dried powder was obtained, which corresponds to net mass of the synthesized powder of 0.0369 g. Assuming that the converted TEOS in the synthesized powder occurred in a homogeneous form corresponding to Q_2 peaks, the conversion rate TEOS would be 0.1015. In the other

extreme case, in which the powder existed in the form corresponding to Q_4 the conversion of TEOS would be 0.1300. Finally, if all synthesized powder existed in Q_3 form, the conversion rate would be 0.1140. Considering that the peak corresponding to Q_3 in Fig. 5.7 is dominant, the latter value will be used to represent the conversion of TEOS in a given experiment.

Table 5.4 TEOS conversion for a given mass of the dried powder different hypothetical forms of the converted TEOS in the powder.

Case	Q_2	Q_3	Q_4
Si Bound	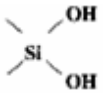	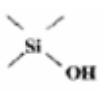	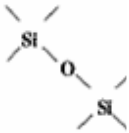
Basic unit	$[SiO_3H_2]$	$[Si_2O_5H_2]$	$[SiO_2]$
Dried Powder:			
Net reacted TEOS mass(g)	0.0369	0.0369	0.0369
Si in Dried powder(g)	0.0144	0.0162	0.0185
Si conversion	0.1015	0.1140	0.1300

Using the above approach, the conversion of TEOS in the emulsion polymerization experiments involving pure TCE ranged 1.51% to 18.14%. In general, the conversion increases with the total mass of the dried powder. Consequently, the results reported in Figs. 5.2 – 5.6 provide qualitative trends for the conversion of TEOS as a function of different experimental parameters. The exception is Fig 5.3, in which plots the mass of the dried powder versus the relative amount of TEOS. In this case, the observed increase in the dried mass powder with an increase in the relative amount of TEOS used does not necessarily indicate an increase in the conversion rate.

Fig. 5.8 presents the results, previously shown in Fig. 5.3, in terms of the conversion TEOS rather than the total mass of the dried powder. It can be noticed that using less than the stoichiometric amount of TEOS relative to amount of aluminum hydroxonitrate, leads to the lowest conversion of TEOS. With the stoichiometric amount of TEOS, its conversion reaches the highest value of 18.14%. Increasing the amount of TEOS beyond its stoichiometric volume leads to a drop in the conversion rate despite an increase in the synthesized dried powder. For the experiment with the excess of TEOS, the conversion appears to be independent of the actual excess of TEOS.

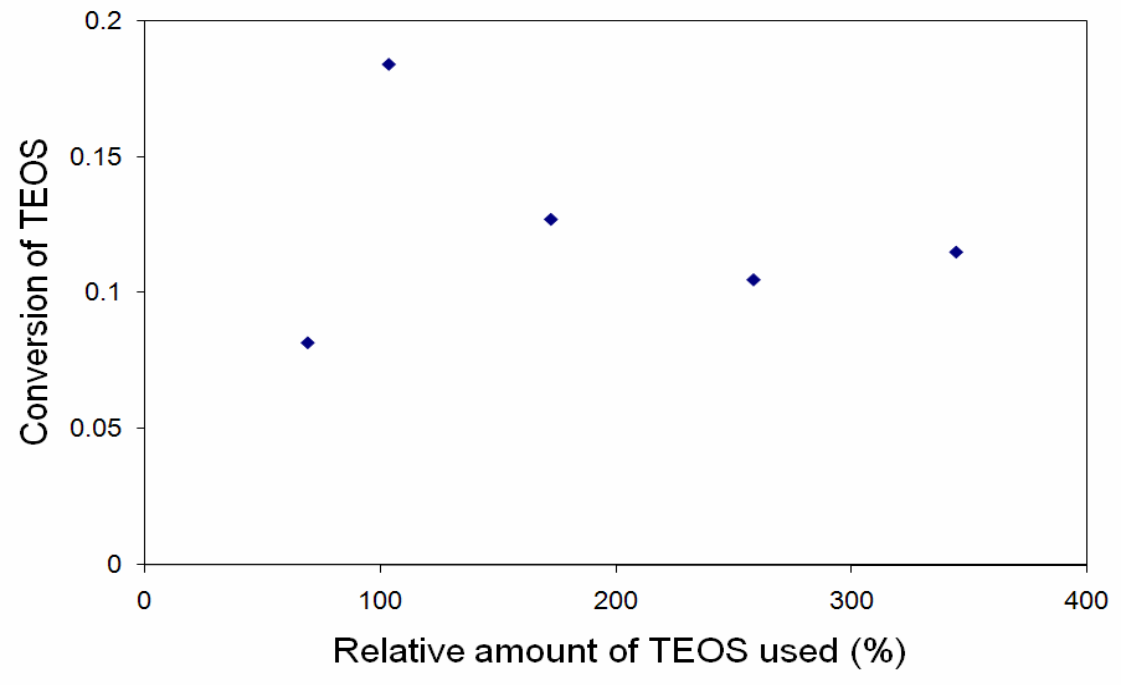

Figure 5.8 Effect of the relative amount of TEOS on its conversion in the emulsion polymerization experiments with pure TEOS.

5.3. New EPMM Membranes

Considering successful emulsion polymerization of TEOS in the system with pure TCE, the next step was to utilize the procedure developed for the Gravimetric Powder Method in synthesis of new EPMM membranes by replacing pure TCE with a 10 wt% solution of PPO in TCE. Similarly to the Gravimetric Powder Method, the new EPMM membranes were prepared using a three-step synthesis similar to the one shown in Fig. 5.1, except for the 3rd step in which the secondary emulsion was cast on a silicon wafer installed on a spin-coating machine.

5.3.1. Synthesis protocol for new EPMM membranes

The major objective in this last part of the project was to prove that the synthesis protocol developed for the Gravimetric Powder Method could be successfully used for the synthesis of the membranes. Due to the time constraint, only one set of new EPMM membranes was be synthesized and characterized. It is important to keep in mind that in the emulsion system involving a polymer solution rather than a pure solvent, the Gravimetric Powder Method is not feasible, because an increase in the mass of the solid residuals due to the polymerization of TEOS is insignificant compared to the mass of the dry polymer. As a result, to prove polymerization of TEOS in the emulsion system involving the actual polymer solution ultimately requires the ^{29}Si NMR analysis of the synthesized membrane. In turn, to detect the peaks characteristic to the polymerized

TEOS, requires a minimum threshold amount of silica in the analyzed sample. Consequently, the specific parameters of the synthesis protocol were selected to maximize the amount of the polymerized TEOS in the final membrane, rather than to produce a defect free membrane. Table 5.5 summarizes the specific parameters used in the synthesis of the new EPMM membranes.

Table 5.5 Parameters for the synthesis on new EPMM membranes.

Composition of the aqueous solution	10.50 g of aluminum hydroxonitrate in 15.0 mL of deionized water + sodium carbonate solution as a buffer
Polymer solution	10 g of PPO in 100 mL of TCE
Compatibilizer	0.3 mL of ethanol
Primary emulsion	0.1 mL of aqueous solution in 10 mL of polymer solution
Ultrasonication of primary emulsion	Power level 7 for 1 minute
Volume of TEOS added	1.0 mL or 345% relative to aluminum hydroxonitrate
Ultrasonication of secondary emulsion	Power level 3 for 180 minutes
Magnetic stirring following ultrasonication	None
Membrane casting	Spin coating – three layers
Boiling in deionized water of dry membrane	Yes
Thermal post-treatment	225^{o}C in vacuum oven for 48 hr

The volume of the aluminum hydroxonitrate solution of 0.1 mL doubles the largest volume of the aqueous solution used for the synthesis of the old EPMM membranes. In

case of TEOS, 1.0 mL represents a 6.7 fold increase compared to the largest volume used in the old synthesis protocol. In addition, there is no 1-octanol, which is replaced by 0.3 mL of ethanol, in the new synthesis protocol. Compared to the Gravimetric Powder experiments, the secondary emulsion was only ultrasonicated, however for a significantly longer time of 3 hours. On the other hand, with no magnetic stirring after ultrasonication of the secondary emulsion, the total reaction time was significantly reduced compared to the Gravimetric Powder experiments. The rationale for this change comes from the fact that ultrasonication, as shown by the results of Gravimetric Powder experiments, was more effective than magnetic stirring and had led to greater conversion rates of TEOS. Moreover, an increase in the conversion of TEOS in the Gravimetric Powder experiments was only marginal for long total reaction times. In addition, ultrasonication as a more effective way of mixing than magnetic stirring was thought to minimize aggregation of the dispersed inorganic phase.

A quick visual inspection of the new EPMM membranes after the complete post-treatment protocol revealed some noticeable differences compared to the old EPMM membranes. Unlike the old membranes, the new ones were not completely transparent. They had a very light white color, not uniformly distributed over the entire area. Moreover, one could observe small beige particles, which were also randomly distributed over the entire surface.

.

5.3.2. Characterization of new EPMM membranes

In total four new EPMM membranes were synthesized according to the protocol discussed in the previous section. The new membranes were characterized using the techniques discussed in Chapter 3, which included gas permeation (O_2 and N_2) and air separation tests, as well as the following analyses: DSC, ICP-MS, ^{29}Si NMR, and ^{27}Al NMR.

Out of the four synthesized membranes only one survived the complete gas permeation/separation protocol. Two of these membranes were found to be defective right after placing them in the permeation cell and one became defective during the tests. The gas transport properties of the lone surviving membrane were however very promising. In particular the oxygen permeability was found to be 33.76 Barrer, which is more than double the O_2 permeability of the base PPO membrane and the best old EPMM membrane. At the same time, this increase in the O_2 permeability was associated with a modest increase in the O_2/N_2 permselectivity from 4.67 for the base PPO membrane to 4.75 for the new EPMM membrane. This represents a very desirable and unique departure from the typical trade-off behavior of polymeric membranes, in which an increase in permeability is associated with a decrease of selectivity and vice-versa. Table 5.6 provides the comparison of the permeability and permselectivity of the new EPMM membrane with the best old EPMM membrane and the pure PPO membrane.

Table 5.6 Comparison of gas transport properties of the EPMM membrane with the best old EPMM and the PPO membranes.

Parameter	New EPMM membrane	Best old EPMM membrane	PPO membrane
O_2/N_2 permselectivity (-)	4.75	4.58	4.67
O_2 permeability coefficient (Barrer)	33.76	14.68	15.26
N_2 permeability coefficient (Barrer)	7.11	3.21	3.27

It is difficult to draw any definite conclusions based on the performance of a single membrane, in particular considering that three other membranes prepared using the same synthesis protocol were defective. Nevertheless, this might be an indication of the anticipated improvement of the gas transport properties of the EPMM membranes compared to those made from the pure polymer.

The DSC analysis of the new EPMM membranes revealed their average T_g of 228.2°C, which considerably greater that the highest T_g of the old EPMM membranes as well as the T_g of PPO of 217.2°C. The observed increase in T_g of the EPMM membranes compared to the base PPO was anticipated because the presence inorganic nanoparticles should decrease the chain mobility of the host polymer. More importantly, a change in the T_g compared to the base polymer indicates that the synthesized silica particles interact with polymer chains at the molecular level, which would not be possible with large inorganic particles. Therefore, the observed increase in the T_g is an indication that at least a part of the synthesized silica particles must be in the nano-range that are well dispersed in the continuous phase of the host polymer, leading to a unique properties of the new

nanocomposite material.

The results of the ^{29}Si NMR analysis of the new EPMM membrane are shown in Fig. 5.9. The overlapping peaks at around -100 ppm can be resolved into four peaks with the maxima located at -82.2 ppm, -89.08 ppm, -100.75 ppm and -110.70 ppm. The first of these peaks located at -82.2 ppm, which is the smallest of the four overlapping peaks can be attributed to a hydrolyzed TEOS. On the other hand, the other three peaks at -89.08 ppm, -100.75 ppm and -110.70 ppm can be attributed to the Q_2, Q_3, and Q_4 bounds, the presence of which provides the direct proof for the emulsion polymerization of TEOS in the new EPMM membranes.

Similarly to the ^{29}Si NMR spectrum of the Dried Powder, the main peak in Fig. 5.9 corresponds to Q_3. On the other hand, the intensities of the Q_2 and Q_4 peaks in Fig. 5.9 are comparable, while the peak corresponding to Q_4 in Fig 5.7 was clearly larger than the peak Q_2. In addition, there is one small peak near -24 ppm in Fig. 5.9. Despite an extensive literature survey, the origin of this peak could not be identified. However, this peak is certainly not related to any form of the Si-O-Si bound. This small peak could be an indication of a Si-O-Al bond, but there is no information in the literature to confirm this hypothesis. Furthermore, this peak was not present on the ^{29}Si NMR of the dried powder.

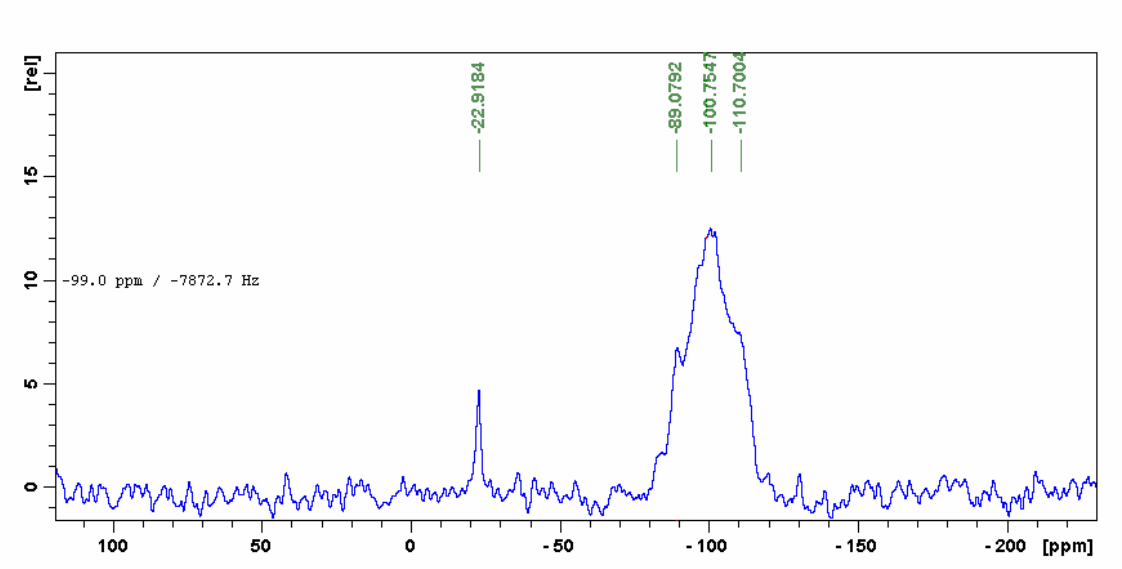

Figure 5.9 ^{29}Si NMR spectrum of the new EPMM membrane.

The ^{27}Al NMR spectrum of the new EPMM membrane is shown in Fig. 5.10. There are two major peaks on this spectrum, which correspond to Al from Groups IV and VI. The first peak, corresponding to Al Group IV can be attributed to the $\left[AlO_{1/4}(OH)_{4/2}(H_2O)\right]^{0.5+}$ while the second one to the core part of the $Al_{13}{}^{7+}$ Keggin structure ($AlO^{+}_{4/4}$). The co-existence of these two peaks proves the existence of the aluminum in the Keggin structure. However, it also indicates that despite boiling of the dry membranes in the deionized water, the residual aluminum remains in the final membrane.

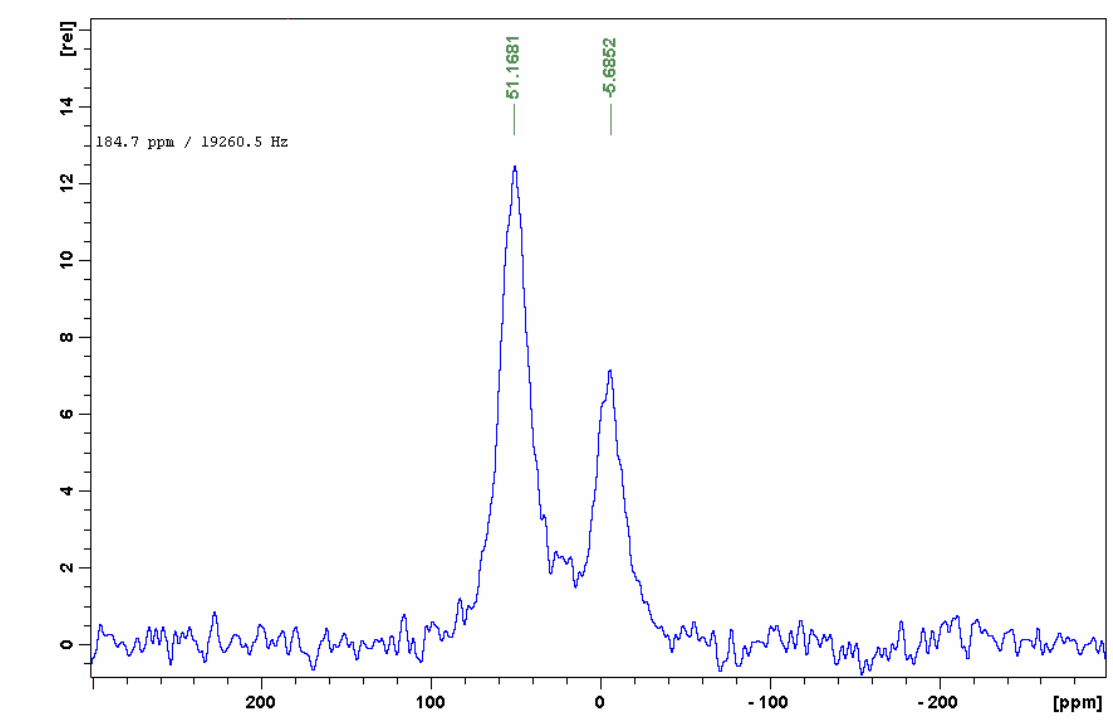

Figure 5.10 ^{27}Al NMR spectrum of the EPMM membrane.

The ICP-MS analysis of the new EPMM membrane revealed 2.87 wt% and 0.495 wt% of the elemental Si and Al, respectively. These amounts are significantly larger than in the largest amounts in the old EPMM membranes. Considering the fact that TEOS did polymerize in the new EPMM membrane the significant increase in the Si and Al contents was anticipated. However, as already indicated most of the detected aluminum came probably from the unreacted aluminum in the Keggin structure. Assuming that polymerized TEOS exist entirely in the form corresponding to Q_3 peak (the largest peak in Fig. 5.9), 2.87 wt% of Si in the new EPMM membrane corresponds to the TEOS conversion of 21.46%, which is significantly greater than 11.40% in the corresponding

Gravimetric Powder experiment.

The fact that the conversion of TEOS in the emulsion system involving the actual polymer solution is greater than that involving the pure solvent is very important from the practical point of view. First of all, this result indicates the positive effect of a greater viscosity of the polymer solution compared to the pure solvent. It is possible that as the viscosity of the continuous organic phase increases, while all other parameters remain approximately the same, the stability of the emulsion increases. This means that it might be possible to synthesize relatively large absolute amounts of polymerized silica using just a stoichiometric amount of TEOS, which would be very desirable from the point of view of the integrity of the final membrane.

Chapter 6.
Conclusions and Recommendations

6.1. Conclusions

Using the synthesis protocol developed by Sadeghi (2007), the resulting EPMM membranes showed virtually no effects of the theoretical Si loading and the post-treatment protocol on the O_2 permeability and the O_2/N_2 permselectivity. Moreover, in comparison to the base PPO membranes, the observed O_2 permeability and the O_2/N_2 permselectivity have generally decreased. The DSC analysis of the synthesized membranes showed a great scatter in the T_g of the EPMM membranes with the values generally lower than the T_g of the base PPO. Moreover, ICP-MS analysis showed the silica content in the selected EPMM membranes far below the expected theoretical level. This, in combination with the ^{29}Si NMR results, which showed that most of the already low silica content come from the unreacted TEOS, indicates that either the conditions required for the emulsion polymerization of TEOS in the old synthesis protocol were not present, or the conversion of TEOS was insufficient to influence the properties of the base polymer. In addition, the thermal post-treatment even at 225^{o}C, i.e. above the T_g of the base PPO, for 48 hours appears to be not sufficient to remove all unreacted TEOS from the final membrane. This low but highly variable content of the residual TEOS appears to be the major factor

behind a large scatter in the permeability, permselectivity, and the T_g of the EPMM membranes synthesized using the original synthesis protocol.

The critical analysis of the original synthesis protocol has suggested the replacement of 1-octanol by ethanol in the primary emulsion, and an increase in concentration of the reactants, i.e., aluminum hydroxonitrate and TEOS, in the casting emulsion system. It is important to emphasize that increasing the concentrations of aluminum hydroxonitrate and TEOS was also recommended by Sadeghi (2007). However, the implementation of this recommendation in the old synthesis protocol did not lead any changes in the properties of the old EPMM membranes. To verify the effect of these changes in the new synthesis protocol, an intermediate experimental procedure, which is referred to as a Gravimetric Powder method, has been developed. In this method, the polymer solution is replaced by the pure solvent, which allows determination of the conversion of TEOS in the emulsion system by measuring the mass of the resulting dried powder.

The results obtained from the Gravimetric Powder experiments show a positive effect of all studied parameters on the mass of the dried powder, which included the total reaction time, excess of TEOS, ultra-sonication time of the secondary emulsion, ultra-sonication power in primary emulsion. Out of these parameters, the power used in the primary emulsion appears to have the strongest effect on the mass of the dried powder. On the other hand, the mass of the dried powder is sensitive to the total reaction time and the ultrasonication time of the secondary emulsion at relatively short times. The mass of

the dried powder increased with the amount of TEOS used, but the largest conversion of the latter was obtained for the stoichiometric amount of TEOS. The polymerization of TEOS in the Gravimetric Powder experiments has been directly confirmed by the ^{29}Si NMR analysis.

Using the conditions for the maximum powder formation, one set of four new EPMM membranes has been synthesized. The new EPMM membranes have the T_g of 228.2^{o}C, which is distinctly greater compared to the base PPO, and contain one order of magnitude more of silica compared to the old EPMM membranes. More importantly, the ^{29}Si NMR analysis has proven that the silica content in the new EPMM membranes originates from the reacted rather than unreacted TEOS. Interestingly, the observed conversion of TEOS in the new EPMM membranes exceeding 20% is greater than the largest conversion in the Gravimetric Powder experiments. The oxygen permeability in the new EPMM membrane of 33.8 Barrer is more than twice that of the base PPO membrane. Moreover, this increase in O_2 permeability is associated with a modest increase in the O_2/N_2 permselectivity (4.75 versus 4.67).

6.2. Recommendations

The following recommendations are formulated based on the research results in this project for the future work:

- Considering that maximum conversion of TEOS occurs when using its stoichiometric amount and the fact that conversion of TEOS appears to be greater in the emulsion with the actual polymer solution rather than pure solvent, it is recommended to use the new synthesis protocol with the stoichiometric volumes of TEOS and even decreasing the volume of the aqueous solution used in formation of the primary emulsion
- In the new experimental protocol n-octanol has been replaced by ethanol. The roles of n-octanol and ethanol are different. The former acts as a surfactant while the latter as compatibilizer. It might be interesting to carry out experiments with both the compatibilizer and the surfactant to see if the latter has any effect on the properties of the EPMM membranes.
- The kinetics of TEOS polymerization under the EPMM conditions (with and without surfactant) should be studied quantitatively with the special focus on the effects of the ethanol concentration, the reaction temperature and the ultra-sonication on/off settings. All experiments involving the ultrasonicator in this project were performed with a 30 s on / 30 s off mode. While keeping the equal the on and off times, it is recommended to decrease them.
- The ^{29}Si NMR analyses in this project were used only to qualitatively confirm polymerization of TEOS. It is recommended to use the ^{29}Si NMR analyses in the quantitative mode, which would allow determination of the contribution of Q2,

Q2 and Q4 peaks. This would provide more inside into the structure of the synthesized inorganic phase.

- It is recommended to study the emulsion polymerization TEOS in an environment other than aqueous solution of aluminum hydroxonitrate. The results of this project do not allow concluding if the aluminum hydroxonitrate copolymerizes with TEOS or just provides the environment of a weak acid. Moreover, it is difficult to remove the residual content of the aluminum salt used, which may promote the formation of the defects in the final membrane. It is therefore, proposed to study the acid catalyzed polymerization of TEOS using a system with no solid residual, for example a hydrochloric acid. In addition, it is proposed to study base-catalyzed polymerization of TEOS using ammonia.
- The new EPMM membranes should also be characterized by testing with other gas mixtures such as methane/carbon dioxide, nitrogen/methane and methane/carbon dioxide
- The potential applications of the new EPMM membranes in other membrane separations such as pervaporation and ultra-filtration should also be investigated.

References

Akkit, J.W., and Farthing, A., Aluminum-27 Nuclear Magnetic Resonance studies of the Hydrolysis of Aluminium (III). Part 4. Hydrolysis using Sodium Carbonate., Journal of the Chemical Society Dalton Transactions, 1617, 1981

Augilar-Vega, M., and Paul, D. R., Gas transport properties of polyethylene ethers, Journal of polymer science: Part B, 31, 1557, 1993

Aycock, D., Polyphenylene tether, in Encyclopedia of Polymer Science and Technology, V12, Interscience Publisher, New York, 1974

Baker, Richard W., Future directions of membrane gas separation technology, Industrial and Engineering Chemistry Research, 41, 1393, 2002

Bottero, J.Y., Cases, J.M., Fiessinger, F., and Poirier, Studies of hydrolyzed aluminium species and compensation of aqueous solutions, Journal of Physical Chemistry, 84, 2933, 1980

Bouma, R.H.B., Checchetti, A., Chidichimo, G., and Drioli, E., Permeation through a heterogeneous membrane: the effect of the dispersed phase, Journal of Membrane Science. 128, 141, 1997

Bradley, D.C., Mehrotra, R.C., and Gaur, D.P., Metal alkoxides, Academic, London, 1978.

Breck, D.W., Zeolite molecular Sieves: structure, chemistry and use, Wiley, New York, 1974

Brinker, C.J., Scherer, G.W., Sol-gel Science:the Physics and Chemistry of Sol-Gel processing., Academic Press, San Diego, 1990

Buonomenna, M.G., Figoli, A., Jansen, J.C., Davoli, M., and Drioli, E., Asymmetric membranes with controlled morphology from modified polyetheretherketone

(PEEKWC): Preparation and characterization, Materials Research Society Symposium - Proceedings, Volume 752, 2003

Chang, C., and Fogler, H.C., Kinetics of Silica Particle Formation in Nonionic W/O Mircoremulsions from TEOS, Materials, Interfaces, and Electrochemical Phenomena, 42, 3153, 1996

Chiang, A.S.T., and Chao, K.J., Membranes and films of zeolite and zeolite-like materials, Journal of Physics and Chemistry of Solids, 62(9-10), 1899, 2001

Chiew, Y.C., and Glandt, E.D., The effect of structure on the conductivity of a dispersion, Journal of Colloid Interface Science, 94, 90, 1983.

Daynes, H.A., The process of diffusion through a rubber membrane, Proceeding of Royal Society of London, 97, 286, 1920

Eliseev, A. A, Kalinin, S.V., Pivalov, V. I., Vertegel, A. A., and Tretyakov, Yu. D, The effect of copolymerization of tetraethylorthosilicate and aluminium hydroxonitrate, Jounal of solid state chemistry, 147, 304, 1999

Furrer, G., Ludwig, C., and Schindler, P.W., On the Chemistry of the Keggin Al_{13} Polymer, Journal of colloid and interface science, 149, 56, 1992

Gonzo, E.E., Parentis, M.L., and Gottifredi, J.C., Estimating models for predicting effective permeability of mixed matrix membranes, Journal of Membrane Science, 277, 46, 2006

Hamilton, B., Porous Silicon, Semiconductor Science and Technology, 10, 1187, 1995

Harris, M. T., Brunson, R. R., and Byers, C. H., The base catalyzed hydrolysis and condensation reactions of dilute and concentrated TEOS solutions, Journal of Non-crystalline Solids, 121, 397, 1990.

Hay, A.S., Blanchard, H.S., Enders, G.F., and Eustance, J.W., Polymerization by oxidative Coupling, J.American Chemical Society, 81, 6335, 1959

Hench, L.L., and West, J.K., The sol-gel process, Chemical Reviews, 90(1), 33, 1990

Ishihara, T., Kilner, J.A., Honda, M., Sakai, N., Yokokawa, H. and Takita, Y., Oxygen

surface exchange and diffusion in $LaGaO_3$ based perovskite type oxides, Solid State Ionics, 113, 593, 1998

Julbe, A., Zeolite Membranes – Syntheses, Characterization and Application, Chap. 6, Introduction to Zeolite Science and Practice, Elsevier, 2007

Karger, J. and Ruthven, D.M., Diffusion in Zeolites and Other Microporous Solids, John Wiley & Sons, New York, 1992

Karasz, F.E., and Reilly, J.M., Thermal properties of Poly (2,6-dimethyl phenylene ether. Journal of polymer science, 3, 561, 1965

Kickelbick, G., Hybrid Materials, Wiley-VCH, Wemheim, 2007

Kesting, R. E. and Frizsche, A. K., Polymeric gas separation membranes, John Wiely & Sons Inc., 1993

Kesting, R. E., Synthetic polymeric membranes. A structural prospective, John Wiley & Sons, New York, 1985

Koros, W.J., and Pinnau, I., Polymeric Gas Separation Membrane, CRC Press, Boca Raton, 1993

Krause, S., Paul D.R., and Newman, S., Polymer blends I, Academic Press Inc. Orlando, Fl, 1978

Kruczek, B. and Matsuura, T., Development and Characterization of Homogeneous Membranes made from High Molecular weight Sulfonated Polyphenylene Oxide, Journal of Membrane Science, 146, 263, 1998.

Kruse, J., Ratzke, K., Faupel, F., Sterescu, D.M., Stamatialis, D.F., and Wessling, M., Free Volume in C60 Modified PPO Polymer Membranes by Positron Annihilation Lifetime Spectroscopy, Journal of Physical Chemistry B, 111, 13914, 2007

Laine, R.M., Nanobuilding blocks based on $[OSiO_{1.5}]_8$ silsesquioxanes, Journal of Material Chemistry, 15, 3725, 2005

Lashkari, S., and Kruczek, B., Fundamental Aspects of Membrane Characterization by Constant Volume and Constant Pressure Techniques, University of Ottawa, 2008

Li, K., Ceramic membranes for separation and reaction, John Wiley & Sons Ltd, Chichester, 2007

Liu, Y.L., Chang, Y.H., and Liang, M., Poly(2,6-dimethyl-1,4-phenylene oxide) (PPO) multi-bonded carbon nanotube (CNT): Preparation and formation of PPO/CNT nanocomposites, Polymer, 49, 5405, 2008

Mahajan, R. and Koros J.W., Factors controlling successful formation of mixed matrix gas separation, Industrial and Enginerring Chemistry Research, 39, 2692, 2000

Makke, A., Perez, M., Lame, O., and Barrat J.L., Mechanical testing of glassy and rubbery polymers in numerical simulations: Role of boundary cpmditioms in tensile stress experiments, The Journal of Chemical Physics, 131, 14904, 2009

Mark, J. E., Physical properties of polymer handbook, Springer, New York, 2007

Matsuura, T., Synthetic Membranes and membrane separation process, CRC press, Boca Raton, 1994

Mueller, U., and Witte, M., Ceramic membrane applications for filter backwash water treatment, Techneau, 2008

Mulder, M., Basic Principles of Membrane Technology, Kluwer Academic Publishers, 1996.

Osada, Y., and Nakagawa, T., Membrane science and technology, Marcel Dekker Inc., New York, 1992

Porter, M. C., Handbook of Industrial Membrane Technology, Noyes Publications, 1990

Rao, M.B. and Sircar, S., Nanoporous carbon membranes for separation of gas mixture by selective surface flow, Journal of Polymer Science, 85, 253, 1993

Robeson, L. M., Correlation of separation factor versus permeability for polymeric membranes, Journal of Membrane Science, 62, 165, 1991

Ruiz-Hitzky, E., Letaief, S., and Prevot, V., Novel organic-inorganic mesophases: Self templating synthesis and intratubular swelling, Advanced Materials, 14, 439, 2002

Rutherford, S.W. and Do, D.D., Review of time lag permeation technique as a method for

characterization of porous media and membranes, Adsorption, 3, 283, 1997

Sadeghi, F, Development of Nanocomposite Materials for Gas Separation Membranes, Masters' Thesis. University of Ottawa, 2007

Sadeghi, F., Tremblay, A.Y. and Kruczek, B., Synthesis and characterization of emulsion polymerized mixed matrix aluminum silicate/poly (2,6-dimethyl 1,4-phenylene oxide) films, Journal of Applied Polymer Science, 109(3), 1454, 2008

Sanchez, J., and McCormick, Kinetic and thermodynamic study of the hydrolysis of silicon alkoxides in acidic alcohol solutions, Journal of Physical Chemistry, 96, 8973, 1992

Sanders, E.S., Koros, W.J., Sorption of CO_2, C_2H_4, N_2O and their binary mixtures in poly(methyl methacrylate), Journal of Polymer Science, Polymer Physics Edition, 24, 175, 1986

Sharp, K.G., Inorganic/organic hybrid materials, Advanced Material, 10, 1243, 1998

Smith, R. L., and Collins, S. D., Porous silicon formation mechanisms, Journal of Applied Physics, 71, R1, 1992

Sperry, D.P., Falconer, J.L., and Noble, R.D., Methanol-hydrogen separation by capillary condensation in inorganic membranes, Journal of Membrane Science, 60, 185, 1991

Vollet D.R., Donatti, D.A., and Campanha, J.R., A kinetic model of the ultrasound catalyzed hydrolysis of solventless TEOS-Water mixtures and role of the initial additions of ethanol, Journal of Sol-gel Science and Technology, 6, 57, 1996

Wijmans, J.G. and Baker, R.W., The Solution-Diffusion Model: a Review, Journal of Membrane Science, 107, 1, 1995

Wrasidlo, W., Transitions and Relaxations in poly (1,4-phenylene ether), J. Polym.Sci., Part A-2 58,1719, 1972

Xu, T., Advances in Membrane Science and Technology, Nova Science Publishers Inc., New York, 2009

Yang, H., Ding, Z., Jiang, Z., and Xu, X., Sol-Gel process kinetics for $Si(OEt)_4$, Journal of non-Crystalline solids, 112, 449, 1989

Yonkoski, R.K., and Soane, D.S., Model of spin coating in microelectronic applications,

Journal of Applied Physics, 72, 725, 1992

Ziegel, K.D., Frensdorff, H.K., and Blair, D.E., Measurement of hydrogen transport in poly-(vinyl Fluoride) films by the permeation-rate method, Journal of polymer Science: Part A-2, 7, 809, 1969

Zolandz, R.R. and Fleming, G.K., Gas Permeation, in Membrane Handbook, Ho and Sirkar editors, Van Nostrand Reinhold: New York, USA, 1992

APPENDIX A: Sample Calculations

A.1 Calculation of TEOS conversion in the membrane:

Taking 1 g of EPMM membrane as basis.

PPO solution: 10% W/V

TEOS density: 0.94g /ml

Reactant Ratio: TEOS:PPO solution = 1ml : 10 ml

With the assumptions listed in Chapter 5.3.3, for the ultimate case that all Si is bounded as 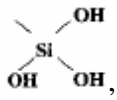 ,

In 1 g membrane, amount of Si = 2.87% x 1 g = 0.0287 g

Si is all in 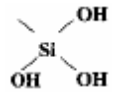 with a basic unit of $[Si_2O_7H_6]$

Si concentration in 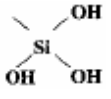 is $\frac{32\times 2}{32\times 2+16\times 7+1\times 6}=0.3516$

PPO concentration in membrane is $1-\frac{0.0287}{0.3516}=0.9184$

Thus from 1 g of PPO, or 1 ml of TEOS, there is

$\frac{0.0287}{0.9184}=0.03125$ g of 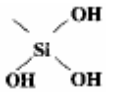 structure.

$$Si\ conversion=\frac{\text{Re}acted\ TEOS}{TEOS\ \text{Re}ac\tan t}=\frac{Amount\ of\ Si\ in\ \text{Pr}oduct}{Amount\ of\ Si\ in\ \text{Re}ac\tan t} \quad \text{A.1}$$

$$Si\ Conversion = \frac{0.03125g}{0.94g/ml \times 1ml \times (32g/212g)} = 0.2203$$

A.2 Calculation of TEOS conversion in dried powder.

Taking the Gravimetric Powder of 0.0674 g as sample.

The net mass of reacted TEOS = 0.0674 g – 0.0305 g = 0.0369 g

Si concentration in 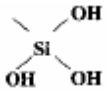 $= \frac{32 \times 2}{32 \times 2 + 16 \times 7 + 1 \times 6} = 0.3516$

$$\text{Si Conversion} = \frac{0.012976\text{g}}{0.94\text{g/ml} \times 1\text{ml} \times (32\text{g}/212\text{g})} = 0.09145$$

APPENDIX B: Characterization of EPMM Membranes

B.1 EPMM membranes analysis result

Table B.1 EPMM membranes analysis result.

id	Si Loading (%)	US time (S)	Boiling	PT Temp	PT time (h)	α_{air}	$P_{O2,air}$	$P_{N2,air}$	P_{O2}	D_{O2}	P_{N2}	D_{N2}	Tg (˚C)	Si Concentration (%)	Al Concentration (%)
1	5	420	1	225	48	3.84	16.34	4.25	19.60	17.04	3.96	5.02	191.32		
4	10	1800	1	225	48	2.82	16.93	6.01	19.52	16.92	6.17	9.26	215.03		
7	5	420	1	120	48	3.01	19.81	6.57	24.08	12.51	6.52	6.13	218.48		
8	5	420	1	120	48	2.79	13.69	4.91	17.42	15.07	4.57	5.20	217.06		
9	5	420	1	225	48	3.41	15.07	4.42	19.91	21.64	3.95	6.15	207.30		
10	5	420	1	225	48	3.56	13.20	3.71	16.99	15.72	3.46	5.43	188.29		
13	0	0	0	0	0	3.53	9.35	2.65	12.50	6.78	2.51	2.63			
16	5	420	1	120	48	3.53	16.81	4.76	19.99	19.98	4.62	5.53	219.36		
17	5	420	1	120	48	2.94	11.29	3.85	14.72	13.69	3.69	5.44	187.86		
18	5	420	1	225	48	4.28	15.28	3.57	17.06	16.64	3.48	4.30	218.70		
22	0	0	0	0	0	3.79	20.49	5.41	23.95	16.64	4.77	5.59			
27	10	0	0	0	0	3.55	15.82	4.45	19.99	13.80	3.95	4.91			
28	5	420	1	25	48	3.65	13.56	3.70	17.94	7.75	3.49	3.02	198.68		
29	10	840	1	25	48	2.66	17.88	6.73	25.13	27.51	6.30	8.66	187.36		
32	15	840	1	225	1	2.85	17.11	6.01	19.33	20.18	6.16	13.60	194.49		

35	10	840	1	25	48	2.58	14.47	5.61	21.12	23.76	5.10	8.40	219.76		
41	10	1800	1	25	48	3.08	14.21	4.61	17.61	17.48	4.42	7.21	184.76		
44	15	1800	1	225	1	3.72	13.83	3.72	15.13	16.11	3.61	8.30	194.30	0.804	0.0406
46	5	420	1	225	48	3.82	16.07	4.21	18.27	14.92	4.53	5.46	198.59	0.507	0.0067
47	5	420	1	225	48	3.11	14.95	4.81	19.46	15.37	4.77	6.64	215.94	0.376	0.0064
48	3	420	1	25	48	3.38	11.40	3.38	14.74	14.23	3.27	4.58	217.92	0.741	0.0179
49	4	420	1	225	48	3.74	14.75	3.95	18.31	19.89	3.93	4.61	204.35	0.721	0.0064
50	4	420	1	25	48	3.35	10.61	3.16	13.93	10.26	3.11	3.92	177.95	0.917	0.0496
51	3	420	1	25	48	3.12	14.79	4.74	18.96	19.16	4.66	7.46	176.13	0.8	0.0076
52	4	420	1	225	48	4.02	14.43	3.59	16.94	14.87	3.65	5.97	188.96	0.572	0.0196
54	4	420	1	225	48	2.81	31.14	11.10	25.30	23.69	12.63	18.75	184.08		
55	4	420	1	25	48	3.68	15.92	4.33	20.14	17.57	5.67	9.57	214.42	0.735	0.0047
56	3	420	1	225	48	4.05	14.39	3.56	17.09	15.95	3.57	5.06	204.19	0.538	0.0074
57	2	420	1	25	48	3.43	13.00	3.79	17.54	17.75	3.52	4.60	212.17	0.553	0.0209
58	2	420	1	25	48	3.29	12.66	3.84	17.76	12.53	3.62	4.79	210.42	0.645	0.0151
59	2	420	1	25	48	3.59	13.55	3.78	17.58	11.90	3.67	5.93	203.02		
60	2	420	1	25	48	3.52	11.95	3.39	17.00	14.42	3.23	4.67	199.14	0.446	0.0194
61	2	420	1	25	48	3.27	11.21	3.43	15.03	8.38	3.24	3.42	185.64	0.591	0.0448
62	2	420	1	25	48	2.97	14.29	4.80	19.80	18.46	4.18	6.61	202.18	0.616	0.039
63	2	420	1	225	48	2.77	14.11	5.10	16.12	13.20	4.86	6.87	215.41	0.597	0.0377
64	2	420	1	225	48	3.84	14.41	3.75	17.43	15.92	3.58	5.82	211.41	0.766	0.0272
65	1	420	1	25	48	3.07	12.48	4.07	17.00	14.04	3.89	5.35	210.49	0.553	0.01
66	1	420	1	25	48	3.48	14.53	4.17	19.09	23.32	3.94	7.24	191.38	0.856	0.008
67	1	420	1	25	48	3.06	12.45	4.07	16.93	13.12	3.83	5.70	203.05	0.793	0.0164
68	1	420	1	25	48	3.04	13.87	4.56	19.33	16.16	4.33	6.18	191.66	0.735	0.014
70	1	420	1	225	48	4.58	14.69	3.21	16.44	15.36	3.34	6.00	219.12	0.665	0.0063
71	1	420	1	225	48	3.62	12.75	3.53	18.37	13.07	3.82	6.01	190.01	0.696	0.0043

72	0	0	0	0	0	3.37	16.23	4.82	21.52	15.95	4.20	5.07	
73	0	0	0	0	0	3.45	13.99	4.06	18.24	11.41	3.70	4.04	
74	0	0	0	0	0	3.31	15.67	4.74	20.98	11.41	4.44	4.72	
77	0	0	0	225	0	4.37	15.94	3.65	36.67	15.55	32.24	0.00	
78	3	420	1	225	48	3.87	17.18	4.44	19.92	19.15	4.32	7.60	207.32
79	3	420	1	225	48	3.19	11.13	3.49	15.32	15.71	3.18	4.55	178.92
80	3	900	1	25	48	2.66	9.84	3.70	15.57	13.86	3.40	3.71	197.63
81	3	900	1	25	48	2.70	10.39	3.85	16.31	9.05	3.61	4.59	176.41
82	3	900	1	25	48	2.97	10.42	3.51	15.43	10.41	3.29	4.21	207.62
83	3	1800	1	25	48	3.12	13.95	4.47	20.32	22.39	4.38	6.76	186.05
84	3	1800	1	25	48	3.72	11.97	3.22	15.80	10.23	3.34	5.10	206.71

Appendix C: Gravimetric Powder Experiment Results

C.1 Gravimetric Powder experiment result.

Table C.1 Gravimetric Powder experiment result.

Aqua solution	Ethanol	TEOS	UltraSonication time (min)	UltraSonication power	Reaction time (h)	Stirred	Net powder weight per sample (g)
(ml)	(ml)	(ml)					
0.1	0.3	1	30	7	1	Yes	0.0356
0.1	0.3	1	30	7	2	Yes	0.0379
0.1	0.3	1	30	7	4	Yes	0.0422
0.1	0.3	1	30	7	8	Yes	0.0516
0.1	0.3	1	30	7	16	Yes	0.0569
0.1	0.3	1	30	7	24	Yes	0.0678
0.1	0.3	1	30	7	48	Yes	0.0674
0.1	0.3	0.1	30	7	24	Yes	
0.1	0.3	0.2	30	7	24	Yes	0.0358
0.1	0.3	0.3	30	7	24	Yes	0.0484
0.1	0.3	0.5	30	7	24	Yes	0.0511
0.1	0.3	0.75	30	7	24	Yes	0.056
0.1	0.3	1	30	7	24	Yes	0.0678
0.1	0.3	1	0	7	24	Yes	0.0492
0.1	0.3	1	1.5	7	24	Yes	0.0473
0.1	0.3	1	3	7	24	Yes	0.0517
0.1	0.3	1	7	7	24	Yes	0.0597
0.1	0.3	1	15	7	24	Yes	0.0647
0.1	0.3	1	30	7	24	Yes	0.0678
0.1	0.3	1	60	7	24	Yes	0.0674
0.1	0.3	1	30	2	24	Yes	0.0354

0.1	0.3	1	30	3	24	Yes	0.0403
0.1	0.3	1	30	4	24	Yes	0.0564
0.1	0.3	1	30	5	24	Yes	0.0678
0.1	0.3	1	30	6	24	Yes	0.0737
0.1	0.3	1	30	7	24	Yes	0.0764
0.1	0.3	1	30	7	1	No	0.03225
0.1	0.3	1	60	7	2	No	0.043925
0.1	0.3	1	120	7	4	No	0.061225
0.1	0.3	1	240	7	8	No	0.061575

C.2 Calculated TEOS conversion in dried powder.

Table C.2 Calculated TEOS conversion in dried powder.

Aqua solution	EtOH	TEOS	Ultra-Sonication time (min)	Reaction time (h)	Stirred	Net product weight per sample (g)	Case Q2	Case Q3	Case Q4
(mL)	(mL)	(mL)							
0.1	0.3	0.2	30	24	Yes	0.0358	0.0657	0.0934	0.0819
0.1	0.3	0.3	30	24	Yes	0.0484	0.1479	0.2103	0.1843
0.1	0.3	0.5	30	24	Yes	0.0511	0.1021	0.1452	0.1273
0.1	0.3	0.75	30	24	Yes	0.056	0.0843	0.1198	0.1050
0.1	0.3	1	30	24	Yes	0.0678	0.0924	0.1314	0.1152